FACULTY OF TECHNOLOGY
OULU MINING SCHOOL
DEGREE PROGRAMME IN ECONOMIC GEOLOGY

The origin of high metal tenor in Ni-PGE ores from the Kevitsa Ni-Cu-(PGE) deposit, northern Finland: Constraints from an in-situ trace element study of base metal sulphides

Master's Thesis

Eleanor Grace Capuano

2020

TABLE OF CONTENTS

LIST OF FIGURES

LIST OF TABLES

ABBREVIATIONS

B

BIF ……..banded iron formation
BMS ……...base metal sulphides

C

CLGB …….Central Lapland Greenstone Belt
CLGC…….Central Lapland Granitoid Complex
cpy ……...chalcopyrite

E

EDS ……..energy-dispersive X-ray spectroscopy
EPMA ……...electron probe micro-analyser

F

FESEM ...……...field emission scanning electron microscope
FQML ……First Quantum Minerals Ltd.

G

GTK …….Geological Survey of Finland

I

IOCG .....iron-oxide-copper-gold
IPGE .....Ir-group PGE (Ir, Os, Ru)
iss .....intermediate solid solution

L

LA-ICP-MS ....laser ablation inductively coupled plasma mass spectrometry
LGB .....Lapland Granulite Belt
LREE .....light rare earth element

M

mill .....millerite
mss .....monosulphide solid solution

O

OLWB .....olivine websterite

P

PGE .....platinum group element
PGM .....platinum group minerals
po .....pyrrhotite
pOLWB .....plagioclase-bearing olivine websterite
pn .....pentlandite
PPGE .....Pt-group PGE (Pd, Pt, Rh)
py .....pyrite

R

REE .....rare earth element

T

TRA .....Time Resolved Analysis

V

VMS .....volcanogenic massive sulphide

ACKNOWLEDGEMENTS

Firstly, I would like to thank my supervisor, Prof. Shenghong Yang, for arranging the funding for this project from the K.H. Renlund Foundation and for all of his guidance throughout, and Dr. Kirsi Luolavirta for all of her advice and provision of essential literature. Furthermore, I am grateful to the GTK for allowing me to use their facilities in Espoo, and Dr. Hugh O'Brien and Dr. Matti Kurhila for providing their expertise with the LA-ICP-MS analysis.

I would like to thank my support network of international students at the University of Oulu, in particular: Alexandra, Axel, Brandon, Mauricio, Matthew, Matthias, Semyon and Thomas, for making my time in Oulu a lot less stressful and a lot more memorable. In addition, I tremendously appreciate Josh, Tess, Mo and Robyn for their support from the UK side and providing me with the humour I needed to get through moving abroad.

I would also like to thank my wonderful family; Tracy, Anthony, William, Monty and Spencer, for all their encouragement and giving me endless reasons to be homesick.

Lastly, I am incredibly grateful for my lovely Nico, for his continuous supply of emotional support, patience and chicken nuggets throughout my degree.

ABSTRACT

Research Unit
Oulu Mining School

Author	**Supervisor and Second Examiner**
Eleanor Grace Capuano	Prof. Shenghong Yang, Dr. Kirsi Luolavirta

Name of the Thesis

The origin of high metal tenor in Ni-PGE ores from the Kevitsa Ni-Cu-(PGE) deposit, northern Finland: Constraints from an in-situ trace element study of base metal sulphides

Degree Programme	**Month, Year**	**Pages**
MSc. Economic Geology	May, 2020	91 + 29

Abstract

The Kevitsa mafic-ultramafic intrusion is located in the Central Lapland Greenstone Belt, in Finnish Lapland, and hosts a large Ni-Cu-PGE sulphide deposit. Since 2012, Kevitsa has been one of Europe's most important nickel mines with a pre-mine resource of 274.8 Mt @ 0.30 % Ni, 0.41 % Cu, 0.014 % Co, 0.11ppm Au, 0.15 ppm Pd and 0.2 ppm Pt. There are two main ore types that make up the economic resources, named *normal ore* and *Ni-PGE ore*, of which the normal ore type comprises 90 vol.%. The normal ore has average Ni and Cu grades of 0.3 and 0.42 wt.%, respectively, with the main ore minerals being pyrrhotite, pentlandite, and chalcopyrite. The Ni-PGE ore consists predominantly of pentlandite, pyrite and millerite and has higher and more variable Ni grades, lower Cu grades (Ni/Cu 1.5–15) and extremely high Ni tenors, up to 40 wt.%. The Ni-PGE ore has a high PGE content ranging from >1 ppm to 26.8 ppm, much higher than that of the normal ore (0.5 to 1 ppm of combined Pt, Pd and Au). The uniqueness of the Ni-PGE ore type is amplified further by the high Ni contents of its cumulus silicates, as attested by Ni contents of olivine that reach up to 1.4 wt.%. In addition to the aforementioned ore types, there is an uneconomic type, called *false ore*, which consists of pyrrhotite, with rare chalcopyrite and pentlandite and generally has a low Ni content (<0.1 wt.%).

To enhance our understanding of the ore-forming and post-magmatic processes that occurred in the Kevitsa intrusion, we determined PGE concentrations of the main sulphide phases from the main ore types using laser ablation-inductively coupled plasma mass spectrometry (LA-ICP-MS). According to our results, sulphides in the Ni-PGE ore show the highest PGE contents with >1 ppm Ru, Ir and Os, and up to 51 ppm Pd. Although Pd is found in all of the sulphide phases, pentlandite is the richest, with Pd contents ranging from 0.3 ppm in the false ore to tens of ppm in the Ni-PGE ore. Millerite and pyrite are much lower in PGEs than pentlandite, and pyrrhotite and chalcopyrite record the lowest levels. Platinum contents are low throughout, with the majority of analyses falling below the detection limit (<0.001 ppm). Mass balance calculations show that BMS host a considerable amount of Os, Ir, Ru, Rh, and Pd whilst Pt is preferentially hosted within PGM, arsenides and sulpharsenides. High PGE and semimetal concentrations in the Ni-PGE ore suggest that a semimetal rich residual liquid was critical in the distribution of PGE within BMS. Although the origin of the Ni-PGE ore remains ambiguous, it is clear that the formation was dominated by magmatic processes and hydrothermal processes played an insignificant role.

1 INTRODUCTION

Magmatic sulphide deposits contribute to a significant proportion of global Ni and Cu resources; approximately 60 percent of global nickel production comes from Fe-Ni-Cu sulphides derived from mafic-ultramafic intrusive bodies and flows (Naldrett, 2004). Magmatic Ni-Cu sulphide deposits have been the subject of thorough and extensive research over the last few decades, as they are often accompanied by a wide range of base, precious and semimetals; the most important of which are platinum group elements (PGE), which may be present at g/t level (Barnes & Lightfoot, 2005).

The mining of Ni and Cu as a resource has been ingrained in Finland's history from as early as the 1920s with the exploitation of the Kotalahti and Vammala Ni-Cu belts in central and southern Finland (Makkonen, et al., 2008). With the development and mining of the Kevitsa Ni-Cu-(PGE) deposit and the discovery of the Sakatti Cu-Ni-PGE deposit, the focus of Ni-Cu exploitation has been shifted to northern Finland.

This study aims to enhance our understanding of the magmatic and post-magmatic processes that occurred in the Kevitsa intrusion and perhaps other Ni-Cu-(PGE) deposits, with the use of laser ablation-inductively coupled plasma mass spectrometry (LA-ICP-MS). LA-ICP-MS is a technique which allows the measurement of a full suite of trace elements in magmatic sulphides *in-situ*, which has led to a better understanding of various PGE-rich deposits (Ballhaus & Sylvester, 2000; Holwell & McDonald, 2007; Holwell & McDonald, 2010; Godel, et al., 2007; Barnes, et al., 2008). Analysis of sulphides in this manner can shed light on the magmatic and hydrothermal processes that contributed to the formation of the deposit, which are addressed in the coming sections.

1.1 Magmatic Ni-Cu-(PGE) Deposits

Magmatic Ni-Cu-(PGE) deposits can be broadly divided into two major categories, depending on their sulphide content (Naldrett, 1999, 2004, 2010, 2011):

i. Sulphide-rich magmatic sulphide deposits, with sulphide contents ranging from 20 to 90 percent, are primarily mined for Ni and Cu, with PGE as by-products. (e.g. *Pechenga,* Russia; *Sudbury, Voisey's Bay,* Canada; *Jinchuan*, China; *Kambalda*, Australia)

ii. Sulphide-poor magmatic sulphide deposits, with sulphide contents ranging from 0.5 to 5 percent, are primarily mined for PGE, with Ni and Cu as by-products. (e.g. *Bushveld Complex,* South Africa; *Great dyke*, Zimbabwe; *Penikat, Portimo Complex,* Finland; *Stillwater,* United States)

These categories are then further divided throughout the literature on the basis of their parental magma type (Naldrett, 2004), geological association and rock type (Barnes & Lightfoot, 2005) and magmatic environment (Eckstrand & Hulbert, 2007).

1.1.1 Genesis of Magmatic Ni-Cu-(PGE) Deposits

Fundamentally, magmatic Ni-Cu-(PGE) sulphide deposits are formed as a consequence of the segregation, enrichment and concentration of an immiscible sulphide liquid from a mafic-ultramafic magma (Naldrett, 2004). Formation of an economic deposit in this manner occurs with several stages, much like a 'recipe' in which specific physical conditions must be satisfied. Anthony Naldrett describes this as a pathway, named *"From the Mantle to the Bank"* in his 2010 paper (Naldrett, 2010a) and can be summarised into 7 main stages, illustrated by *Figure 1-1*.

1. *Partial melting* – high-degree partial melting of the mantle to produce a metal-rich mafic-ultramafic magma.

2. *Transport* - magma ascent from the mantle through the crust via crustal-scale structures.

3. *Fertilisation* - sulphide saturation of the silicate magma and the segregation of an immiscible sulphide melt.

4. *Enrichment* - enrichment of the sulphide melt in base and precious metals.

5. *Emplacement* - magma emplacement and the accumulation of sulphides in a physical trap.

6. *Nourishment* - further enrichment of the sulphide melt upon interaction with additional flowing magma and crystallisation of the sulphide liquid.

7. *Full maturity* - post-magmatic modification by hydrothermal and metamorphic processes.

Partial Melting

Parental magmas of magmatic Ni-Cu-(PGE) deposits are derived from the mantle, as the crust is relatively depleted in such metals. For example, there is 1 ppb Pd and 100 ppm Ni and Cr in the average crust as opposed to 4-7 ppb and 2000 ppm respectively in primitive mantle (Taylor & McLennan, 1985; Becker, et al., 2006).

In order to form a magma fertilised with metals such as Ni, Cu and PGE, there must be relatively large degrees of partial melting of the mantle. Although the phases with the highest partition coefficient of Ni are sulphide minerals, the amount of sulphide in the mantle is very low (0.0054 wt.% sulphide; Lorand & Keays, 1993), and has much less influence on the budget of Ni in the magma than olivine. Despite a moderate partition coefficient of Ni into olivine, olivine makes up around 70% of the mantle and is thus the main phase contributing Ni to the magma (Barnes & Lightfoot, 2005). Therefore, in order for the magma to obtain an economical amount of Ni from the mantle, a high degree of partial melting is required with a considerable contribution from olivine (*Fig. 1-1 a*).

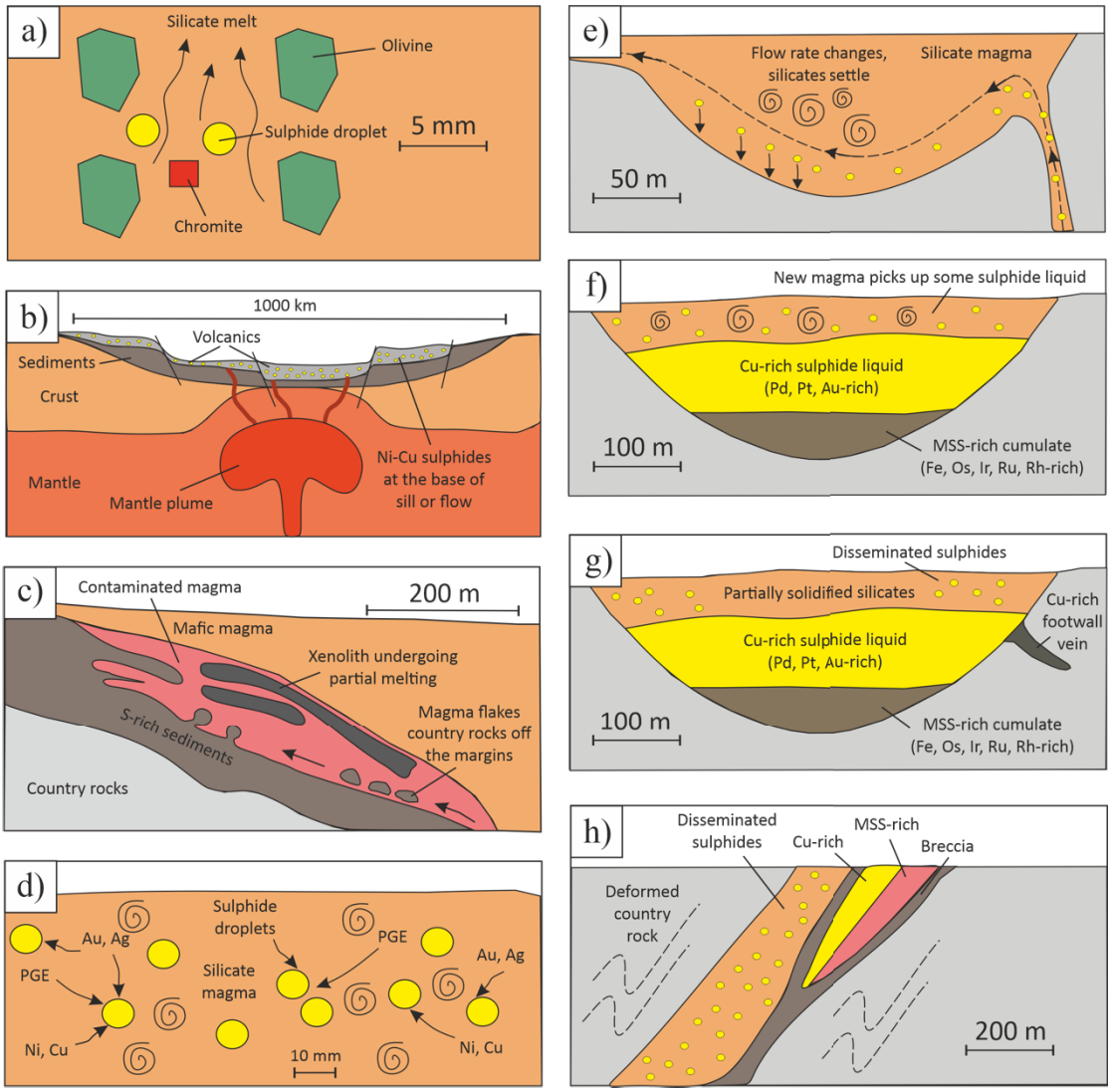

Figure 1-1. Compilation of cartoons illustrating the processes that lead to the formation of magmatic Ni-Cu-(PGE) deposits. **a)** Mantle melting results in the release of Ni from olivine and PGE from sulphides. **b)** Magma ascends to the crust along crust-penetrating faults. **c)** External sulphur is added to the magma from sedimentary country rocks which triggers sulphur saturation and the formation of an immiscible sulphide liquid. **d)** Sulphide droplets collect chalcophile metals. **e)** Sulphide droplets are carried by the magma until a decrease in velocity allows them to settle at the base of the intrusion or flow. **f)** Crystal fractionation of the sulphide liquid produces monosulphide solid solution (*mss*) and Cu-rich residual liquid, intermediate solid solution (*iss*). Injections of new magma may entrain Cu sulphide liquid and moved to new collection sites. **g)** Cu-rich liquid may be injected into the footwall as Cu-rich veins. Silicates begin to solidify. **h)** Post-magmatic deformation may displace sulphides from their parent body, potentially as breccias. *Modified after Barnes & Lightfoot (2005).*

For the magma to become enriched in Cu and PGE, sulphides in the mantle must be dissolved into the melt. Once all of the available sulphides in the mantle have been dissolved, Pt, Pd and Cu reach their maximum concentrations in sulphur undersaturated conditions (Naldrett, 2010b). Assuming that the mantle contains 200 ppm sulphur, a sulphur undersaturated melt could be generated in the mantle to form basaltic or komatiitic magmas with ~20% melting (Naldrett, 2004 and references therein). Smaller amounts of melting may be required in oxidised magmas in which S solubility is much higher (Jugo, et al., 2005). These metals will be subsequently diluted with further melting. However, as olivine contains high Ni, the Ni content in the melt will continue to grow as melting degree increases.

Therefore, if a large, high grade deposit is to form, a large amount of the mantle must undergo high degrees of partial melting. This explains why komatiite-related sulphide deposits generally have high Ni grades, but relatively low Cu and PGE grades as by-products. Favourable tectonomagmatic conditions for this are typically associated with mantle plume events, which produce high degrees of partial melting at high temperatures (*Fig 1-1 b*).

Transport

In order to form a large deposit whilst preserving the amount of Ni in the magma, the magma needs to ascend through the crust with minimal olivine crystallisation and sulphide segregation. This is because Ni will continuously decrease as olivine crystallises and is removed from the magma, although a small amount of crystallised olivine is unlikely to substantially affect a deposit's Ni grade (Barnes & Lightfoot, 2005). In contrast, the PGE content of the magma is very sensitive to any removal of sulphides and as little as 2 percent crystallisation in cotectic proportions can lower PGE contents by a factor of 0.003 to 0.13 (Barnes & Lightfoot, 2005).

Basaltic and komatiitic magmas require efficient transport routes extending to the base of the lithosphere (Naldrett, 2010a), such as crustal-scale structures generated or reactivated during transpression (*Fig 1-1 b*). Ideal conditions for magma ascent include those present in plume-related rifting regimes, where the continental crust is thinner and allows magma to travel unimpeded through major structures (Barnes & Lightfoot, 2005). Such lineaments in the crust are found along craton margins as a result of concentrated deformational strain

in these environments (Begg, et al., 2010). This model of transport explains the occurrence of many Ni-Cu sulphide deposits at intracratonic boundaries.

Fertilisation

Mantle magmas need to achieve sulphur saturation during emplacement in order to form an immiscible sulphide liquid, and hence a Ni-Cu sulphide deposit. The magma is initially sulphur undersaturated due to the inverse relationship between S solubility and pressure (Mavrogenes & O'Neill, 1999). Other factors that affect the S solubility of the magma include temperature, FeO and TiO_2 content, oxidation state and mafic vs. felsic components of the melt (Keays, 1995; Naldrett, 2004; Barnes & Lightfoot, 2005). As cooling and fractionation occurs, the S content of the melt will increase as S is not readily incorporated into the crystallising silicate minerals (Irvine, 1975). Although this will ultimately lead to S saturation, in the case of Ni-Cu deposits, isotopic studies have shown that sulphide immiscibility is more likely induced by the introduction of an external S source than by changes in pressure, temperature, oxygen fugacity or silicate content of the magma (Keays & Lightfoot, 2007; Ripley & Li, 2013). Potential crustal sources of S include black shales (e.g. *Kabanga, Pechenga*), paragneisses (e.g. *Voisey's Bay*), BIF (e.g. *Platreef*), felsic volcanic rocks and sulphidic cherts (komatiite-hosted ores) and evaporites (e.g. *Noril'sk*) (Maier & Groves, 2011 and references therein) (*Fig. 1-1 c*).

Enrichment

Once immiscible sulphide droplets have formed from the magma, chalcophile metals are collected by sulphide in proportions relative to their partition coefficients. Metals such as Ni, Cu, Co, Pt, Pd and Au have their normal partitioning behaviour upset by the presence of the sulphide liquid (Keays, 1995), of which the Nernst partition coefficient is the key control. This coefficient measures how readily metals will partition into sulphide liquid or silicate minerals as opposed to a silicate melt (Rollinson, 1993). Ni more readily partitions into sulphide liquid with a partition coefficient of 500-1500, as opposed to olivine with a partition coefficient of 6-29 (Rollinson, 1993). As a result, the removal of dense immiscible sulphide will deplete the magma in nickel more efficiently than the crystallisation of olivine. Similarly, Cu and PGE have much higher partition coefficients for sulphide than silicate minerals, producing a degree of enrichment in the order of Pd > Pt > Cu > Ni based on partition coefficients in a small closed system (Keays, 1995).

Segregation of metal-rich sulphides also depends on the *"R factor"* which is defined as the ratio of silicate melt to sulphide liquid (Campbell & Naldrett, 1979). Low R factor will produce sulphide-rich deposits with relatively low chalcophile metal tenor whereas high R factor will produce sulphide-poor deposits with a much higher chalcophile metal tenor (Naldrett, 2011). Sulphide-rich deposits occur in small, conduit-type intrusions dominated by Ni-Cu, with PGEs normally occurring as by-products (e.g., *Jinchuan*, *Voisey's Bay*, *Pechenga*, *Sakatti*). Sulphide-poor deposits with high R factor occur in large layered intrusions dominated by PGE, with Ni and Cu as by-products (e.g., *Bushveld*, *Great Dyke*, *Stillwater*, *Penikat*) (Naldrett, 2011). The "*N factor*" supplements this with an explanation of situations where sulphides may undergo a zone refining process, either where sulphide droplets settle through the magma from top to bottom (Brügmann, et al., 1993) or where sulphides are located within a dynamic magma conduit system along which new magma flows and interacts with existing sulphides (Naldrett, et al., 1995, 1996). In the case of the latter, sulphides interact with a continuous stream of magma, collect and retain chalcophile metals, leaving the magma depleted in these (Naldrett, 2004) (*Fig. 1-1 d*).

Emplacement

Once a dense, metal-enriched immiscible sulphide melt has formed, it must be concentrated in a structural trap to form an ore deposit (*e.g.* physical depressions in the magma chamber or breaks in the magma conduit). The density of a sulphide liquid varies with composition, from 4.0 g/cm^3 of pure FeS to about 5.0 g/cm^3 of Cu_2S or NiS (Mungall & Su, 2005). In contrast, the density of a silicate magma is in the range of 2.7 to 3 g/cm^3, which allows sulphide liquids to settle unimpeded, except when phenocrysts are present (Naldrett, 2010a).

As a consequence of this density contrast and a drop in velocity, massive and semi-massive sulphides are concentrated at the base of the magma or flow (*Fig. 1-1 e*). This is especially important in cases where olivine and orthopyroxene crystallise to form cumulates which press down on the accumulating sulphides at the base, thus forming an overlying net-textured ore; this is termed the *"billiard-ball model"* by Naldrett (2004). In contrast, disseminated and blebby sulphide textures may be produced if efficient gravity-aided segregation

is hindered by the presence of crystals or inclusions. In some cases, this style of mineralisation can yield high ore grades (*e.g. Norils'k;* Naldrett, et al., 1996a, b), but most commonly produce sub-economic to uneconomic deposits (Franchuk, et al., 2015).

Nourishment

Many disseminated sulphide ores have higher metal tenors than associated massive or matrix sulphides (Barnes & Lightfoot, 2005). This can be explained by the longer interaction time with surrounding magma that disseminated sulphides experience before settling, thus having a higher R/N factor than their massive or matrix textured counterparts. Furthermore, massive sulphides have lower and more variable Pd/Ir ratios than disseminated sulphides, which is thought to be the result of fractionation of the sulphide liquid upon cooling (Barnes, et al., 1997a).

Once segregated, the immiscible sulphide melt will begin to crystallise and fractionate as temperature falls (*Fig 1-1 f, g*). The crystallisation process is controlled by a combination of sulphide mineral phases and solid solution series (Lightfoot, 2017). This produces a range of mineral assemblages, from typical pyrrhotite-pentlandite-chalcopyrite rich ores to pentlandite-millerite-pyrite mineralisation (Naldrett, 2004).

Figure 1-2 illustrates the behaviour of PGEs during the fractionation process of a sulphide droplet. The sulphide liquid typically segregates from a mafic magma at around 1200°C and initially contains dissolved Fe, Ni, Cu, PGEs, Au and semimetals such as As, Te, Bi, and Se (*Fig. 1-2 a*).

The first phase crystallises at 1000°C in the form of monosulphide Fe-Ni-S solid solution (*mss*) (Naldrett, 2004). Ni, IPGE (Ir, Os and Ru) and Rh are compatible into *mss* at this stage and partition into it (*Fig. 1-2 b*) (Fleet, et al., 1993; Li, et al., 1996; Barnes, et al., 1997a; Ballhaus, et al., 2001; Mungall, et al., 2005). The remaining residual liquid becomes enriched in Cu, Pt, Pd, Au and other semimetals (*Fig. 1-2 b*) (Barnes, et al., 1997a).

At around 900ºC, *iss* crystallises from the Cu-rich residual liquid. Pt, Pd and Au, however, are incompatible in *iss* (Peregoedova, 1998) and concentrate into an immiscible semimetal

rich liquid (*Fig. 1-2 c*). The semimetal-rich liquid remains in liquid form after *iss* has crystallised (Helmy, et al., 2007). Pd and Pt have a stronger affinity for Bi and Te than S (Helmy, et al., 2007), resulting in Pd entering *mss* only when the Pd:semimetal ratio is high enough to produce an excess of Pd that cannot be accommodated by the semimetal-rich melt alone (*Fig. 1-2 c*). This may explain the presence of Pd in pentlandite in some ores, although the mechanism and physical conditions for this are still unknown (Holwell & McDonald, 2010). This may also produce Pt-Bi-Te microinclusions within the sulphide phases (Holwell & McDonald, 2010).

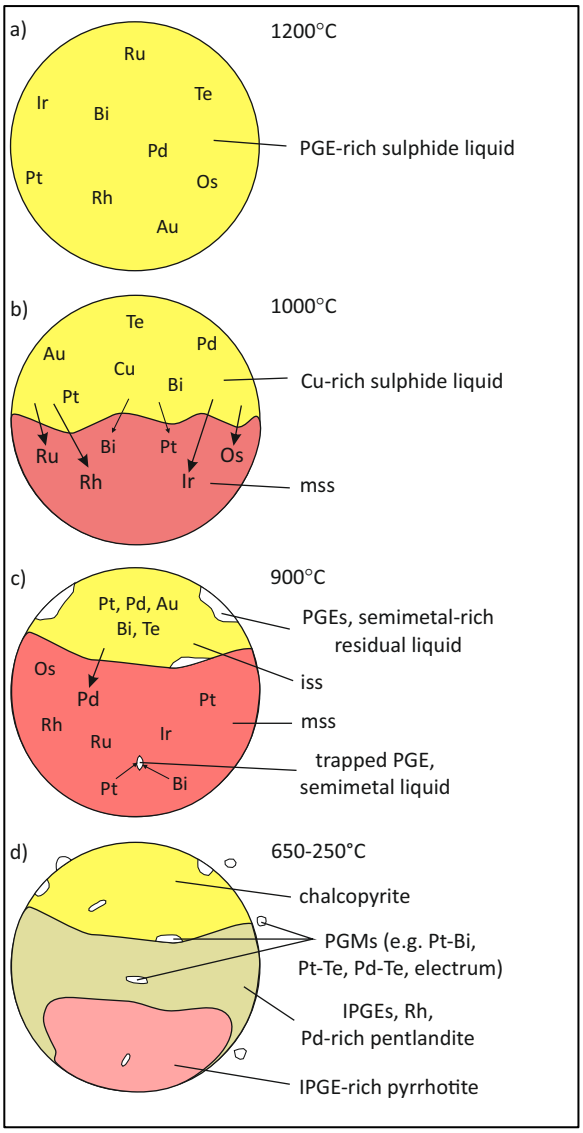

Figure 1-2: Schematic illustration of the behaviour of PGEs within a fractionating sulphide droplet (see text for explanation). *Modified after Holwell & McDonald (2010).*

Finally, at temperatures of 650–200°C, the *mss* recrystallises into pentlandite ($(Fe, Ni)_9S_8$) and pyrrhotite (FeS_{1-x}) (*Fig. 1-2 d*). Both contain IPGEs in solid solution and pentlandite contains Rh and Pd in solid solution, explaining why pentlandite tends to be the principal carrier of Rh in many studies (Holwell & McDonald, 2010 and references therein). The *iss* recrystallises to chalcopyrite ($CuFeS_2$) (Naldrett, 2004) with low PGEs in solid solution and the semimetal-rich liquid crystallises to form platinum group minerals (PGMs) around the margins of sulphide blebs (Cabri & LaFlamme, 1976; Prichard, et al., 2004; Godel, et al., 2007). The precise recrystallisation temperatures are determined by the abundance of sulphur in *mss* (Naldrett, 2004).

Full Maturity

Post-magmatic modification of ores by means of hydrothermal alteration, structural displacement, tectonic deformation and/or metamorphism have the potential to completely reform an ore body, remobilise sulphides and alter the concentrations of metals within sulphides (Lightfoot, et al., 2011b; Farrow & Watkinson, 1997). Since sulphides are able to move in plastic form at relatively low temperatures and pressures, they can be mobilised by *"sulphide kinesis"* along with fragments of country rock, forming sulphide breccias (*Fig. 1-1 h*). At higher temperatures and pressures, sulphides can become completely detached from their parent intrusions and even undergo partial melting, which may result in new fractionation of *mss* and a change in composition of sulphides (Lightfoot, et al., 2011a). Hydrothermal fluids have the potential to remobilise sulphides in economic proportions, as is the case with *Enterprise*, Zambia (Capitrant, et al., 2015) and *Avebury*, Tasmania (Keays & Jowitt, 2013) deposits.

1.1.2 High Tenor Magmatic Ni-Cu-(PGE) Deposits

Some magmatic Ni-Cu-(PGE) deposits have unusually high metal tenors, such as *Noril'sk,* Russia (Naldrett, 2004); *Santa Rita,* Brazil (Barnes, et al., 2011) and Kevitsa (Hanski, et al., 1997). Such deposits may have formed as a consequence of assimilation, or *"cannibalisation"* of early-stage magmatic proto-ores by later magma surge(s), resulting in upgradation and re-precipitation of sulphides downstream (Maier, et al., 1998; Maier & Barnes, 2010).

For example, Li & Ripley (2009) proposed a multi-stage genetic model for the Kharaelakh intrusion of the Noril'sk region which follows this model of enrichment of sulphides via later magma pulses. Firstly, sulphide segregation occurred early in a deep staging chamber where magma was contaminated with granitic crustal material, before rising to erupt as lavas on the surface and producing weakly mineralised intrusions in the crust. The sulphide liquid in the staging chamber was left with low tenors of Ni, Cu and PGE. This PGE-poor sulphide liquid was then upgraded in chalcophile elements by a secondary pulse of magma named the Morongovsky magma. This formed a PGE-rich sulphide liquid which remained in the staging chamber while the magma erupted to form Morongovsky lavas. A third, S-undersaturated pulse of magma entered the chamber from the mantle, progressively re-

dissolving the PGE-rich sulphide liquid in the staging chamber, which produced a new magma that was enriched with PGE. This new enriched magma rose through the upper crust where it interacted with anhydrite-bearing evaporite country rocks, triggering sulphide saturation. An immiscible PGE-rich sulphide liquid was produced, which then settled in traps in the Kharaelakh conduit system to form a high metal tenor sulphide deposit.

Similarly, the unusually high Ni-tenor of Kevitsa ores has been attributed to cannibalisation of komatiitic proto-ores by the Kevitsa basaltic magma, which created an enriched zone of entrained and dissolved sulphides that produced the high Ni contents in the Ni-PGE ores of Kevitsa (Maier & Groves, 2011; Yang, et al., 2013).

Alternatively, metal tenors in magmatic Ni-Cu-(PGE) deposits may be enriched by post-magmatic processes such as hydrothermal alteration, metamorphism and serpentinisation. Although nickel and PGEs usually have low solubilities, they can become more readily soluble in acidic fluids as bisulphide and chloride complexes in reducing and oxidising conditions, respectively (Barnes & Liu, 2012). There are many examples globally that feature modification of Ni-Cu and/or PGE-rich ore as a result of hydrothermal remobilisation, such as the Fraser, Strathcona and West McCreedy deposits and the Barnet property within the Sudbury Igneous Complex, Canada (Farrow & Watkinson, 1997); and ore bodies around the Kambalda Dome in Western Australia (Lesher & Keays, 1984; Heath, et al., 2001). Regarding Kevitsa, the role of fluid enrichment and remobilisation of metals has been considered as a contributing factor of high metal tenor by some authors (Hanski, et al., 1997; Mutanen, 1997; Gervilla & Kojonen, 2002; Standing, et al., 2009).

1.2 Aims of the Study

The Kevitsa Ni-Cu-(PGE) deposit (67°41’51.09″N, 26°58’18.35″E), also referred to as the Keivitsansarvi deposit in the literature (Gervilla & Kojonen, 2002), is located 140 km north of the Arctic Circle in Finnish Lapland. Dated at 2058 ± 4 Ma (Mutanen & Huhma, 2001), the Kevitsa deposit is found within the Central Lapland Greenstone Belt (CLGB) and is hosted by Palaeoproterozoic volcano-sedimentary sequences, including komatiites and black schists. The deposit has been the subject of numerous studies, providing detail on the

geometry, structural controls, petrology, ore compositional variations, effects and extent of hydrothermal alteration and models of petrogenesis (Hanski, et al., 1997; Mutanen, 1997; Mutanen & Huhma, 2001; Gervilla & Kojonen, 2002; Grinenko, et al., 2003; Yang, et al., 2013; Le Vaillant, et al., 2016; Santaguida, et al., 2015; Luolavirta, et al., 2018, 2018a, b)**.**

The economic mineralisation consists of disseminated sulphides in the centre of the ultramafic lower unit of the intrusion and features two main types: *normal ore* and *Ni-PGE ore.* The normal ore type represents the bulk of the economic resource (90%) and yields average Ni and Cu ore grades of 0.3 and 0.42 wt.% respectively. The Ni-PGE ore has higher and more variable Ni grades, lower Cu grades and extreme Ni tenors up to 40%. The Ni-PGE ore also contains high PGE, from >1 ppm to 26.75 ppm (Gervilla, et al., 2004), much higher than the normal ores. It is this unusually high tenor Ni-PGE ore that makes Kevitsa unique and somewhat enigmatic in origin. Although genetic models have been proposed for the Kevitsa deposit (Hanski, et al., 1997; Mutanen, 1997; Gervilla & Kojonen, 2002; Yang, et al., 2013; Le Vaillant, et al., 2016; Luolavirta, et al., 2018a, b, c) and other similar deposits (Li, et al., 2009; Maier & Groves, 2011), the origin of these different ore types remains fairly controversial.

The aim of this study is to examine the distribution of trace elements, including PGE, within base metal sulphides (BMS) to better understand the petrogenesis of the Kevitsa deposit, and provide insight into the genesis of high metal tenor magmatic Ni-Cu-(PGE) deposits. By measuring PGE distribution in BMS from the different ore types, in particular the atypical assemblage of the Ni-PGE ore, this study can either support or refute the current models of formation and consider effects of post-magmatic processes (see *Section 1.1.2*). The presence of fresh, primary millerite in the Ni-PGE ore (Yang, et al., 2013) also presents an opportunity to examine the behaviour of trace elements in relation to this mineral, which at present is not well understood.

2 GEOLOGICAL BACKGROUND

An overview of the regional geology and local geology of the Kevitsa Ni-Cu-(PGE) deposit is provided in this section, with a detailed description of the deposit's ore types, mineralogy and various genetic concepts.

2.1 Geology of Finland

The bedrock of Finland is comprised of mainly Precambrian rocks belonging to the Fennoscandian Shield (*Fig. 2-1 A*). Exposures of the Fennoscandian Shield are found throughout Finland, but also in Sweden and north-western Russia (Lehtinen, et al., 2005), representing the oldest exposed rocks in Europe together with the Ukrainian Shield (Hanski, 2015). The oldest known occurrences are the Siurua trondhjemitic gneisses, dated at ~3.5 Ga in the Mesoarchaean (Mutanen & Huhma, 2003; Lauri, et al., 2011), and the most significant younger formations are 1.65-1.54 Ga rapakivi granites (Vaasjoki, et al., 2005).

Three large-scale crustal units divide the Precambrian bedrock in the central and eastern parts of the shield: (1) Archaean basement (3.5-2.5 Ga), (2) overlying Palaeoproterozoic volcano-sedimentary sequences (2.5-1.9 Ga), and (3) the Svecofennian orogenic belt (1.93-1.8 Ga) (Vaasjoki, et al., 2005; Hanski, 2015).

The Archaean basement occurs in the northern and eastern parts of the Fennoscandian Shield, either exposed or hidden beneath Palaeoproterozoic cover. The Archaean crust in this area consists of two main crustal domains, the Karelian and Kola cratons (*Fig. 2-1 A*), which are thought to have collided with one another during the Palaeoproterozoic Lapland-Kola orogeny (Lahtinen, et al., 2005), separated by a belt of Belomorian rocks and the Lapland Granulite Belt (LGB) (Lehtinen, et al., 2005) (*Fig. 2-1 A*). The basement is composed of typical Archaean granitoid-greenstone terranes, however recent research has revealed a complex lithology and tectonomagmatic history, including an array of different magmatic suites within the Karelian craton (Mikkola, et al., 2011; Hölttä, et al., 2012b). Amongst supracrustal belts surrounded by broadly tonalitic to granodioritic granitoids and migmatites (Vaasjoki, et al., 2005) (*Fig. 2-1 B*), the Archaean basement consists of paragneiss complexes derived from immature greywackes (Kontinen, et al., 2007) and blocks of

mafic to felsic high grade granulites. These terranes experienced a major collisional orogeny at around 2.73-2.67 Ga, linked to the assembly of the Archean supercontinent Kenorland. A period of stabilisation at around 2.6 Ma was followed by subsequent rifting events at the Archaean-Proterozoic transition (Lahtinen, 2012; Hanski, 2015).

Rifting provided a substrate onto which continental margin sediments and volcanic rocks were deposited, forming the Palaeoproterozoic *Karelian formations* (Hanski, 2015) (shown in *Fig. 2-1 B* as two supracrustal groups aged between 2.50 and 1.95 Ga). The Karelian formations record geological evolution of about 600 Ma, and feature episodes of sporadic continental mafic magmatism between 2.5-1.97 Ga as well as several generations of mafic dyke swarms in the Archaean basement (Vuollo & Huhma, 2005). Emplacement of layered gabbro-norite intrusions occurred ~2.5-2.44 Ga, the most significant examples of which include the Tornio-Näränkävaara belt (*Fig. 2-1* B) and the Koitelainen and Akanvaara intrusions of central Finnish Lapland (Mutanen, 1997; Hanski, et al., 2001b; Iljina & Hanski, 2005). Starting from about 2.45 Ga, multiple generations of mantle derived mafic-ultramafic lavas erupt onto Archaean basement and begin forming the Central Lapland Greenstone Belt (CLGB, described in more detail in *Section 2.2*) (Hanski & Huhma, 2005) which hosts the ~2.06 Ga Kevitsa intrusion.

The Svecofennian orogenic belt is present in central and southern parts of Finland (Lahtinen, et al., 2005) and typically comprise calc-alkaline volcanic and intrusive rocks resulting from arc magmatism and associated accretionary prism sediments including turbiditic greywackes and mudrocks (Kähkönen, 2005). Granitic magmatism occurred at this time (1.95-1.77 Ga) creating several intrusion complexes such as the Central Finland Granitoid Complex (CFGC) (Peltonen, 2005b) (*Fig. 2-1 B*). There are also a number of mafic-ultramafic intrusions formed during this period, located in the Kotalahti and Vammala belts which host significant Ni-Cu sulphide mineralisation (Papunen, 1986, 1989; Makkonen et al., 2008; 2017). This period records two major orogenies which occurred between 1.91-1.90 Ga and 1.83-1.81 Ga (Kähkönen, 2005).

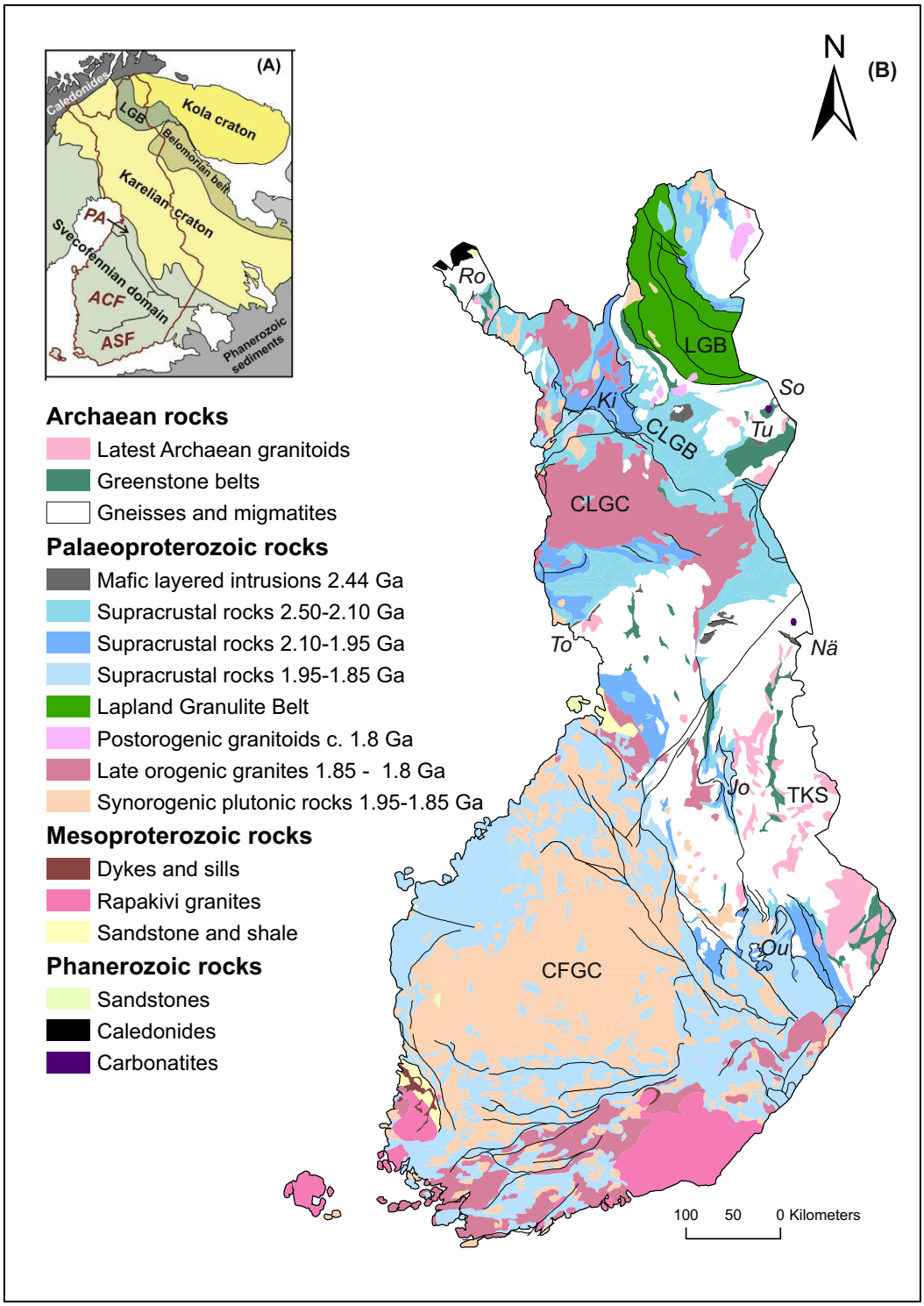

Figure 2-1: (A) Main bedrock units of the Fennoscandian Shield. *Modified after Hanski (2015).* **(B)** Simplified geological map of Finland. *After Hanski (2015), data from GTK's Suomen Kallioperä 1:5 000 000 (URL-1).* **(A)** abbreviations: PA = Primitive arc complex of central Finland, ACF = Accretionary arc complex of central and western Finland, ASF = Accretionary arc complex of southern Finland, LGB = Lapland Granulite Belt. **(B)** abbreviations: CFGC = Central Finland Granitoid Complex, CLGB = Central Lapland Greenstone Belt, CLGC = Central Lapland Granitoid Complex, Jo = Jormua ophiolite, Ki = Kittilä greenstone area, Nä = Näränkävaara, Ou = Outokumpu ophiolite, Ro = Rommaeno complex, So = Sokli carbonatite, TKS = Tipasjärvi-Kuhmo-Suomussalmi belt, To = Tornio, Tu = Tulppio.

2.2 The Central Lapland Greenstone Belt (CLGB)

The Palaeoproterozoic Central Lapland Greenstone Belt (CLGB) forms the largest greenstone belt in the Fennoscandian Shield (Hanski & Huhma, 2005). The CLGB records depositional evolution over almost 600 Ma, beginning with mantle-plume related eruptions of komatiitic to rhyolitic lavas on Archaean cratonic basement at ~2.54 Ga and ending soon after ~1.88 Ga with synorogenic felsic plutonism and minor volcanism (Hanski & Huhma, 2005). The CLGB is exposed over an area 100 km x 200 km and runs as an almost uninterrupted zone from northern Norway through central Finnish Lapland, where it reaches both the western and eastern borders of Finland (*Fig. 2-2*). In Finland, the CLGB runs parallel to and plunges beneath the south-western contact of the Lapland Granulite Belt (LGB) and is bordered by Archaean granite-gneiss terranes in the west and east. The south-western rocks of the CLGB have been affected by the Svecofennian orogeny whereas the north-eastern part has experienced thrusting of the LGB.

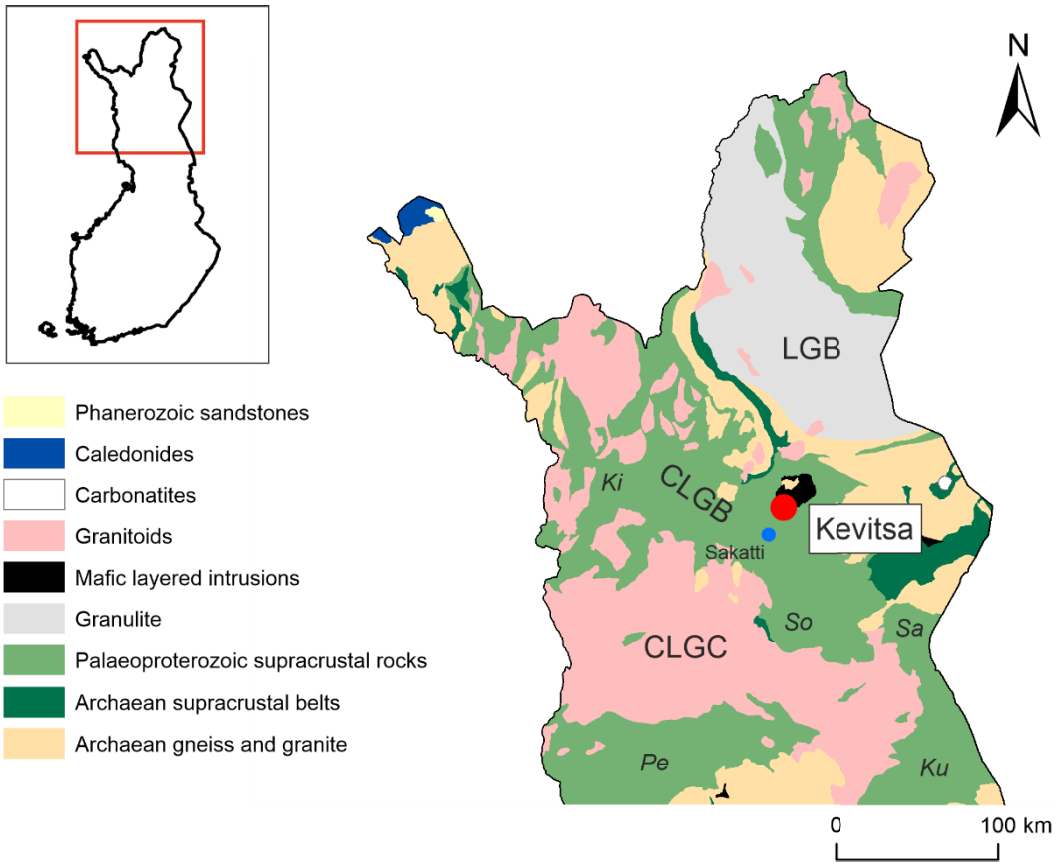

Figure 2-2: Simplified geological map of northern Finland showing the spatial distribution of the CLGB amongst other major units. Large red circle shows the location of the Kevitsa deposit, smaller blue circle shows the Sakatti deposit. Ki = Kittilä greenstone area, Ku = Kuusamo schist belt, Pe = Peräpohja schist belt, Sa = Salla greenstone area, So = Sodankylä schist area. *After Hanski & Huhma (2005), data from GTK's Suomen Kallioperä 1:5 000 000 (URL-1).*

This acts as a foreland fold-and-thrust belt to two nearly coeval convergent systems with opposing polarity (Sorjonen-Ward, et al., 1997). Later tectonic activation generated significant shear zones, including the *Sirkka-line* at the southern margin of the Kittilä greenstone area (Hanski & Huhma, 2005). The CLGB is characterised by a complex pattern of metamorphic zonation, from greenschist facies in the core zone of the belt, to amphibolite facies towards the CLGC. Middle-amphibolite facies is prevalent in the east, whereas upper amphibolite and granulite facies takes over towards the north-east (Hanski & Huhma, 2005).

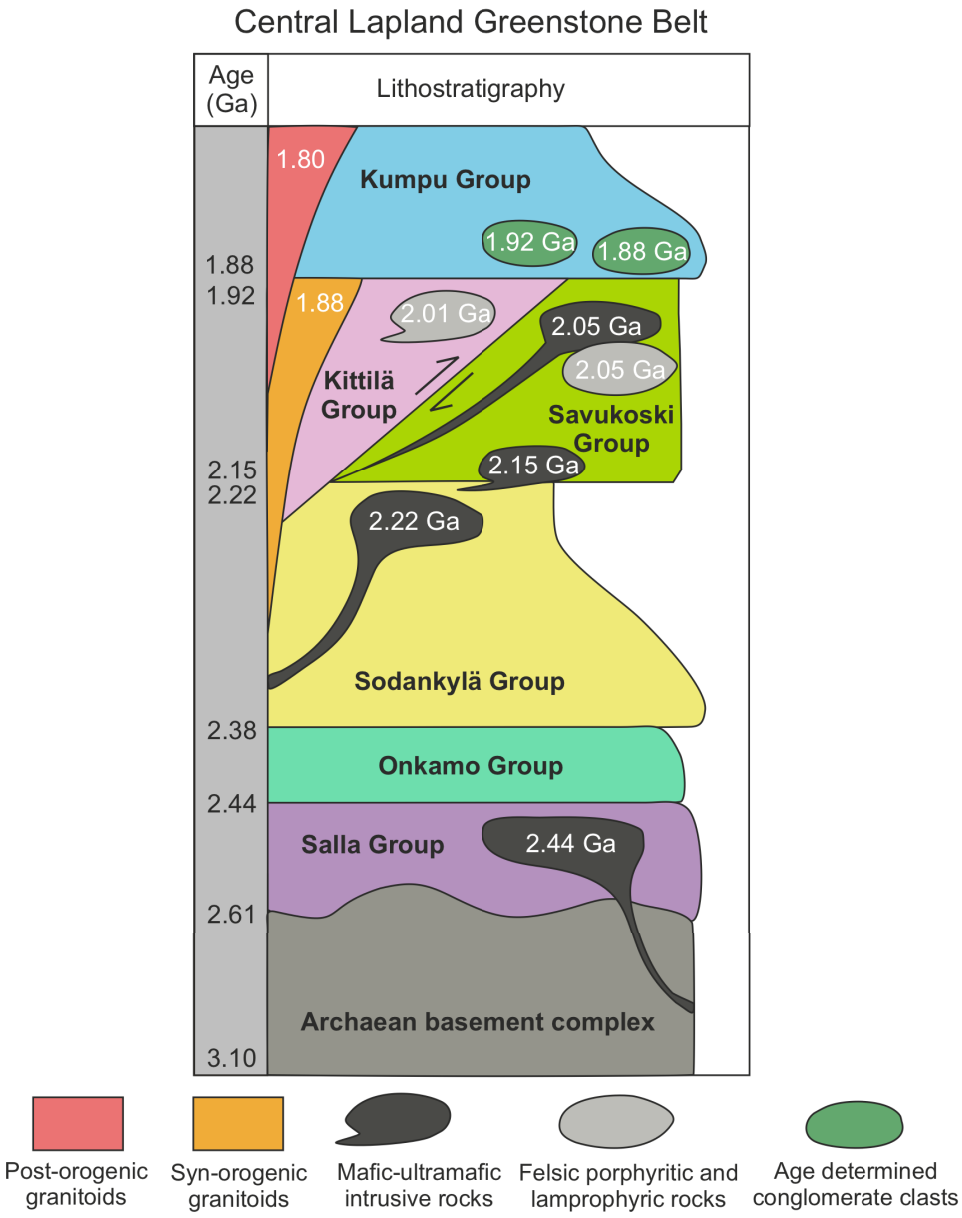

Figure 2-3: Simplified stratigraphic column of the CLGB showing main lithostratigraphic groups, intrusive features and conglomerate clasts. Magmatic intrusive ages from Huhma, et al. (2018). *After Hanski, et al. (2001) and Köykkä, et al. (2019).*

The rocks of the CLGB have been assigned to seven lithostratigraphic groups, shown in *Figure 2-3*, from oldest to youngest: *Salla, Onkamo, Sodankylä, Savukoski, Kittilä, Lainio* and *Kumpu*, each with their own subdivisions (Lehtonen, et al., 1998; Hanski & Huhma, 2005; Hanski, et al., 2011). The lowermost units, the *Salla* and *Onkamo* Groups, aged ~2.45 Ga, occur in the south-east and occupy a combined area of around 40 km x 100 km (Hanski & Huhma, 2005). Both are comprised of subaerial or shallow-water komatiitic to rhyolitic volcanic rocks. The volcanic rocks generally become more evolved higher up in the stratigraphy and retain original volcanic structures, although primary minerals have been exposed to greenschist metamorphism (Hanski & Huhma, 2005). Both groups show a clear geochemical signature of crustal contamination.

The *Onkamo* Group is overlain by the *Sodankylä* Group epiclastic sedimentary sequence (*Fig. 2-3*). These sediments consist of quartzites and mica schists, accompanied by minor carbonates and mafic metavolcanic rocks (Hanski & Huhma, 2005). This lithostratigraphic group represents a widening depositional basin featuring structures such as cross-bedding, graded bedding, and desiccation cracks typical of a tidal environment (Nikula, 1988).

The *Savukoski* Group, represents the deepening of the depositional basin, with the first occurrences of graphite- and sulphide-bearing black schists amongst phyllites and mafic tuffites (Hanski & Huhma, 2005). The mafic and tuff interbeds present important key horizons for geophysical mapping due to their magnetism (Lehtonen, et al., 1998; Hanski & Huhma, 2005). The *Savukoski* Group also hosts crosscutting mafic intrusive bodies, including the Kevitsa intrusion (Rastas, et al., 2001; Hanski & Huhma, 2005).

The *Kittilä* Group, often called the Kittilä greenstone area (*Fig. 2-3*), covers an area of over 2600 km^2 and represents one of the largest accumulations of mafic metavolcanic rocks in the Fennoscandian Shield. The *Kittilä* Group consist of various submarine mafic metavolcanic units, sheeted dyke complexes and minor felsic rocks. Although dominated by metavolcanic rocks, there are also sedimentary interbeds of greywackes, phyllites, graphite- and sulphide-bearing schists, and banded iron formations (BIFs) (Hanski & Huhma, 2005). The *Kittilä* Group developed at 2.0 Ga during the opening of the oceanic basin.

The *Lainio* and *Kumpu* Groups were deposited following a depositional hiatus (Hackman, 1927) and make up 200-2000 m of meta-arkoses, quartzites, polymictic conglomerates and siltstones. Sedimentary features of these units suggest deposition in a fluvial environment, typical of alluvial fans and braided rivers (Kortelainen, 1983; Nikula, 1988).

The CLGB is highly prospective for mineralisation, namely Ni-Cu-(PGE) (Papunen, 1986, 1989; Makkonen, et al., 2017) and orogenic gold deposits (Eilu, et al., 2007; Eilu, et al., 2012). Most economic ore deposits of the CLGB formed exclusively within 2.06-1.78 Ga, beginning with the emplacement of mafic intrusions around 2.06 Ga. Rifting during this period was the mechanism whereby Ni-Cu-(PGE) deposits formed, such as those found at Kevitsa (Weihed, et al., 2005), and perhaps Sakatti (Brownscombe, et al., 2015; Makkonen, et al., 2017).

2.3 The Kevitsa Ni-Cu-(PGE) Deposit

The Kevitsa mine is Europe's most recent nickel mine, with a pre-mine resource of 274.8 Mt @ 0.30 % Ni, 0.41 % Cu, 0.014 % Co, 0.11ppm Au, 0.15 ppm Pd and 0.2 ppm Pt (First Quantum Minerals Ltd., 2011). The approximate mine life will be over 20 years after plans for expansion to accelerate production rates (Santaguida, et al., 2015). First discovered in 1987 by the Geological Survey of Finland (GTK), the deposit has since been the subject of extensive research, from Mutanen (1997) providing the first comprehensive studies, to projects relating to many of the deposit's unique characteristics, i.e. PGE mineralogy (Gervilla & Kojonen, 2002), radiogenic and stable isotope characteristics of the ore types (Hanski et al. 1997; Grinenko, et al., 2003), effects of hydrothermal alteration on metal contents (Le Vaillant, et al., 2016), structural geometry with the use of 3D geophysical models (Koivisto, et al., 2015), and origin of enigmatic dunitic rocks (Luolavirta, et al., 2018a).

The Kevitsa deposit is a large (237 Mt), low grade, disseminated Ni-Cu-(PGE) sulphide ore body within a mafic-ultramafic intrusion (Santaguida, et al., 2015). A detailed description of the geology of the Kevitsa deposit is provided in *Section 2.3.2*. The 2.058 Ga Kevitsa intrusion (Mutanen, 1997; Mutanen & Huhma, 2001) is located in the CLGB and is

part of a suite of medium to small sized mafic-ultramafic intrusions in the area. It should be noted that the intrusion is located in proximity to the newly discovered Sakatti intrusion, hosting the Ni-Cu-(PGE) Sakatti deposit (Ahtola, et al., 2012) (*Fig. 2-2*). The Sakatti deposit is the largest high-grade nickel sulphide discovery in Europe (Coppard, et al., 2013). The Kevitsa deposit features several peculiarities, including the presence of mineralisation in the central part of the ultramafic section of the intrusion rather than at the base, as is typical of magmatic sulphide deposits (Barnes & Lightfoot, 2005 and references therein). The mineralisation is also characterised by an unusually wide variety of metal contents within sulphides, with Ni tenor ranging from ~2 wt.% to as high as 40 wt.% (Mutanen, 1997; Yang, et al., 2013). The composition of these sulphides at trace element level provides the scope of investigation for this study.

2.3.1 History

In 1987, the Kevitsa Ni-Cu-(PGE) deposit was discovered by GTK after a drilling campaign to investigate a glacial till geochemical anomaly following the findings of outcropping peridotite containing pyrrhotite. However, low metal grades classified the deposit as uneconomic. Subsequent exploration programs by GTK, who drilled 278 holes totalling 32,845 metres (Mutanen, 1997) and Outokumpu Oy, who drilled 15 holes totalling 2200 metres, did not improve the economic outlook of the deposit. Outokumpu Oy reported mineral reserves of 87 Mt @ 0.25% Ni, 0.39% Cu, 0.6 g/t PGM+Au and 0.015% Co (Kojonen, et al., 2008), yet the deposit was not economic at the time.

The Scandinavian Gold Prospecting company acquired the mineral rights to the Kevitsa deposit in 2000 and conducted further exploration and metallurgical studies. First Quantum Minerals Ltd. (FQML) acquired the deposit in 2008 and a mine development decision was made in 2009. FQML initiated a comprehensive drilling campaign to confirm previous results and define the previous resource model (Santaguida, et al., 2015). The updated mineral reserve, along with improved metal prices encouraged the development of the Kevitsa Ni-Cu-(PGE) mine. In March 2011, FQML published its second NI 43-101 compliant technical report which showed a significant increase in mineral resource and reserves compared to calculations made in 2009 (Lappalainen & White, 2010). Mine production began in 2012 and has a published combined resource of 166 Mt @ 0.22% Ni, 0.35% Cu, 0.13 Pt, and

0.08 g/t Pd (Luolavirta, et al., 2018b) with Ni grades up to around 0.6%. The mine has been operated by Boliden Mineral AB since mid-2016.

2.3.2 Geology

The Kevitsa mafic-ultramafic intrusion is a funnel-shaped body occupying a surface area of around 16 km^2, of which 6.4 km^2 is made up of ultramafic rocks (Mutanen, 1997). The intrusion consists of a 1.5 km-thick ultramafic lower section, overlain by >500 metres of gabbroic rocks with a few tens of metres of granophyre at the top (Mutanen, 1997).

A large dunitic body outcrops in the middle of the intrusion (Luolavirta, et al., 2018b) named the *Central Dunite*. Dunitic cumulates, named the *Kevitsa Dunite*, also occur within olivine pyroxenites in the ore deposit area, in addition to small, cm-scale fragments of recrystallised ultramafic rocks scattered around the ore-bearing area of the intrusion (*Fig. 2-6*).

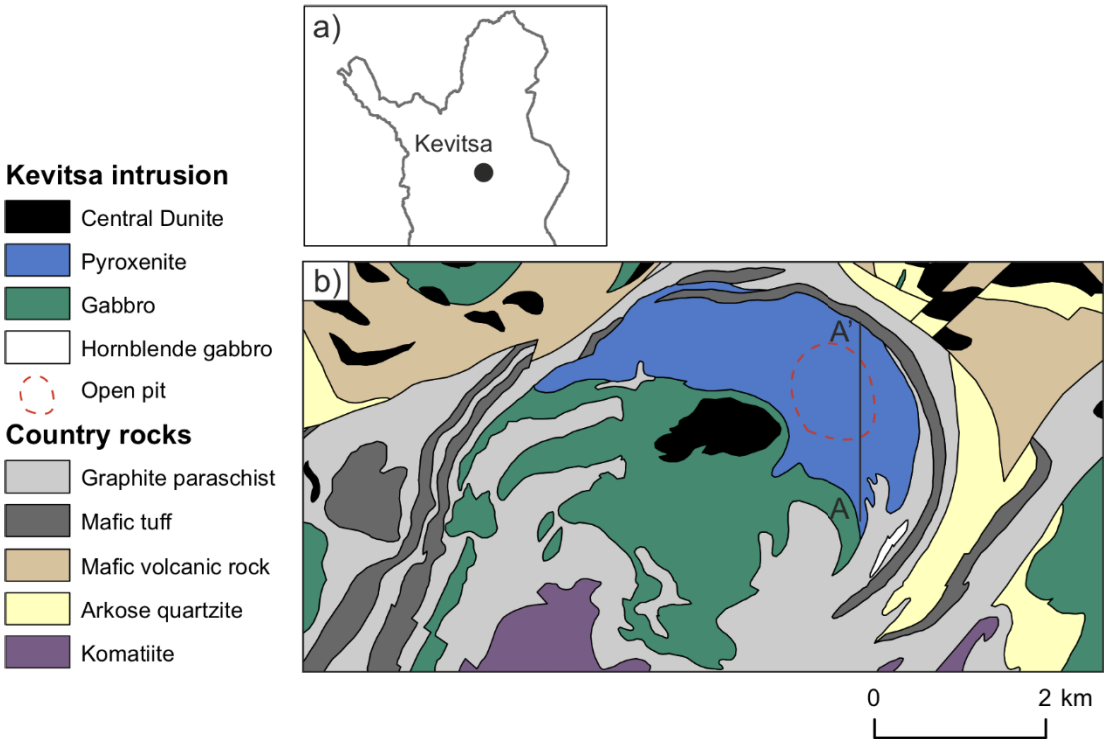

Figure 2-4: a) Location of the Kevitsa intrusion, northern Finland. *Modified after Hanski et al. (2001).* **b)** Simplified geological map of the Kevitsa intrusion, showing the approximate location of the Kevitsa Ni-Cu-(PGE) deposit by the outline of the open pit. A'-A cross section illustrated in *Figure 2-4*. *After Luolavirta et al. (2018b), data from GTK's Kallioperä 1:200 000 (URL-2).*

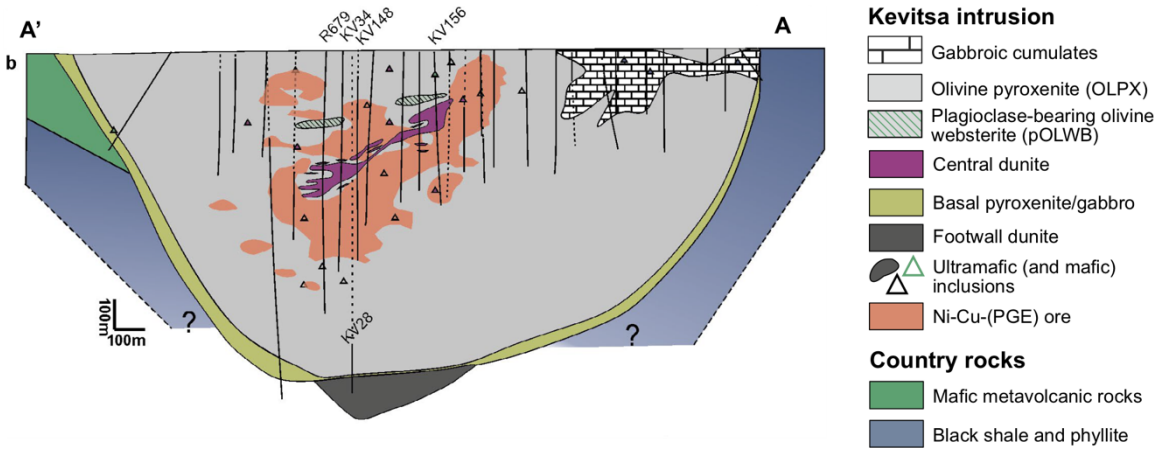

Figure 2-5: S-N cross section showing main lithological units of the Kevitsa intrusion, country rocks and outline of Ni-Cu-(PGE) ore. *After Luolavirta (2018c)*.

The dunite has been found to extend as far as below the Kevitsa intrusion (shown in *Fig. 2-5* as *Footwall dunite)* (Koivisto, et al., 2015; Luolavirta, et al., 2018a).

The Kevitsa magma was emplaced into pelitic metasediments and metavolcanic rocks of the *Savukoski* Group which comprise phyllites, graphitic black shales and mafic and ultramafic volcanic lava flows and tuffs that are locally recrystallised to a hornfels aureole (Lehtonen, et al., 1998). Komatiites of the *Savukoski* Group have yielded a Sm-Nd age of 2056 ± 25 Ma (Hanski, et al., 2001b), similar to that of the Kevitsa intrusion.

2.3.2.1 Magmatic Units and Rock Types

The Ultramafic Zone

The ultramafic zone overlies the basal *marginal chill zone*, a variably thick (a few metres to >50 m) unit of microgabbros and quartz-rich pyroxenites (Mutanen, 1997). The ultramafic zone is dominated by fairly uniform olivine pyroxenites (OLPX) (shown in *Fig. 2-6* and *2-8 b*) with modal mineralogy ranging from olivine websterites to olivine clinopyroxenites. There is some local development of cyclic units, but overall the ultramafic unit lacks obvious lithological layering (Santaguida, et al., 2015). The zone is thickest (up to 2 km) in the north-east of the intrusion, where the ore deposit is located.

Olivine websterite (OLWB) (shown in *Fig. 2-6* and *2-8 a*) is the dominant rock type and host rock for the sulphide mineralisation. It is composed of about 20% olivine, 70% clinopyroxene, and over 5% oikocrystic orthopyroxene (Santaguida, et al., 2015). Plagioclase, magnetite, sulphides and apatite occur as common accessory minerals.

Plagioclase-bearing olivine websterites (pOLWB) (*Fig. 2-8 c*) and associated microgabbros (*Fig. 2-8 b*) occur within the ore-bearing domain where they form distinct, discontinuous zones within the OLWB (*Fig. 2-6*). The pOLWB show orthocumulate textures with plagioclase (>10%) as an intercumulus phase. Orthopyroxene oikocrysts are more abundant (15-25%) whereas olivine is less abundant (<15%) than in the OLWB (Santaguida, et al., 2015). Contacts between OLWB and pOLWB tend to be diffuse but may appear sharp locally. In some places, marker horizons of magmatic layering may be visible within the pOLWB, although they are mostly discontinuous and difficult to trace beyond a few hundred metres. pOLWBs are generally weakly mineralised and do not occur outside of the ore-bearing part of the Kevitsa intrusion. The uppermost ultramafic cumulate unit are composed of pyroxenites containing <5% olivine, with a gradational contact with the OLWB.

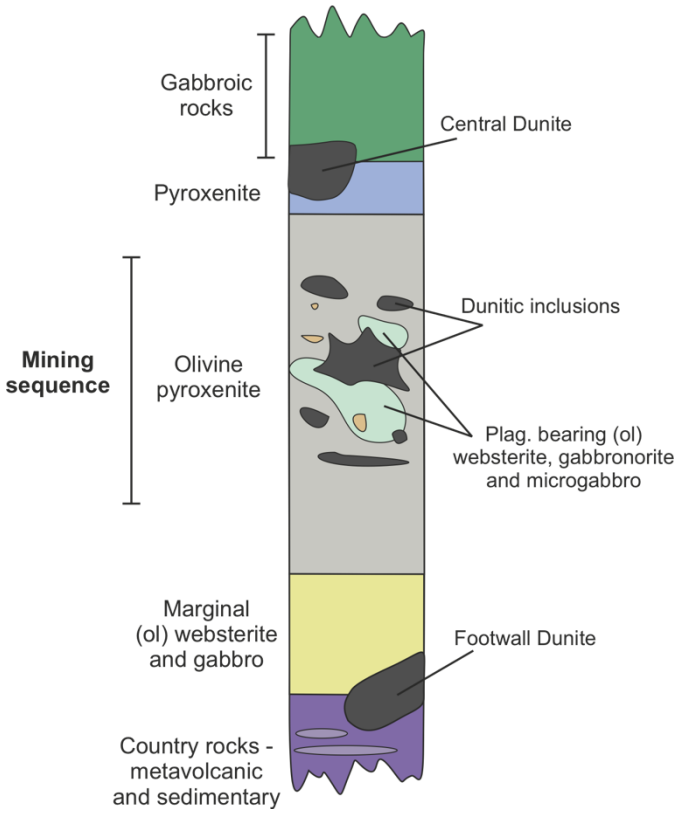

Figure 2-6: Simplified stratigraphic column of the Kevitsa intrusion showing main lithological units and the relative location of inclusions.

The intrusion contains peculiar olivine-rich lenses (>50% olivine), termed *dunite* in mine terminology, although they are lherzolitic to wehrlitic in composition (Santaguida, et al., 2015). In addition, a large body of dunitic rock crops out in the middle of the intrusion, termed the *Central Dunite* (*Fig. 2-4, 2-5, 2-6*). This has been interpreted as a conduit to picritic volcanic rocks of the *Savukoski* Group (Luolavirta, et al., 2018a). Large irregular rafts of these dunitic cumulates occur as clasts throughout the ore-bearing domain. Komatiitic xenoliths are also widespread within the Kevitsa deposit (*Fig. 2-7*) (Mutanen, 1997; Yang, et al. 2013; Luolavirta, et al., 2018a). Pelitic sedimentary xenoliths occur at and near the basal margin of the intrusion (Gervilla & Kojonen, 2002).

Figure 2-7: Photograph of Kevitsa drill core showing ultramafic/mafic xenoliths.

The Gabbroic Zone

The gabbroic zone is ~500 m thick and overlies the ultramafic cumulates (*Fig. 2-6*) (Mutanen, 1997). The rocks are compositionally gabbros, olivine gabbros and gabbronorites, with plagioclase as the dominant mineral (shown in *Fig. 2-8 e*). The gabbros also contain clinopyroxene, olivine and accessory apatite, magnetite and ilmenite (Santaguida, et al., 2015). Visible layering is uncommon and the internal structure is not well under-

stood. Prospective Cu-Au mineralisation occurs along the gabbroic margins, but the gabbros are otherwise devoid of sulphide minerals with the exception of pyrite (Santaguida, et al., 2015).

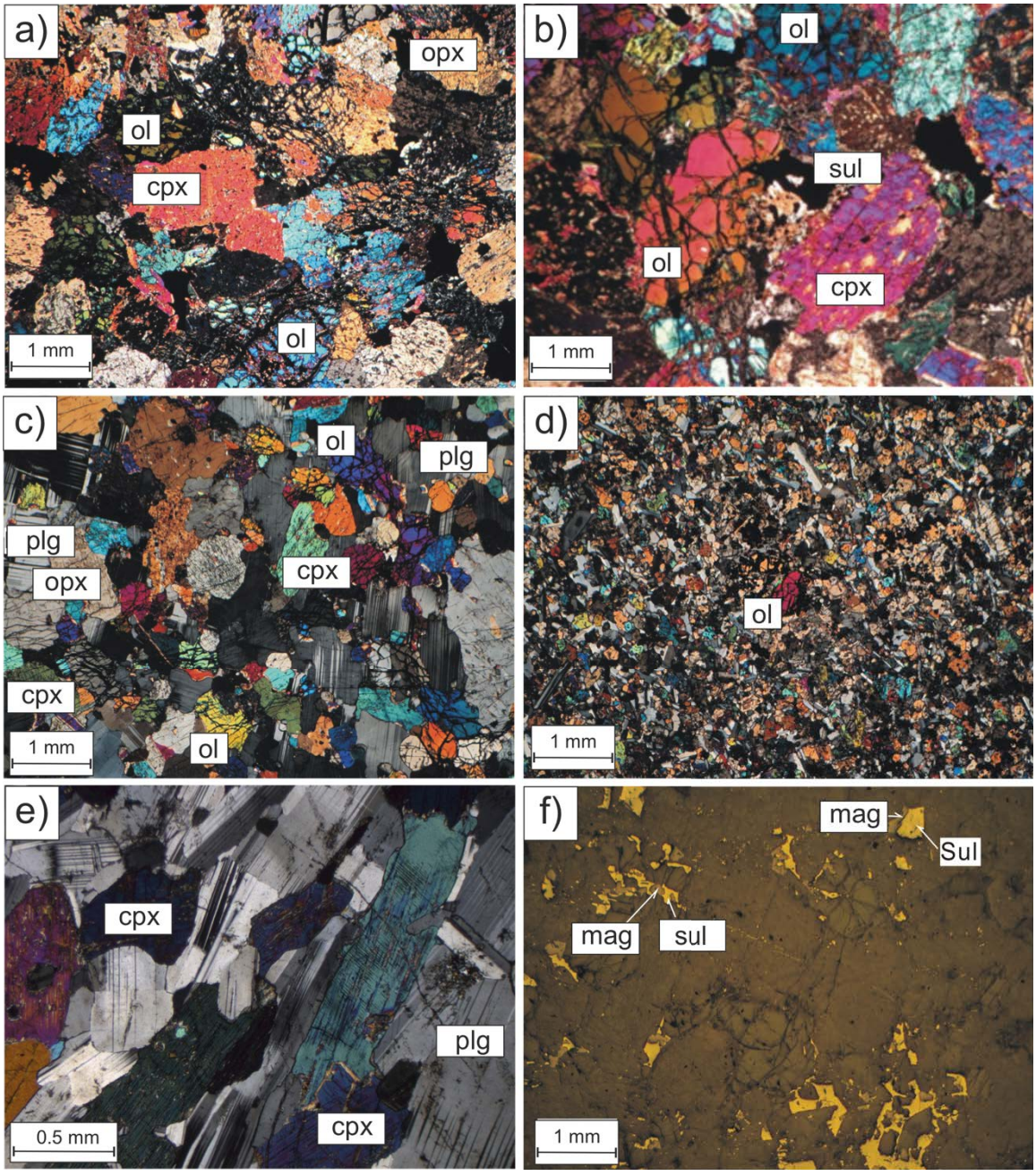

Figure 2-8: Photomicrographs of rock types found in the Kevitsa intrusion. **a)** Olivine websterite, **b)** Olivine pyroxenite, *after Yang, et al. (2013)*, **c)** Plagioclase-bearing olivine websterite, **d)** Microgabbro, **e)** Gabbro, **f)** Texture of sulphides in olivine websterite.

Granophyre

According to Mutanen (1997), the uppermost magmatic unit of the intrusion is made up of <20 m thick granophyre, composed of plagioclase, quartz and secondary hornblende. However, these granophyres have not been encountered by subsequent exploration drilling nor mining operations. Several tens of metres of albitised gabbros and dykes have been found along the southern margin (Santaguida, et al., 2015), although the lack of mineralisation in these units has not yet prompted any in-depth study.

2.3.2.2 Hydrothermal Alteration

The Kevitsa intrusion and surrounding greenstone sequence were metamorphosed and hydrothermally altered during regional greenschist facies metamorphism (Mutanen, 1997). This can be seen in many of the host rocks to mineralisation in the form of an amphibole overprint, replacement of clinopyroxene and in some places complete alteration of olivine and orthopyroxene to amphibole, chlorite and serpentine (Santaguida, et al., 2015). Alteration tends to be the most intense in proximity to late stage mafic dykes and veins. A detailed study of these veins by Le Vaillant et al. (2016) revealed that this has had only a minor effect on primary metal concentrations.

2.3.3 Mineralisation

The Kevitsa Ni-Cu-(PGE) deposit has an irregular shape due to the disseminated style of sulphide mineralisation. The ore body forms a large, low grade deposit hosted by olivine pyroxenites in the centre of the ultramafic cumulate succession (Luolavirta, et al., 2018a, b, c). Sulphides occur as granular masses interstitial to the silicate mineral crystals, and in places appear net-textured, although this cannot usually be defined beyond a couple of diamond drill holes (Santaguida, et al., 2015). The main ore minerals are pentlandite and chalcopyrite, accompanied by pyrrhotite and magnetite.

Mutanen (1997) identified four ore types based on Ni tenor: *false ore, normal ore* (or *regular ore*)*, transitional ore,* and *Ni-PGE ore.* However, the transitional ore likely represents a lower grade counterpart of the Ni-PGE ore (Lappalainen & White, 2010), and thus will not be considered as a separate ore type in this study. *Figure 2-10* shows photomicrographs of sulphide mineralogy under reflected light.

2.3.3.1 Ore Types

False ore

The false ore type consists of pyrrhotite, with rare chalcopyrite and pentlandite (Santaguida, et al., 2015) (*Fig. 2-10 a, b*). Ni content is generally low, <0.1 % with a record low of 87 ppm (Mutanen, 1997). False ore is easily recognised by geophysical methods, due to the high interconnection of disseminated sulphides creating good electromagnetic conductors (Santaguida, et al., 2015). Due to low metal grades, this ore type is largely uneconomic.

Normal ore

The normal ore (or regular ore) type forms the main mass of the deposit (90%) and occurs as continuous bodies which may extend for hundreds of metres. Normal ore is characterised by 2-6 vol.% sulphide (pyrrhotite, pentlandite, chalcopyrite, *Fig. 2-10 c, d*) and yields average Ni and Cu ore grades of 0.3 and 0.42 wt.% respectively (Ni/Cu <1) (Santaguida, et al., 2015).

Ni-PGE ore

The Ni-PGE ore type has a similar sulphide content to the normal ore, but instead occurs as irregular, discontinuous, lens-like bodies in both the upper and lower parts of the mineralised zone. Ni-PGE ore consists predominantly of pentlandite, pyrite and millerite (*Fig. 2-10 e, f*), with much higher and more variable Ni grades, lower Cu grades (Ni/Cu 1.5-15) and extreme Ni tenors reaching 40%. Ni-PGE ore has higher PGE contents, from >1 ppm to 26.75 ppm (Gervilla, et al., 2004), in comparison to normal ore which has about 0.5-1 ppm of Pt, Pd and Au combined. Ni-PGE ore is also characterised by unusually high Ni content in olivine, up to 14,000 ppm (Hanski, et al., 1997; Yang, et al., 2013). In contrast to normal and false ores, the Ni-PGE ore type has LREE-enriched chondrite-normalised REE patterns (Hanski, et al., 1997; Luolavirta, et al., 2018b).

2.3.3.2 Ore Mineralogy

The major sulphide minerals are pentlandite ($Ni_{4.5}Fe_{4.5}S_9$), pyrite (FeS_2), chalcopyrite ($CuFeS_2$), cubanite ($CuFe_2S_3$) and hexagonal pyrrhotite (Fe_7S_8), with millerite (NiS) and heazlewoodite (Ni_3S_2) also present in the Ni-PGE ore (Kojonen, et al. 2008). Arsenides

including nickeline (NiAs), gersdorffite (NiAsS), cobaltite (CoAsS) and maucherite ($Ni_{11}As_8$) are abundant in some samples, oxidic minerals are mostly chromite ($FeCr_2O_4$) and magnetite (Fe_3O_4) (Kojonen, et al., 2008). Sulphide minerals occur in the intercumulus spaces of primary cumulus silicates or intergrown with secondary minerals such as amphibole, chlorite and serpentine (Kojonen, et al., 2008).

In the upper part of the deposit, pyrite, millerite, heazlewoodite, pentlandite and chalcopyrite often show fine graphical intergrowths and pyrite is replaced along fractures by pentlandite (*Fig. 2-9 a*). Monoclinic pyrrhotite is found associated with pyrite, chalcopyrite and granular pentlandite, exhibiting distinct pentlandite flames or exsolution blebs of pentlandite (Gervilla & Kojonen, 2002). Millerite is closely associated with pentlandite, as is gersdorffite which forms euhedral to subhedral crystals.

Platinum group minerals (PGM) mostly form monomineralic grains <75 μm in size included within hydrosilicates or around the boundaries of sulphide grain aggregates (*Fig. 2-9 b*) Gervilla and Kojonen (2002) found that 54% of PGMs occur as isolated grains within silicates, 39% are associated with sulphides (at the boundaries of sulphide grains) and only 6% occur within the sulphides themselves. 80% of the PGM form from the Pt-Pd-Ni-Te-Bi system, including moncheite, merenskyite, michenerite, melonite and sperrylite. Additional photomicrographs and back-scattered electron images of PGM, sulphides, arsenides and sulpharsenides are provided in the *Appendix 8.1*.

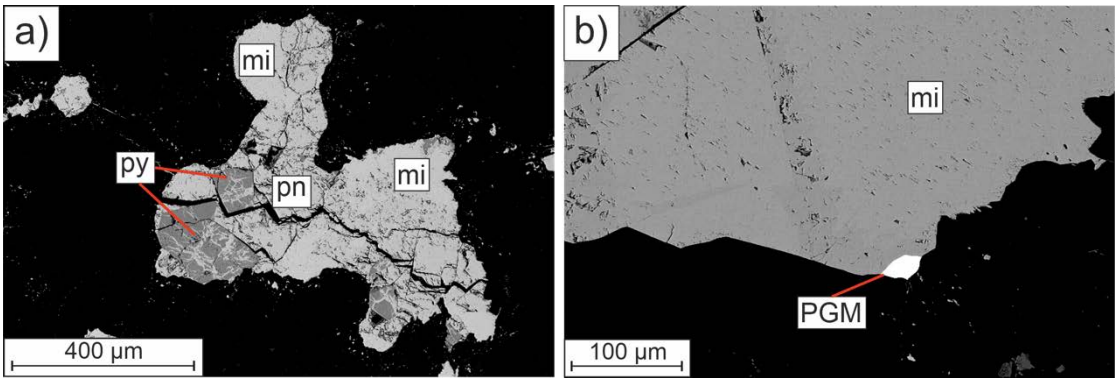

Figure 2-9: Backscattered electron image of sulphide grains from Ni-PGE ore, showing **a)** replacement of pyrite by pentlandite along fractures, and **b)** a PGM (merenskyite) at the edge of a sulphide grain. *mi* = millerite, *pn* = pentlandite, *py* = pyrite, *PGM* = platinum-group element.

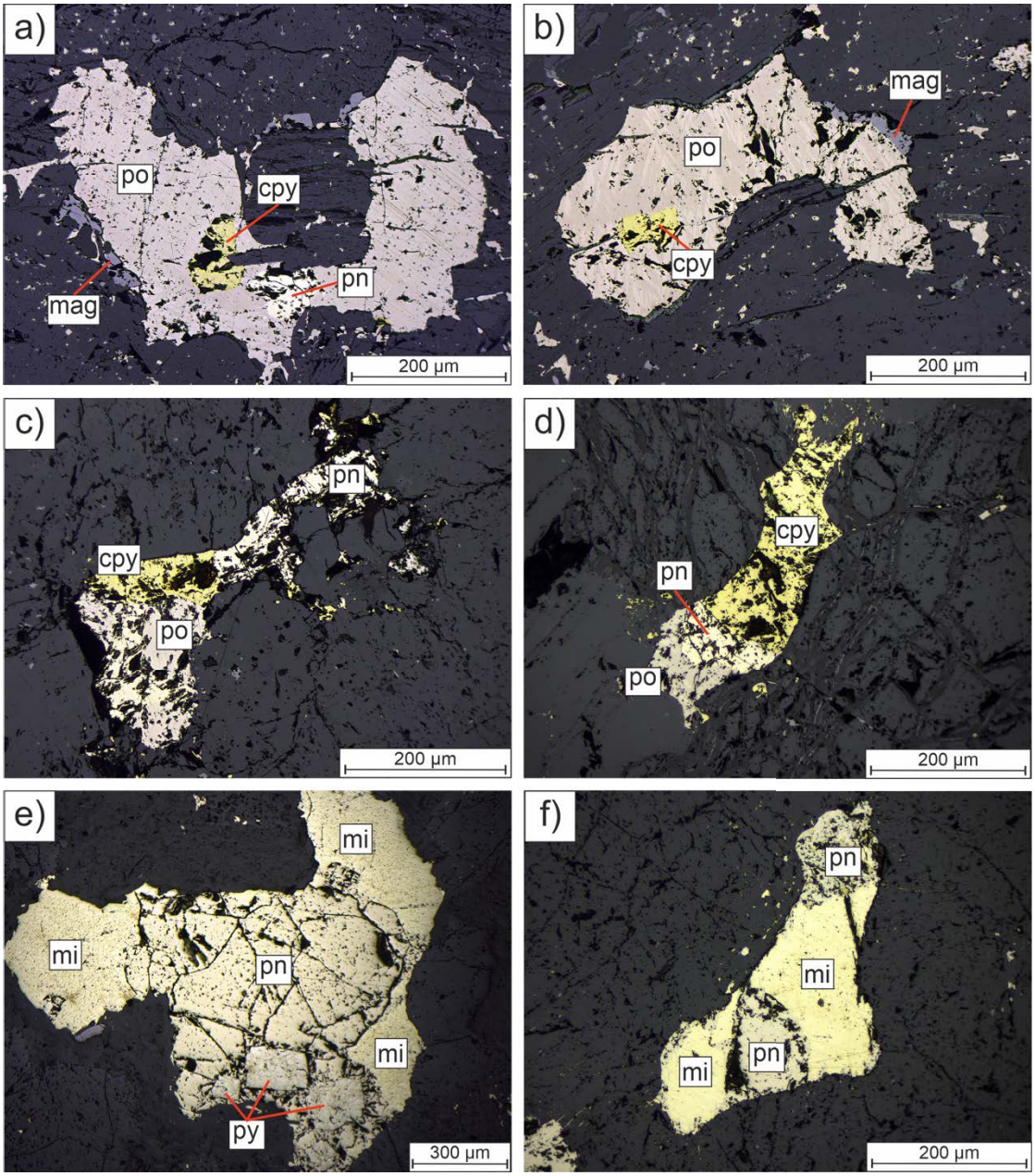

Figure 2-10: Photomicrographs of sulphide blebs under reflected light from different ore types of the Kevitsa deposit. **a)**, **b)** false ore, **c)**, **d)** normal ore, and **e)**, **f)** Ni-PGE ore. *cpy* = chalcopyrite, *mag* = magnetite, *mi* = millerite, *pn* = pentlandite, *po* = pyrrhotite, *py* = pyrite.

2.3.4 Genetic Models

As previously explained in *Sections 1.1.1* and *1.1.2*, mafic-ultramafic intrusions exhibit complex evolutionary histories including magma mixing, crystal fractionation and multiple episodes of magma replenishment to form economic deposits (Depaolo, 1985; Meyer & Wilson, 1999; Namur, et al., 2010).

Varied whole-rock and trace element compositions and abrupt changes in fractionating mineral assemblages are examples of evidence for replenishment by multiple injections of magma (Eales, et al., 1986; Kruger, 1994; Namur, et al., 2010). The Kevitsa deposit is odd in that it does not occur at the base of the intrusion and the mineralisation involves a wide variety of metal contents which form distinct ore types (Mutanen, 1997; Yang, et al., 2013). Such lithological and geochemical variations and uncertain internal structure of the Kevitsa intrusion suggest that the deposit is unusual and has led to many unanswered questions about its petrogenesis.

According to the preliminary model by Mutanen (1997), the Kevitsa intrusion was formed by differentiation of a single pulse of basaltic magma, with lithological and chemical variations reflecting variable degrees of contamination with country rocks *in-situ*. Although this may be true for the unmineralised part of the intrusion, this explanation is not sufficient to account for the distinct differences exhibited by the ore types. In contrast, more recent studies suggest multiple magma injections as an explanation for variability within the ore-bearing domain (Gregory, et al., 2011; Luolavirta, et al., 2018b). A fundamental aspect of the formation of magmatic sulphide ores is the presence of a dynamic magma plumbing system, allowing sulphide liquid to interact with a larger volume of silicate magma, thus increasing chalcophile element contents within sulphides (Naldrett, 1999, 2010, 2011). Indications of open system processes and magma recharge include stratigraphic variations/reversals and changes in types and proportions of fractionating minerals (Cox & Hawkesworth, 1985; Eales, et al., 1986, 1990), all of which occur particularly within the ore-bearing domain of the Kevitsa deposit.

Le Vaillant et al. (2017) proposed that the unmineralised zone around the deposit formed as a result of early-stage xenoliths choking an interconnected sill complex, producing high viscosity conditions that restricted the mixing of magma with sulphide liquid. This resulted in high S, low tenor sulphides of the false ore type. However, chemical and Sr isotopic conditions show homogeneity within ultramafic cumulates around the unmineralised domain of the Kevitsa intrusion (Luolavirta, et al., 2018c), indicating continuous input of chemically and isotopically uniform basaltic magma and its subsequent crystal fractionation. False ores contain slightly heavier S isotope compositions than 'barren' rocks, and vary more than Sr isotopic compositions, which may be a result of bulk contamination at

depth, in a deep staging chamber followed by variable degrees of assimilation of crustal sulphur en route to the Kevitsa magma chamber (Luolavirta, et al., 2018c).

In the ore-bearing domain of the intrusion, variations in mineral and whole-rock compositions reflect episodes of magma replenishment (Luolavirta, et al., 2018b). High $^{87}Sr/^{86}Sr$ values of Ni-PGE ore further support open magma chamber processes, although restricted to the ore-bearing domain of the intrusion (Luolavirta, et al., 2018c). Dynamic emplacement of the ore deposit is supported by the abundance of dunitic inclusions and komatiitic xenoliths (Mutanen, 1997; Luolavirta, et al., 2018a), emphasising the ability of intruding magmas to entrain fragments from adjacent wall rocks. These inclusions may have decreased the flow rate of the magma, aiding in the settling of sulphide droplets (Luolavirta, et al., 2018a).

The formation of the Ni-PGE ore is fairly controversial. Yang et al. (2013) proposed that the Ni-PGE ore formed as a result of assimilation of Ni-rich sulphides from komatiitic xenoliths, enriching the magma in Ni and allowing Ni-enriched olivine to crystallise within this ore type. Contrary to this model, Gervilla and Kojonen (2002) suggested that the PGE-enriched Ni-PGE ore formed as a result of hydrothermal remobilisation by chloride-rich fluids. The hydrothermal fluids are interpreted to be chloride-rich due to the spatial association between Ni-PGE ore and chlorapatite. This hydrothermal remobilisation would have been coeval with greenschist facies metamorphism, potentially leaching out PGE and Au from mineralised zones and depositing them in PGE-rich horizons (Gervilla & Kojonen, 2002). Le Vaillant et al. (2016) argued against this hydrothermal model, as hydrothermal enrichment in Pd is commonly associated with an enrichment in Cu and Au, which is not the case for the Ni-PGE ore at Kevitsa. Low temperature hydrothermal alteration is unlikely to have had a significant effect on the Ni and PGE distribution within the Kevitsa deposit (Le Vaillant, et al., 2016).

The most recent integrated geological model for the genesis of the Kevitsa Ni-Cu-(PGE) by Luolavirta (2018b), shown in *Figure 2-11,* takes these aspects of previous literature into account, and is as follows:

1) Intrusion(s) of picritic basalt magma formed olivine-chromite cumulates in the conduits (*Fig. 2-11 Stage 1*), which would later be referred to as *Central Dunite* (Luolavirta, et al., 2018a).
2) Differentiation and comprehensive country rock contamination of the picritic basalt magma in a lower staging chamber. The basaltic magma intruded as a continuous, stable flow into the Kevitsa magma chamber, crystallising olivine-pyroxene cumulates. There were variable degrees of contamination with external sulphur from country rocks during the flow of magma pulses into the Kevitsa magma chamber. Sulphur saturation was achieved, depositing sulphidic proto-ore(s) into depressions within the conduit. Metal-depleted magma continued to gain sulphur from country rocks and transported sulphide melt to the Kevitsa magma chamber, precipitating metal-poor false ores. Later crystal fractionation resulted in the formation of pyroxenites in a largely closed system (*Fig. 2-11 Stage 2*).
3) The Kevitsa magma chamber began operating as a dynamic open system, with magma intruding into the hot interior of the Kevitsa intrusion. Subsequent magma injections assimilate earlier formed sulphides, collecting metals and forming Ni-Cu-(PGE) enriched sulphides (*Fig. 2-11 Stage 3*). Dunitic cumulates which formed at Stage 1 and komatiitic xenoliths were further brecciated by these magmas and redistributed throughout the olivine-pyroxene cumulates. These inclusions and xenoliths decreased the magma's flow rate and aided in the settling of sulphides. Ni-PGE type magmas intrude via a different route into the Kevitsa magma chamber.

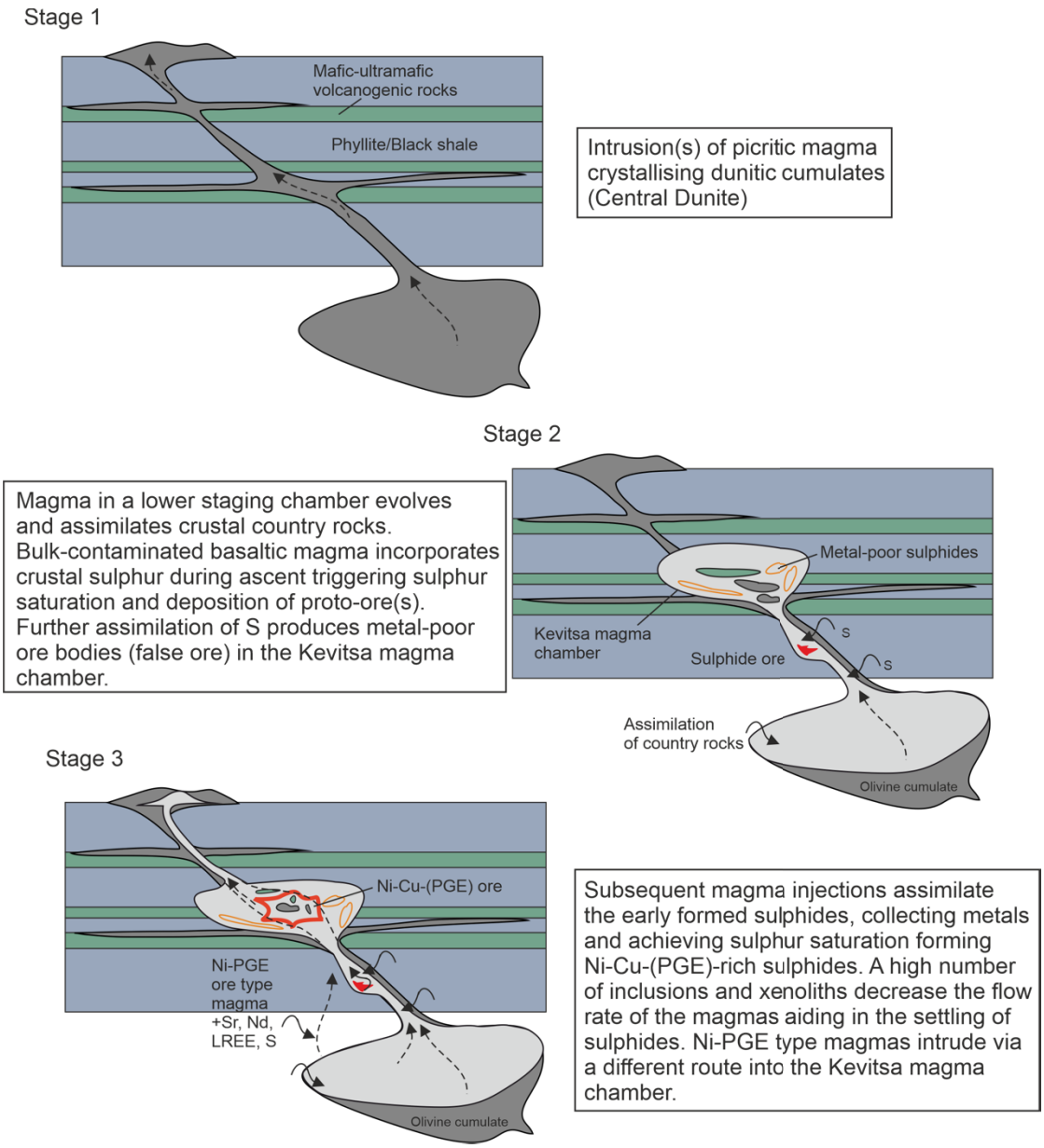

Figure 2-11: Schematic illustration of the processes that led to the emplacement of the Kevitsa intrusive rocks and formation of Ni-Cu-(PGE) deposit. *Modified after Luolavirta, et al. (2018c).*

3 METHODS

3.1 Samples

Altogether, fourteen thick sections representing different ore types were selected for this study. The locations of sampled drill holes are provided in *Figure 3-1*. Characteristics of each ore type are described in *Section 2.3.3.1*. Details of each thick section, including ore type, whole rock concentrations of major elements and metal tenors in 100% sulphide are presented in *Table 3-1*.

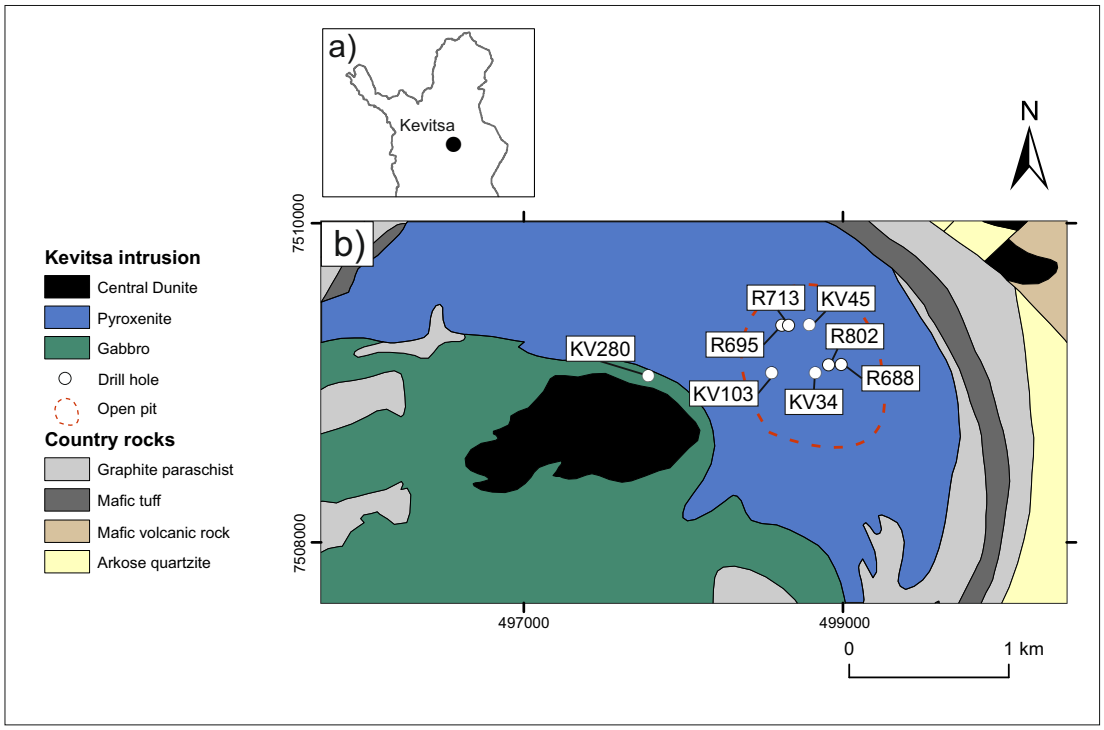

Figure 3-1: a) Location of the Kevitsa intrusion, northern Finland. *Modified after Hanski et al. (2001).* **b)** Simplified geological map of the Kevitsa intrusion, showing the location of sampled drill holes and approximate location of the open pit. *Bedrock data from GTK's Kallioperä 1:200 000 (URL-2), drill hole location data from Boliden.*

Table 3-1: Sample list containing 14 thick sections from 8 drill holes showing their respective depth, whole rock concentrations of main metals and sulphide composition in 100% sulphide.

Samples						Whole rock composition			Sulphide composition							
Name	From	To	Ore Type	Alteration	No. of grains	S (wt.%)	Ni (wt.%)	Cu (wt.%)	Ni (%)	Cu (%)	Pd (ppb)	Pt (ppb)	Ir (ppb)	Os (ppb)	Ru (ppb)	Rh (ppb)
KV280 574.95	573	575	False ore	n/a	7	1.87	0.04	0.04	0.84	0.78	n/a	n/a	n/a	n/a	n/a	n/a
KV280 620.4	619	621	False ore	n/a	6	0.79	0.04	0.04	1.92	1.94	n/a	n/a	n/a	n/a	n/a	n/a
R688 65.7	65.70	65.90	False ore	n/a	6	3.09	0.03	0.06	0.32	0.69	n/a	n/a	n/a	n/a	n/a	n/a
R802 81.4	81.00	82.00	False ore	n/a	6	2.17	0.02	0.04	0.35	0.62	n/a	n/a	n/a	n/a	n/a	n/a
KV34B 327.73	327	328.9	Normal ore	n/a	4	3.67	0.4	0.64	4.12	6.52	4194	3601	n/a	n/a	n/a	n/a
KV34B 554.48	553	555	Normal ore	n/a	5	3.54	0.71	0.99	7.30	10.23	4981	3090	n/a	n/a	n/a	n/a
KV45-32	136	138	Normal ore	n/a	6	2.73	0.38	0.67	5.09	9.09	5717	4156	n/a	n/a	n/a	n/a
KV45-35	146	148	Normal ore	n/a	6	2.74	0.38	0.95	5.04	12.67	6126	3999	n/a	n/a	n/a	n/a
KV103 421.2	421	423	Normal ore	n/a	6	1.96	0.17	0.37	3.34	7.15	1060	765	n/a	n/a	n/a	n/a
KV45-63	264	266	Ni-PGE ore	Moderate	5	1.53	0.57	0.2	11.38	4.05	11643	7997	n/a	n/a	n/a	n/a
KV45-75	314	316	Ni-PGE ore	Fresh	8	1.82	0.75	0.39	15.44	7.96	26039	21079	n/a	n/a	n/a	n/a
R695 68.1	68	68.55	Ni-PGE ore	Fresh	8	2.9	2.54	0.2	33.24	2.58	24602	37295	1349	912	1764	1064
R695 69	68.9	69.2	Ni-PGE ore	High	7	1.79	1.74	0.15	32.61	2.72	35244	51179	1002	652	1278	930
R713 37.3	36	38	Ni-PGE ore	Fresh	8	0.68	0.85	0.04	43.15	2.09	34577	45541	1305	867	2050	1351

Values sourced from the Kevitsa assay database. *n/a* data not available, *wt.%* weight percent, *ppb* parts per billion.

3.2 Reflected Light Microscopy

The thick sections were studied using a *Leica DM750P* transmitted- and reflected-light microscope and photographs were taken using a *Zeiss Axioplan 2* transmitted- and reflected-light microscope equipped with and *Axiocam 105* colour camera and a *Zen 2 core 2.4* computer programme. The sections were investigated in terms of sulphide mineral assemblage using reflected light as a prerequisite to further analysis. Individual sulphide grains were chosen based on size, general condition (few pits and fractures, less altered, etc.) and ore mineralogy to provide a good spread of sulphide minerals to be used throughout the study. An average of 5 sulphide grains per section were chosen, totalling 88 grains.

3.3 FESEM & EDS

The field emission scanning electron microscope (FESEM) was used primarily to confirm ore mineralogy of selected sulphide grains and note the location of PGMs, which if included in LA-ICP-MS analysis would interfere with the results. Prior to the use of the FESEM, all the thick sections were carbon-coated. The *Zeiss ULTRA plus FESEM* was used at the University of Oulu, allowing high resolution backscattered images of sulphide grains to be taken to highlight arsenide phases and PGMs that may go unnoticed using regular microscopy (see *Fig. 2-9* and in *Appendix 8.1*). Backscattered images from the FESEM were used to plan laser ablation spots and lines. The FESEM is also equipped with energy-dispersive X-ray spectroscopy (EDS) for element analysis, which aided in the identification of unknown mineral phases and confirmation of elemental composition of known minerals.

3.4 LA-ICP-MS

Trace element concentrations for each of the sulphide phases were analysed by laser ablation inductively coupled plasma mass spectrometry (LA-ICP-MS) at the Geological Survey of Finland (GTK) research laboratory in Espoo, Finland. The LA-ICP-MS analyses were carried out using the Nu Instruments™ AttoM single-collector high-resolution ICP-MS system, equipped with a Photon Machines™ deep UV (193 nm wavelength) excimer laser. Analyses were conducted using 50 μm diameter spots, a laser frequency of 10 Hz,

power of 2.5 J/cm^2 with He-Ar carrier gas and a 25 sec pattern start pause for gas background analysis before ablation. Data reduction was conducted using Glitter™ software, with ^{57}Fe as an internal standard for the majority of samples. Millerite was analysed separately due to a higher Ni content, with ^{61}Ni used as the internal standard. Aside from 50 μm diameter spot analysis, slow sampled traverse lines were measured with some grains from rim to core. Time resolved analysis (TRA) allowed signal intensity *vs.* time profiles to be generated, revealing any zoning that may be present within the sulphide grains as well as any mineral inclusions.

Concentrations of elements S, Fe, Ni, Cu, Co, Ru, Rh, Pd, Pt, Re, Os, Ir, Au and Ag were analysed in this manner. Si, Sc, Ti, V, Cr, Mn, Zn, Ga, Ge, As, Se, Mo, Cd, Sn, Te, Bi, Pb, and Hg were also measured to monitor the mineral phase and identify possible inclusions and interferences. Obvious peaks of these elements could indicate a hidden PGM or semi-metal inclusion.

3.4.1 Standards and QAQC

The LA-ICP-MS methodology employed an analytical sequence of 2 analyses of a primary calibration standard (MASS-1) and 2 analyses of a secondary calibration standard (UQAC) before running analyses on the Kevitsa sulphides. This sequence was repeated every 10-15 spots, depending on the amount of spots per sample. The calibration standards MASS-1 and UQAC take the form of nano-particulate pressed pellets (Garde-Schönberg & Müller, 2014). MASS-1 (Fe-Zn-Cu-S) is sourced from the United States Geological Survey (USGS) and is doped with ~50-70 ppm As, Se, Mo, Ag, Cd, In, Sn, Sb, Ir, Pt, Au, Hg, Pb and Bi (Wilson, et al., 2002). Reference values and statistical analysis for each standard are shown in *Table. 3-2.* Cu was found to be unreliable, with great variations in the results (see *Table 3-2*) and frequent 'dead' signals which would appear as very low or even minus values in the presence of significant amounts of Cu.

Table 3-2: Analyses of reference materials used for calibration during LA-ICPMS to monitor data quality.

Standard		^{34}S (%)	^{65}Cu (%)	^{67}Zn (ppm)	^{75}As (ppm)	^{77}Se (ppm)	^{109}Ag (ppm)	^{111}Cd (ppm)	^{118}Sn (ppm)	^{121}Sb (ppm)	
MASS-1	avg	27.8376439	481.96	213660.56	65.31	51.22	50.26	60.48	59.28	60.30	
(n=79)	stdev	1.76	1688.14	19884.50	4.43	3.43	3.51	5.36	3.64	3.98	
	Rel. Diff.	0.009	34.967	0.017	0.005	0.004	0.005	0.008	0.005	0.005	
	reference value	27.6	13.4	210000	65	51	50	60	59	60	
		^{61}Ni (%)	^{99}Ru (ppm)	^{101}Ru (ppm)	^{103}Rh (ppm)	^{106}Pd (ppm)	^{108}Pd (ppm)	^{190}Os (ppm)	^{193}Ir (ppm)	^{195}Pt (ppm)	^{197}Au (ppm)
UQAC	avg	2.51	65.21	65.21	64.28	60.62	60.58	75.78	60.55	50.86	65.57
(n=79)	stdev	0.14	2.64	2.65	3.36	6.02	5.82	6.76	4.91	6.11	5.87
	Rel. Diff.	0.003	0.003	0.003	0.004	0.010	0.010	0.010	0.009	0.017	0.009
	reference value	2.5	65	65	64	60	60	75	60	50	65

Reference values provided by the GTK Lab, Espoo. LA-ICP-MS used for analysis of each isotope. *stdev* standard deviation; *Rel. Diff.* relative difference of this study/reference value; *n* number of analyses.

3.4.2 Interferences

LA-ICP-MS analysis can be particularly problematic in PGE-bearing sulphides due to significant interferences of isotopes with the ICP support gas, Ar. Some interferences are so severe, namely CuAr interferences on ^{103}Rh and ^{105}Pd in chalcopyrite and NiAr interferences on ^{101}Ru in pentlandite and millerite, that it is difficult to generate data without unacceptable losses of certainty. Potential interferences on PGE are shown in *Table 3-3.*

Table 3-3: Table of the main interferences on PGE in sulphide minerals. *After Cabri & LaFlamme, 1976.*

Ruthenium	Rhodium	Palladium
$^{59}Co^{40}Ar^{+} \rightarrow {}^{99}Ru^{+}$	$^{63}Cu^{40}Ar^{+} \rightarrow {}^{103}Rh^{+}$	$^{65}Cu^{40}Ar^{+} \rightarrow {}^{105}Pd^{+}$
$^{61}Ni^{40}Ar^{+} \rightarrow {}^{101}Ru^{+}$	$^{206}Pb^{++} \rightarrow {}^{103}Rh^{+}$	$^{66}Zn^{40}Ar^{+} \rightarrow {}^{106}Pd^{+}$
$^{62}Ni^{40}Ar^{+} \rightarrow {}^{102}Ru^{+}$		$^{68}Zn^{40}Ar^{+} \rightarrow {}^{108}Pd^{+}$
		$^{106}Cd^{+} \rightarrow {}^{106}Pd^{+}$
		$^{108}Cd^{+} \rightarrow {}^{108}Pd^{+}$

Since all the noble metals, except for Rh and Au, possess multiple isotopes, PGE isotopes can be selected or avoided based on the likelihood that they are being interfered with. For instance, ^{65}Cu in chalcopyrite and ^{40}Ar interfere with ^{105}Pd; whereas ^{106}Pd and ^{108}Pd tend to have little to no interferences. Similarly, ^{61}Ni and ^{62}Ni with ^{40}Ar create large interferences on ^{101}Ru and ^{102}Ru respectively, and there is little interference with ^{99}Ru provided there is low ^{59}Co.

3.5 Mass Balance

To determine the proportion (wt.%) of each PGE hosted by each BMS phase, a mass balance calculation was carried out according to the method of Barnes et al. (2008). Firstly, the calculation requires the weight fraction of each of the BMS phases (*F*) to be estimated using whole rock data (for whole rock composition of each sample see *Table 3-1*). For chalcopyrite, all of the Cu was assumed to be within chalcopyrite, and was calculated as follows:

$$F_{Cpy} = (\mathrm{Cu}_{wr})/(\mathrm{Cu}_{Cpy})$$

Where Cu_{wr} = Cu concentration in whole rock and Cu_{Cpy} = Cu concentration in chalcopyrite (approx. 0.345 wt.%). Similarly, all of the whole rock Ni was assumed to be within pentlandite, thus:

$$F_{Pn} = (\mathrm{Ni}_{wr})/(\mathrm{Ni}_{Pn})$$

Where Ni_{wr} = Ni concentration in whole rock and Ni_{Pn} = Ni concentration in pentlandite (approx. 0.356 wt.%). For two of the Ni-PGE ore samples, the whole rock concentration of Ni was halved, the other half being assigned to millerite. In the particularly Ni-rich samples from the Ni-PGE ore, the whole rock Ni content was reduced by 0.4 before being used in the calculations to account for silicates. The amount of S attributed to chalcopyrite, pentlandite and millerite was then calculated and the amount left over was assigned to pyrrhotite (and pyrite in the Ni-PGE ore samples):

$$F_{Po} = (\mathrm{S}_{wr} - F_{Cpy} * \mathrm{S}_{Cpy} - F_{Pn} * \mathrm{S}_{Pn} - F_{Mill} * \mathrm{S}_{Mill}) / \mathrm{S}_{Po}$$

Where S_{Cpy} = S in chalcopyrite, S_{Pn} = S in pentlandite, S_{Mill} = S in millerite and S_{Po} = S in pyrrhotite. The sum of the wt.% of all mineral phases was then used to calculate the proportion of each BMS normalised to 100% sulphide, the results of which are shown in *Table 3-1*. The proportion (wt.%) of each element in each sulphide phase (F_{sul}^{i}) was calculated using the following equation:

$$F_{sul}^{i} = (F_{sul} C_{sul}^{i} / C_{wr}^{i})$$

Where F_{sul} = weight fraction of the given BMS phase, C_{sul}^{i} = concentration of element *i* in the BMS phase and C_{wr}^{i} = concentration of element *i* in the whole rock.

Results of the 100% sulphide and mass balance calculations are provided in the *Appendix 8.2* and *8.3*.

4 RESULTS

The results of the in-situ trace-element LA-ICP-MS analysis of sulphide phases in the Kevitsa Ni-Cu-(PGE) ore (see *Table 4-1* and *4-2* for summary) and subsequent mass balance calculations are presented here in the following sections. All LA-ICP-MS data is provided in the *Appendix 8.4*.

4.1 Platinum-Group Elements in Different Ore Types

Sulphides in the Ni-PGE ore type host more PGE than sulphides in the other ore types, except Pt, where normal ore marginally exceeds the Ni-PGE ore average by 0.06 ppm (*Table 4-1, Fig. 4-1*). Sulphides in the false ore are almost barren of PGEs (<0.1 ppm on average, except Pd with 0.23 ppm on average) and contain 20 times less Ru, Rh and Pd and nearly 150 times less Os and Ir than sulphides in the Ni-PGE ore. Maximum values for false ore sulphides do not exceed 1 ppm for any of the PGEs, whereas normal ore only exceeds an average of 1 ppm for Pd, with a maximum of 7.33 ppm. Although the average concentrations of Os, Ir and Pt are low in normal ore sulphides (0.08, 0.05 and 0.1 ppm respectively), maximum values of over 1 ppm are encountered for each. Similarly, Ni-PGE ore sulphides contain up to 26.4 ppm Os and 18.06 ppm Ir, although the averages are fairly low (0.7 and 0.9 ppm, respectively). The Pd contents in the Ni-PGE ore sulphides range from 0.04 to 51 ppm with an average of 5.7 ppm. The PGE contents in Ni-PGE ore sulphides also vary considerably, in particular Pd, Os and Ir (*Fig. 4-1*). The false ore sulphides record consistently low PGE values with little spread of data. Overall, Pd is the most abundant PGE in the Kevitsa sulphides.

In general, there is a positive correlation between Pd and Os, and Os and Ir in both Ni-PGE and normal ore sulphides (*Fig. 4-2 c, f*). There is a clear correlation between Pd and Ru in Ni-PGE ore sulphides (*Fig. 4-2 a*), while Os and Ru appear to weakly correlate in normal ore sulphides, as do Ru and Rh (*Fig. 4-2 d, e*).

Table 4-1: LA-ICP-MS results for each BMS phase in false ore, normal ore and Ni-PGE ore. All values given in ppm.

Ore Type	BMS	Element	Ru	Rh	Pd	Os	Ir	Pt	Co	Ni	Zn	As	Se	Ag	Te	Re	Au	Bi
		Isotope	99/ 101	103	106/ 108	190	193	195	59	61	67	75	78	107	126	185	197	209
False ore	Po	avg	0.07	0.02	0.22	0.006	0.005	0.004	82.7	899.4	0.84	0.31	60.7	0.35	0.27	0.034	0.002	0.19
(n=77)		min	0.02	0.01	0.12	0.001	0.001	0.002	22.5	2.0	0.27	0.13	27	0.05	0.05	0.003	0.001	0.07
		max	0.16	0.04	0.48	0.015	0.014	0.007	437	2214	4.3	0.61	98.6	1.51	1.29	0.289	0.005	0.79
	Pn	avg	n/a	0.04	0.32	0.009	0.007	0.005	422	210209	5.95	0.25	56	4.03	3.51	0.044	0.013	1.05
		min	n/a	0.007	0.17	0.002	0.003	0.003	0.9	170354	0.2	0.13	40.2	0.1	0.24	0.003	0.004	0.06
		max	n/a	0.12	0.51	0.015	0.011	0.007	2961	309609	41.7	0.52	87.1	29.2	26.9	0.318	0.044	3.59
	Cpy	avg	0.15	n/a	0.12	0.006	0.002	0.004	1767	12688	1800	0.35	64.8	12.7	6.58	0.048	0.009	0.84
		min	0.03	n/a	0.04	0.002	0.001	0.003	2.2	38.4	5.7	0.12	24.6	0.16	0.21	0.004	0.001	0.11
		max	0.26	n/a	0.23	0.01	0.002	0.004	11537	128219	21822	0.65	91.9	86.3	14.3	0.373	0.016	3.24
	All	avg	0.09	0.02	0.23	0.006	0.005	0.004	481	33676	555.5	0.31	61	3.48	2.15	0.038	0.005	0.45
		min	0.02	0.01	0.04	0.001	0.001	0.002	0.9	2	0.2	0.12	25	0.05	0.05	0.003	0.001	0.06
		max	0.26	0.11	0.51	0.015	0.014	0.007	11537	309610	21822	0.65	99	86.3	26.9	0.373	0.044	3.59
Normal ore	Po	avg	0.27	0.02	0.17	0.118	0.093	0.074	96.6	3453	17.35	0.4	196	1.31	0.32	0.051	0.006	0.61
(n=125)		min	0.04	0.01	0.07	0.005	0.001	0.002	4.0	21.4	0.31	0.06	135	0.07	0.04	0.003	0.001	0.05
		max	0.74	0.08	0.34	0.87	1.890	1.680	3521	82247	328.1	4.15	273	36.2	2.48	0.660	0.051	5.48
	Pn	avg	n/a	0.16	2.61	0.121	0.010	0.019	12403	301431	22.96	0.66	179	2.3	10.2	0.024	0.015	1.63
		min	n/a	0.01	0.43	0.004	0.001	0.002	2268	77204	0.330	0.09	123	0.31	0.15	0.002	0.002	0.22
		max	n/a	0.74	7.3	1.100	0.087	0.147	18808	400514	151.1	3.62	273	13.7	54.7	0.204	0.095	4.24
	Cpy	avg	0.19	n/a	0.24	0.011	0.026	0.168	64	1400	677.8	0.31	185	4.64	10.2	0.005	0.023	2.29
		min	0.04	n/a	0.07	0.001	0.001	0.001	0.1	5.2	23.91	0.06	138	0.54	0.1	0.001	0.002	0.1
		max	0.45	n/a	0.63	0.206	0.501	1.66	1919	33680	7895	1.46	289	25.5	45.6	0.012	0.468	9.31

Table 4-1 (continued)

Ore Type	BMS	Element Isotope	Ru 99/ 101	Rh 103	Pd 106/ 108	Os 190	Ir 193	Pt 195	Co 59	Ni 61	Zn 67	As 75	Se 78	Ag 107	Te 126	Re 185	Au 197	Bi 209
	All	avg	0.23	0.08	1.24	0.088	0.055	0.11	2567	62326	314.8	0.42	189	2.68	6.10	0.034	0.015	1.40
		min	0.04	0.01	0.07	0.001	0.001	0.001	0.1	5	0.3	0.06	123	0.07	0.04	0.001	0.001	0.05
		max	0.74	0.74	7.33	1.1	1.890	1.680	18808	400514	7895	4.15	289	36.2	54.7	0.660	0.468	9.31
Ni-PGE ore	Po	avg	0.3	0.04	1.69	0.188	0.008	0.005	1520	24286	5.622	2.2	404	2.12	1.84	0.014	0.075	15.4
(n=137)		min	0.06	0.01	0.12	0.016	0.001	0.002	2.4	1481	0.33	0.12	322	0.06	0.5	0.006	0.002	0.13
		max	0.54	0.17	7.78	0.339	0.021	0.013	14825	202022	16.96	16	852	18.5	10	0.04	0.4	145
	Pn	avg	4.09	1.07	7.81	1.333	1.165	0.074	4088	402188	10.49	243	1041	1.47	104	0.026	0.037	12.7
		min	0.39	0.01	0.1	0.002	0.001	0.002	1049	111314	0.235	0.3	251	0.03	0.75	0.002	0.002	0.02
		max	8.16	4.54	51.6	26.40	18.06	1.84	58279	642453	281.4	1420	41520	21.2	651	0.226	0.486	215
	Cpy	avg	0.22	n/a	0.4	0.007	0.008	0.03	125	12690.3	288.6	1.8	204	0.46	0.53	0.012	0.021	1.67
		min	0.09	n/a	0.05	0.003	0.001	0.002	0.1	10.6	5.07	0.33	134	0.07	0.2	0.002	0.001	0.48
		max	0.77	n/a	1.86	0.014	0.021	0.15	1185	113822	542.1	9.62	333	1.83	1.57	0.036	0.093	4.13
	Py	avg	0.41	0.16	4.06	0.230	0.087	0.004	6052	94815.8	30.31	220	792	3.19	19.4	0.012	0.231	80.9
		min	0.06	0.01	0.08	0.006	0.001	0.002	225	850.6	0.93	1.54	447	0.03	2.83	0.003	0.005	1.07
		max	1.9	0.5	15.9	0.711	0.469	0.013	12094	393627	215.2	2018	1316	13	130	0.039	0.98	332
	Mill	avg	0.36	0.18	1.78	0.403	0.189	0.007	1480	638685	1.522	259	1576	1.21	18.5	0.005	0.016	10.9
		min	0.16	0.01	0.14	0.003	0.001	0.002	758	618433	1.02	9.34	1328	0.03	1.89	0.002	0.003	0.85
		max	0.65	1.81	15.8	3.62	1.76	0.017	4819	677056	2.32	596	2084	5.07	220	0.012	0.064	72.3
	All	avg	1.81	0.74	5.73	0.894	0.725	0.046	3518	335369	44.1	207.9	973	1.66	65.4	0.02	0.07	21.4
		min	0.06	0.01	0.05	0.002	0.001	0.002	0.1	10.6	0.2	0.12	134	0.03	0.20	0.002	0.001	0.02
		max	8.16	4.54	51.6	26.4	18.06	1.84	58279	677056	542.1	2018	41521	21.2	651	0.226	0.98	332

Po pyrrhotite, *pn* pentlandite, *cpy* chalcopyrite, *py* pyrite, *mill* millerite, *avg* average, *min* minimum, *max* maximum, *n/a* data not available, *n* number of lasered spots, *bdl* below detection limit.

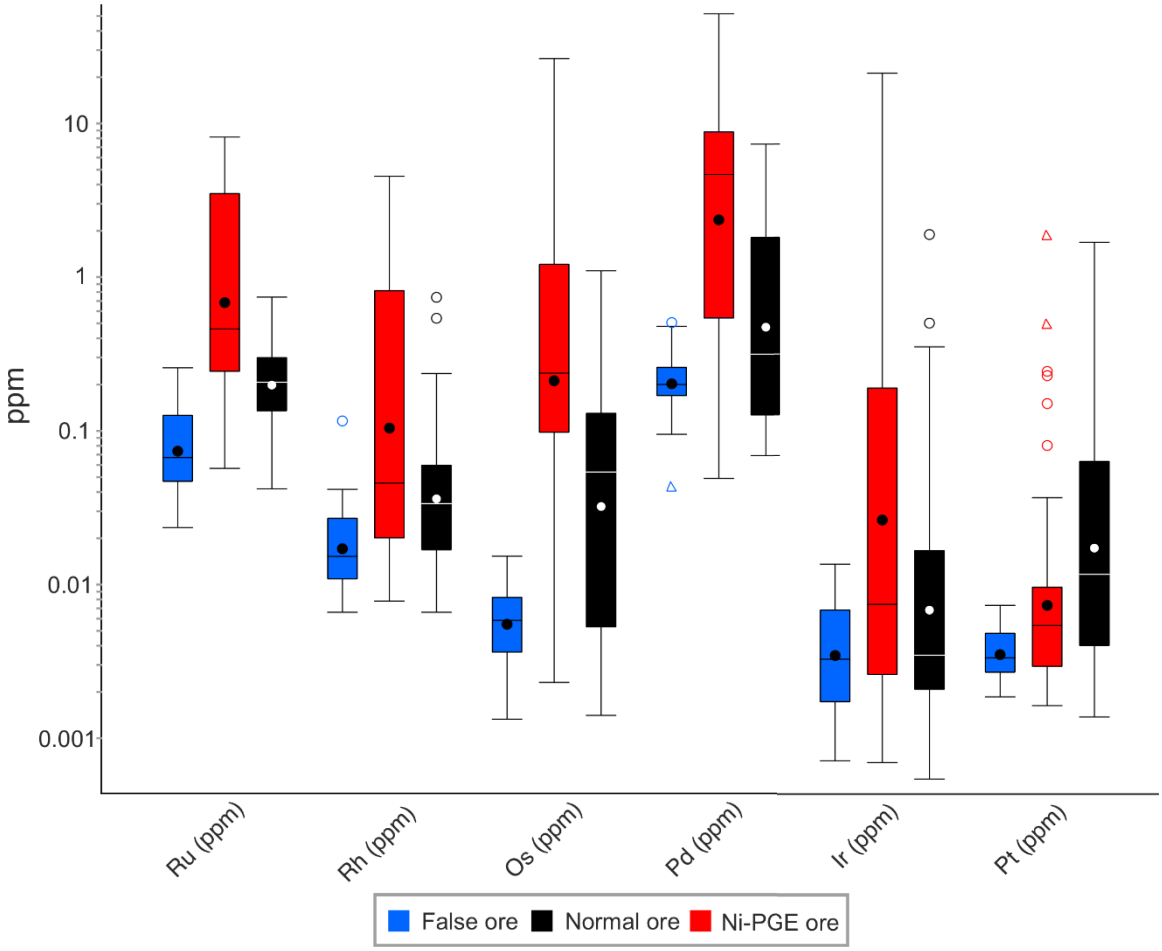

Figure 4-1: Box plot showing the spread of data for PGEs around the mean for sulphides in different ore types at Kevitsa. The box corresponds to the middle 50% of the data, with the bottom of the box representing the 25th percentile (Q1) and the top of the box representing the 75th percentile (Q3). The black circle and the line inside of the box represents the mean and median, respectively. Outliers (circles) are further than 1.5*(Q3-Q1) and far outliers (triangles) are further than 3*(Q3-Q1). Whiskers represent extreme values.

The highest values in the Ni-PGE ore sulphides are attributed to pentlandite (*Fig. 4-3 a, c, e*), chalcopyrite is consistently low (<0.4 ppm on average), and millerite and pyrite contain similar amounts of Ru, Rh, Os, and Pd (~0.4 ppm Ru, ~0.18 ppm Rh, ~0.4 ppm Os, 1.7-4 ppm Pd). Normal ore contains similar amounts of Os and Ir in pentlandite and pyrrhotite, although pentlandite is distinctly higher in Pd (*Fig. 4-3 b, d, f*). Chalcopyrite and pyrrhotite also exceed pentlandite in Pt.

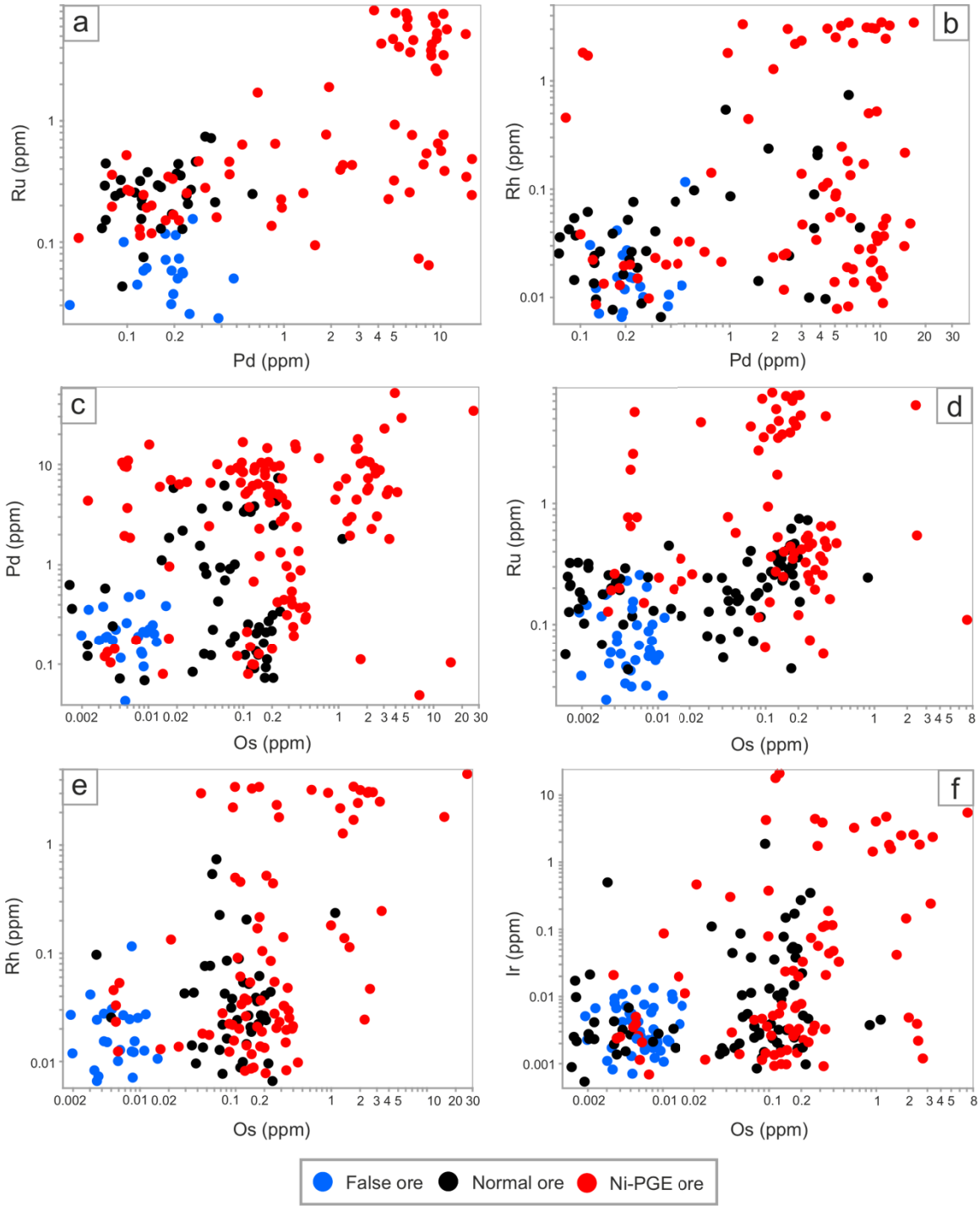

Figure 4-2: Variation of PGE concentration in all BMS from different ore types; false ore, normal ore and Ni-PGE ore.

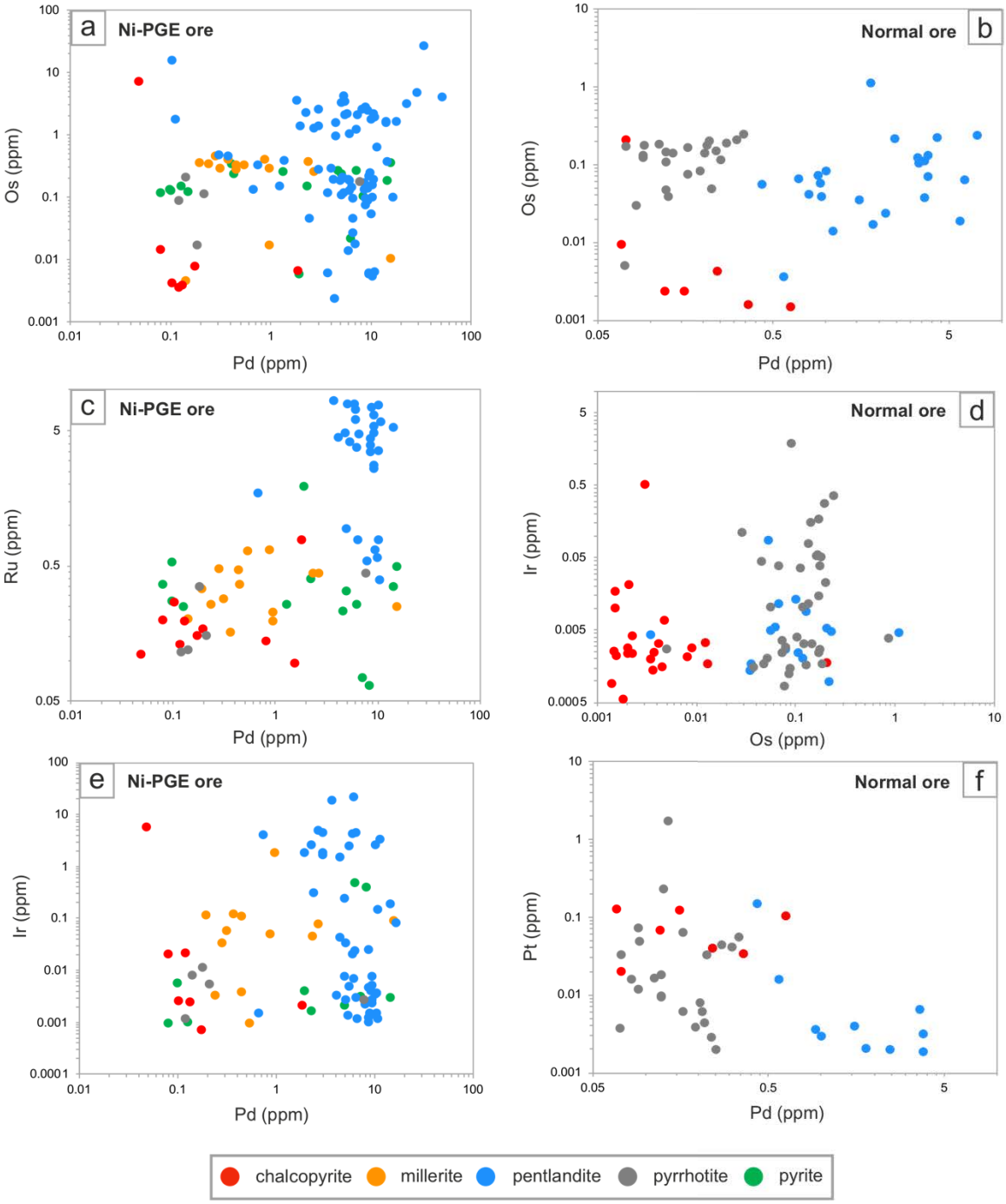

Figure 4-3: Variation in PGE concentration in normal and Ni-PGE ore, showing different base metal sulphide phases.

4.2 Platinum-Group Elements in Different BMS

In general, Pd is the most abundant PGE in all of the sulphide phases, whereas a third of Ir and Pt analyses were below the detection limit (~0.001 ppm) (*Table 4-2, Fig. 4-4*). Pentlandite contains the highest concentration of all PGEs except Pt, and all elements exceed 1 ppm in at least two spots. Pentlandite is richest in Pd, with an average of 6.25 ppm (*Fig. 4-4*). Ru is also high in pentlandite, with an average of 4.09 ppm. Os and Ir have similar averages of 0.99 and 0.82 ppm respectively, and large ranges with high maximum values of >18 ppm. Regarding the other sulphide phases, chalcopyrite contains low concentrations of PGE, and is particularly low in Ir, with an average of 0.019 ppm and Os, with an average of 0.09 ppm. Although Pt contents are low in all sulphide phases, chalcopyrite hosts the most (avg. 0.29 ppm) (*Fig. 4-4*). Similarly, PGE contents are among the lowest in pyrrhotite, with an average of 0.21 ppm Ru, 0.08 ppm Os, 0.03 ppm Rh and Os (averages of 0.21 ppm and 0.08 ppm, respectively). Pyrrhotite also features the lowest concentration of Rh with an average of 0.03 ppm and a maximum value of 0.17 ppm. Pt in pyrrhotite is mostly very low (avg. 0.05 ppm), with the exception of a few spots exceeding 1 ppm. Pyrite and millerite are only encountered in the Ni-PGE ore type, and in comparison to other sulphide phases, these minerals contain moderate concentrations of PGE except Pt (avg. 0.004 and 0.007 ppm, respectively). Pyrite contains marginally higher Ru and Rh than millerite, although millerite contains higher Os (avg. 0.403 ppm, max. 3.62 ppm) and Ir (avg. 0.189 ppm, max. 1.76 ppm). Pyrite also contains higher concentrations of Pd than millerite by a few ppm, although their maximum values are similar (~15.8 ppm).

All BMS show a substantial spread of data (*Fig. 4-4*), particularly for Pd, Rh, Os and Ir. Pentlandite tends to have the most extreme values, whereas chalcopyrite and pyrrhotite have the least spread and least extreme values. Outliers tend to occur with Pt more than any other PGE, especially in pentlandite. Millerite also shows a large spread of data with Os and Ir, and pyrite shows a large spread for Pd. Pentlandite shows varied concentrations of Pd, Os and Ir whereas values tend to be more clustered at the higher end for Ru (>4 ppm) (*Fig. 4-4*). There is a general positive correlation between Pd and Ru, Os and Pd, and Os and Ru with all mineral phases combined (*Fig. 4-5 a, b, c*), although relationships are more clearly seen in pentlandite and pyrrhotite (*Fig. 4-6*).

Table 4-2: LA-ICP-MS results for each BMS phase in all ore types. All values given in ppm.

	Element	Ru	Rh	Pd	Os	Ir	Pt	Co	Ni	Zn	As	Se	Ag	Te	Re	Au	Bi
	Isotope	99/ 101	103	106/ 108	190	193	195	59	61	67	75	78	107	126	185	197	209
Pyrrhotite	avg	0.21	0.03	0.36	0.080	0.048	0.047	213.3	4176	10.3	0.52	155.7	0.97	0.44	0.041	0.01	1.70
(n=116)	min	0.02	0.01	0.07	0.001	0.001	0.002	2.4	2.0	0.3	0.06	27.01	0.05	0.04	0.003	0.001	0.05
	max	0.74	0.17	7.78	0.87	1.89	1.68	14825	202022	328.1	15.98	852	36.2	10	0.660	0.40	145
	stdev	0.17	0.02	1.13	0.111	0.222	0.229	1407	20154	44.1	1.61	114.5	3.79	1.01	0.072	0.053	13.5
Pentlandite	avg	4.09	0.84	6.25	0.99	0.823	0.059	5557	361209	12.3	167	757.2	1.91	74.1	0.028	0.03	9.12
(n=113)	min	0.39	0.01	0.10	0.002	0.001	0.002	0.9	77203	0.2	0.09	40.24	0.03	0.15	0.002	0.002	0.02
	max	8.16	4.54	51.58	26.4	18.06	1.84	58279	642453	281.4	1420	41520	29.3	651	0.318	0.49	215
	stdev	2.47	1.29	6.67	2.697	2.427	0.255	6994	113952	39.8	357.5	3859	4.35	129	0.046	0.07	29.7
Chalcopyrite	avg	0.19	n/a	0.29	0.009	0.019	0.133	467.7	5592	878.8	0.54	160.3	5.88	8.1	0.018	0.02	1.87
(n=70)	min	0.03	n/a	0.04	0.001	0.001	0.001	0.1	5.2	5.1	0.06	24.59	0.07	0.1	0.001	0.00	0.10
	max	0.77	n/a	1.86	0.206	0.501	1.66	11537	128219	21822	9.62	333.5	86.3	45.6	0.373	0.47	9.31
	stdev	0.11	n/a	0.43	0.03	0.085	0.313	1667	21011	2711	1.21	62.18	12.5	9.07	0.062	0.06	2.04
Pyrite	avg	0.41	0.16	4.06	0.23	0.087	0.004	6052	94815	30.3	219.9	791.9	3.19	19.4	0.012	0.23	80.9
(n=19)	min	0.06	0.01	0.08	0.006	0.001	0.002	225.1	850.6	0.9	1.54	446.8	0.03	2.83	0.003	0.005	1.07
	max	1.90	0.50	15.85	0.711	0.469	0.013	12094	393626	215.2	2018	1316	13	130	0.039	0.98	332
	stdev	0.45	0.19	5.03	0.190	0.179	0.003	3456	130189	58.1	525	270.6	3.57	29.6	0.010	0.26	80.5

Table 4-2 (continued)

	Element	Ru	Rh	Pd	Os	Ir	Pt	Co	Ni	Zn	As	Se	Ag	Te	Re	Au	Bi
	Isotope	99/ 101	103	106/ 108	190	193	195	59	61	67	75	78	107	126	185	197	209
Millerite	avg	0.35	0.18	1.78	0.403	0.189	0.007	1480	638685	1.5	259	1576	1.21	18.45	0.005	0.02	10.9
(n=19)	min	0.16	0.01	0.14	0.003	0.001	0.002	758.3	618432	1.0	9.34	1328	0.03	1.89	0.002	0.003	0.85
	max	0.65	1.81	15.80	3.62	1.76	0.017	4818	677056	2.3	596.2	2084	5.07	219	0.012	0.06	72.3
	stdev	0.15	0.54	3.95	0.795	0.474	0.004	1001	14442	0.5	259.3	256.1	1.53	49.7	0.003	0.02	17.2

avg average, *min* minimum, *max* maximum, *stdev* standard deviation, *n/a* data not available, *n* number of lasered spots.

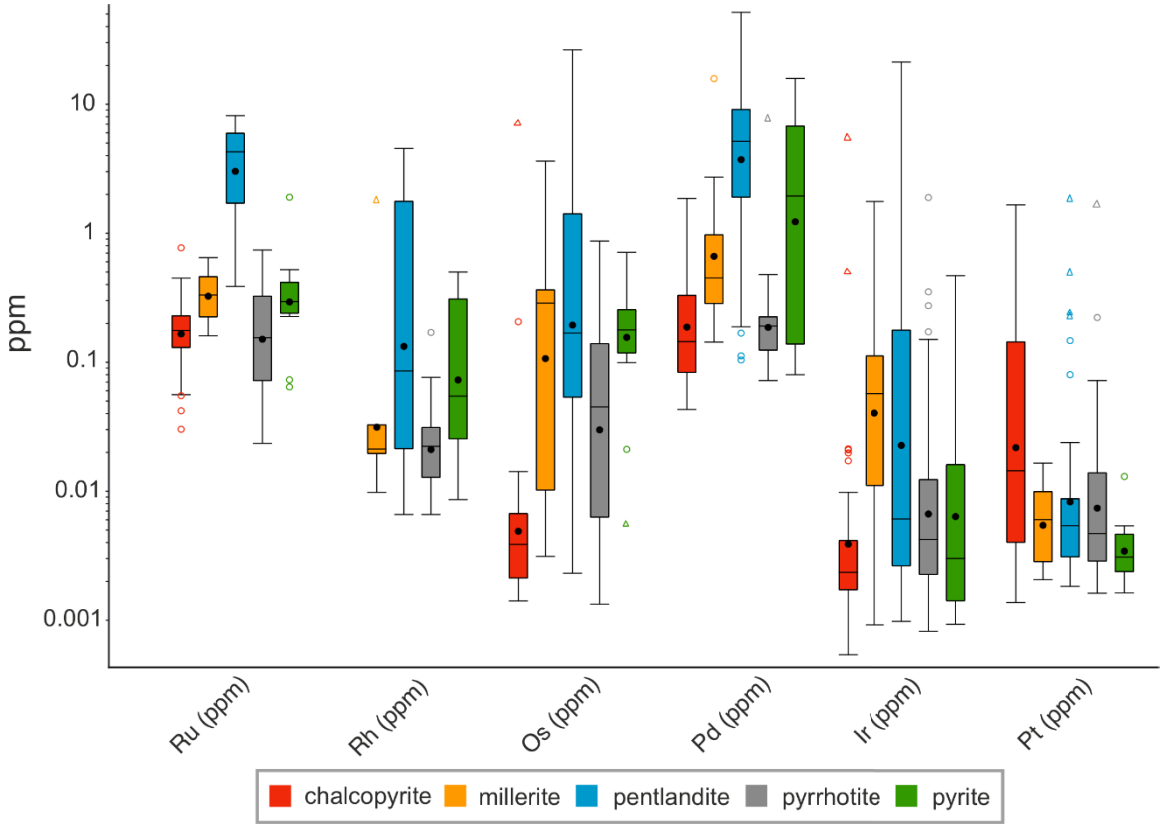

Figure 4-4: Box plot showing the spread of data for PGEs around the mean for different BMS phases at Kevitsa. See *Fig. 4-1* for explanation.

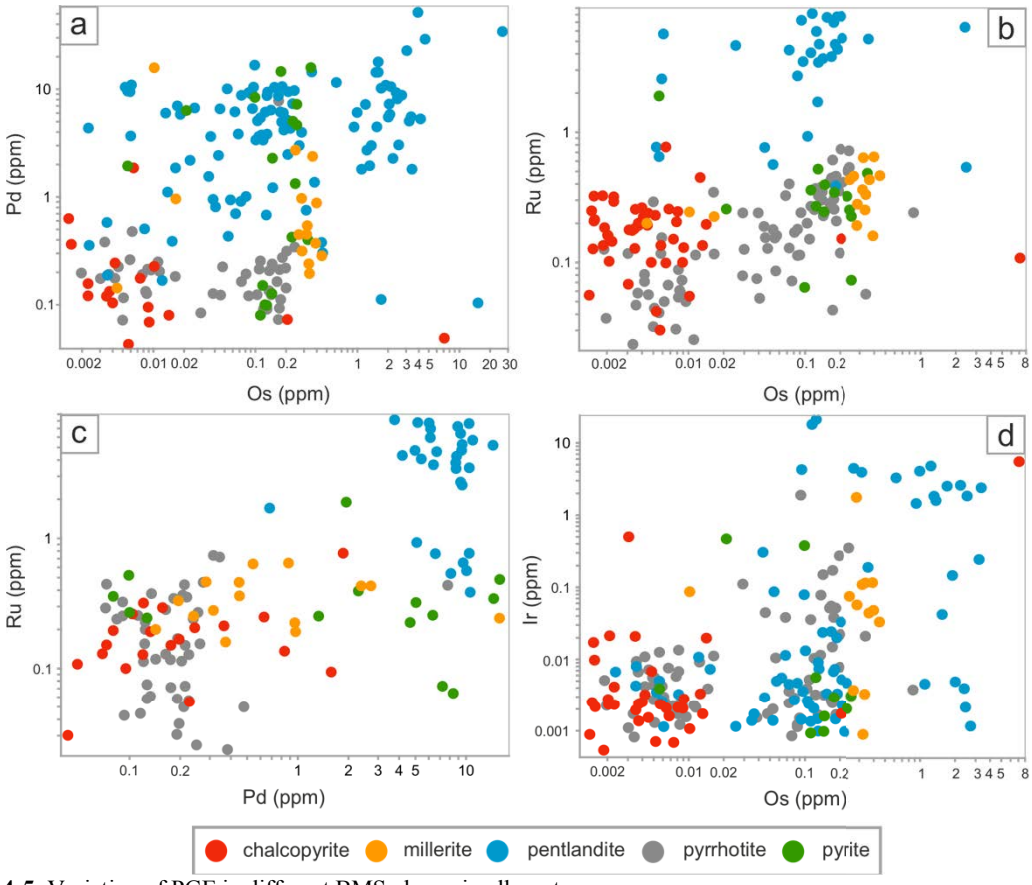

Figure 4-5: Variation of PGE in different BMS phases in all ore types.

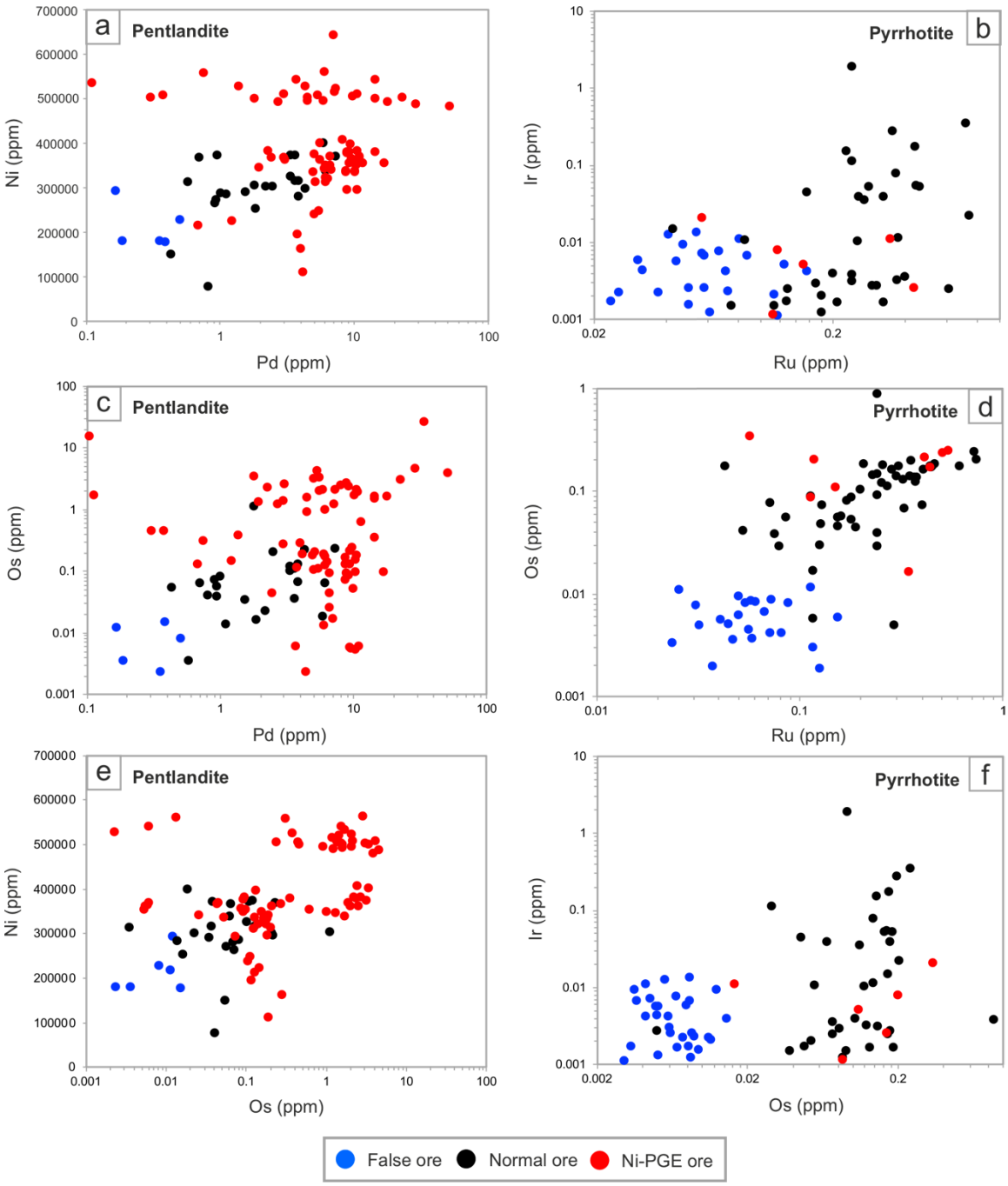

Figure 4-6: Variation of PGE concentrations in pentlandite (**a, c, e**) and pyrrhotite (**b, d, f**) showing the different ore types; false ore, normal ore and Ni-PGE ore.

Pentlandite shows a positive correlation between Pd and Ni, Os and Ru, and Pd and Os (*Fig. 4-6 a, c, e*), particularly in the Ni-PGE ore sulphides. Pyrrhotite shows a positive correlation between Ru and Os (*Fig. 4-6 d*) and a weaker positive correlation between Ru and Ir, and Os and Ir (*Fig. 4-6 b, f*), mostly in the normal ore sulphides.

4.2.1 Traverse Line Analyses

Two examples of TRA spectra from laser ablation spots are shown in *Figure 4-7*: (a) pentlandite from sample *R713 37.3* (Ni-PGE ore) and (b) chalcopyrite from sample *KV34B 327* (normal ore). A flat signal indicates that the element is present in solid solution within the mineral structure, whereas a peak would show with the presence of an inclusion.

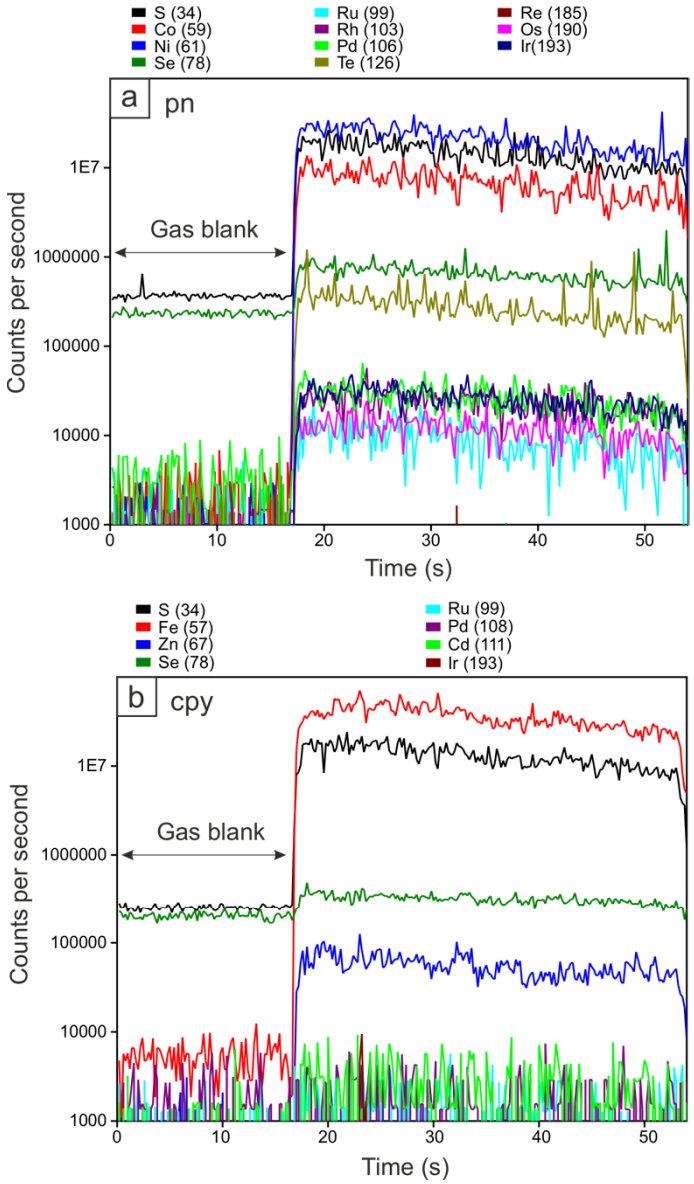

Figure 4-7: TRA spectra (counts per second *vs.* time in seconds) from laser ablation spots. **a** Pentlandite (*pn*) containing S, Co, Ni, Se, Ru, Rh, Pd, Te, Re, Os and Ir in solid solution. **b** Chalcopyrite (*cpy*) containing S, Fe, Zn and Se in solid solution and negligible amounts of Ru, Pd, Cd and Ir.

Pentlandite (*Fig. 4-7 a*) clearly shows higher counts of Ru, Os, Pd and Ir than chalcopyrite (*Fig 4-7 b*), which is the mineral phase with the lowest concentrations of all PGEs except Pt.

Traverse line analyses were conducted on 12 different BMS grains, most of which were pentlandite but also included millerite, chalcopyrite and pyrrhotite grains. Similarly to the spots shown in *Figure 4-7,* the spectra for the traverse line analyses would show peaks with the presence of an inclusion or PGM. These analyses revealed that in a few pentlandites, zoning of PGE could be seen. In one pentlandite grain from rim to core, Rh, Os and Ir decrease whereas Pd increases (*Fig. 4-8 A*). In another grain however, Pd showed no change (*Fig. 4-8 B*). All the pentlandites analysed in this way are from the Ni-PGE ore. No zoning was observed in lines analysed from millerite, chalcopyrite or pyrrhotite.

4.3 Other Chalcophile Elements

Generally, Ni-PGE ore sulphides hosts more Co, Se, As, Te, Au and Bi than the other ore types (*Fig. 4-9*). False and normal ore sulphides host more Zn (avg. 555 ppm and 314 ppm respectively) and Ag (avg. 3.48 ppm and 2.68 ppm respectively). The greatest variation occurs with Co, particularly in the normal ore sulphides (*Fig. 4-9*).

Co is the dominant trace element, hosted in all the base metal sulphide phases to some extent, but particularly in pyrite (avg. 6,052 ppm, up to 12,093 ppm) and pentlandite (avg. 5,557 ppm, up to 58,279 ppm, *Table 4-2, Fig. 4-10*). Pyrrhotite and chalcopyrite contain the lowest average concentrations of Co, although they have quite high maximum values (14,825 and 11,537 ppm, respectively). The largest spread of data occurs with chalcopyrite (*Fig. 4-10*) with a range of 0.1-11,537 ppm of Co. Millerite also contains reasonable amounts of Co, up to 4818 ppm. Pentlandite has the highest concentration of Co in normal ore, chalcopyrite in false ore and pyrrhotite in Ni-PGE ore (*Table 4-1*). Zinc is the most abundant trace element in chalcopyrite, particularly in false ore, with a maximum of 21,822 ppm. Se is found throughout the analyses, featuring a marked increase from false ore sulphides (24-98 ppm), to normal ore (122-289 ppm), to Ni-PGE ore (134-41,520 ppm) (*Fig. 4-11 d)*. Millerite hosts the most Se on average with 1,576 ppm, while pyrrhotite hosts the least with 155 ppm (*Table 4-2, Fig. 4-10*).

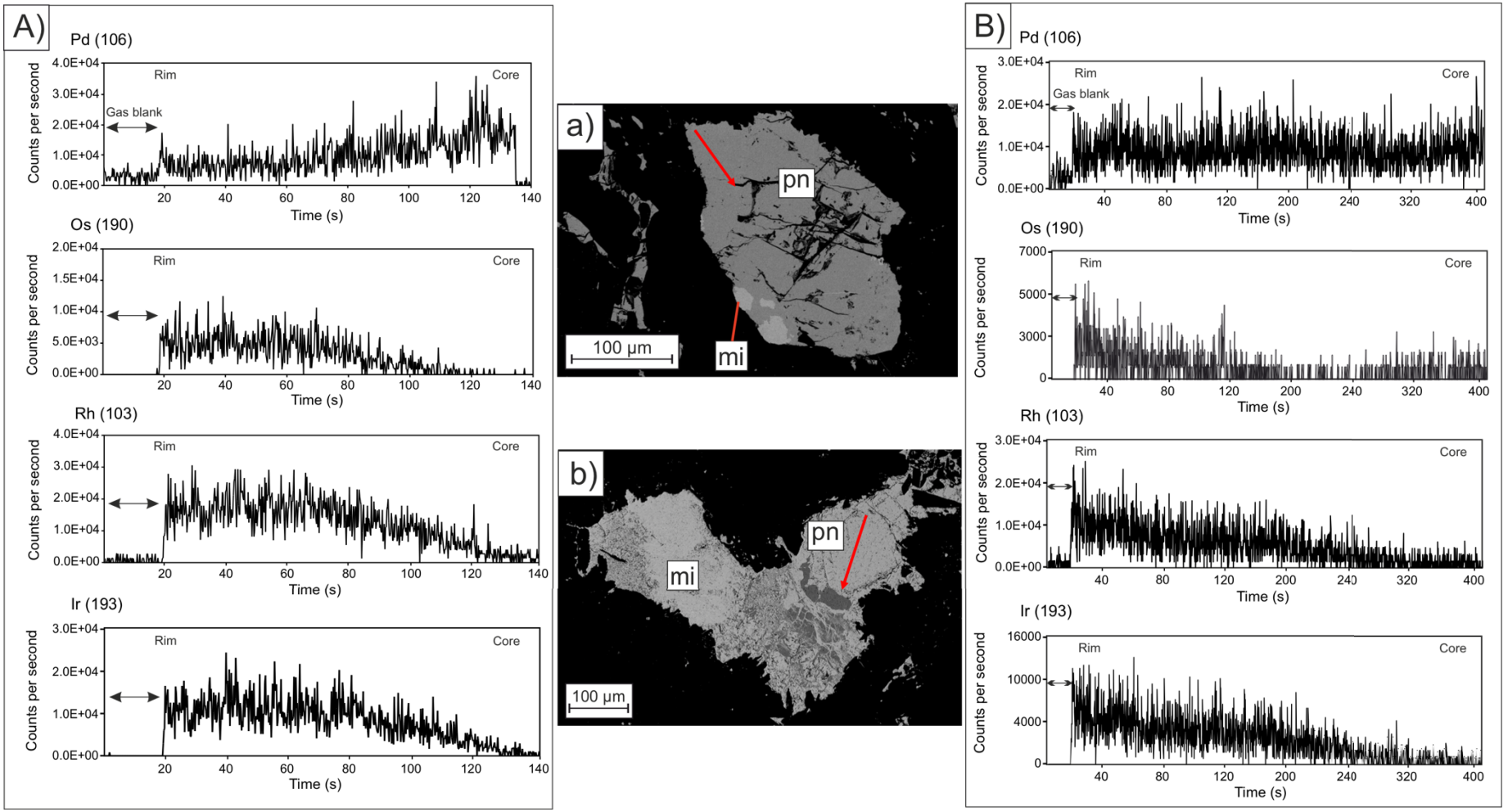

Figure 4-8: TRA spectra (counts per second vs. time in seconds) from a laser ablation lines across two pentlandite grains from Ni-PGE ore. Spectra **A** correspond to grain **a** from sample *R713 37.3*, spectra **B** correspond to grain **b** from sample *R695 68.1*.

Ni-PGE ore sulphides show an elevated amount of As (*Fig. 4-9*), particularly in pyrite (2,018 ppm), pentlandite (1,420 ppm) and millerite (596 ppm) (*Fig. 4-10*). Ag in sulphides is mostly quite low (avg. ~0.9-5 ppm) in all ore types (*Fig. 4-9*), although a small amount is hosted in chalcopyrite (max. 86.3 ppm) and pentlandite (max. 29 ppm) within false ore sulphides (*Table 4-1*). Te is low in false and normal ore sulphides (*Fig. 4-9*), but reaches 650 ppm in Ni-PGE ore pentlandite (*Table 4-1*). Bi is reasonably low in all ore types, but reaches 332 ppm in pyrite, 215 ppm in pentlandite and 145 ppm in pyrrhotite within Ni-PGE ore sulphides (*Table 4-1, Fig. 4-9*) . Au is very low throughout all sulphide phases (*Fig. 4-10*), with the highest value being 0.98 ppm in pyrite (*Table 4-2)*. Au and Ag and Te and Au show a positive correlation (*Fig. 4-11 b, c*), as does Te with all of the PGE. Se also produces a positive correlation with all PGE, with distinct zones for each ore type (*Fig. 4-11 d*).

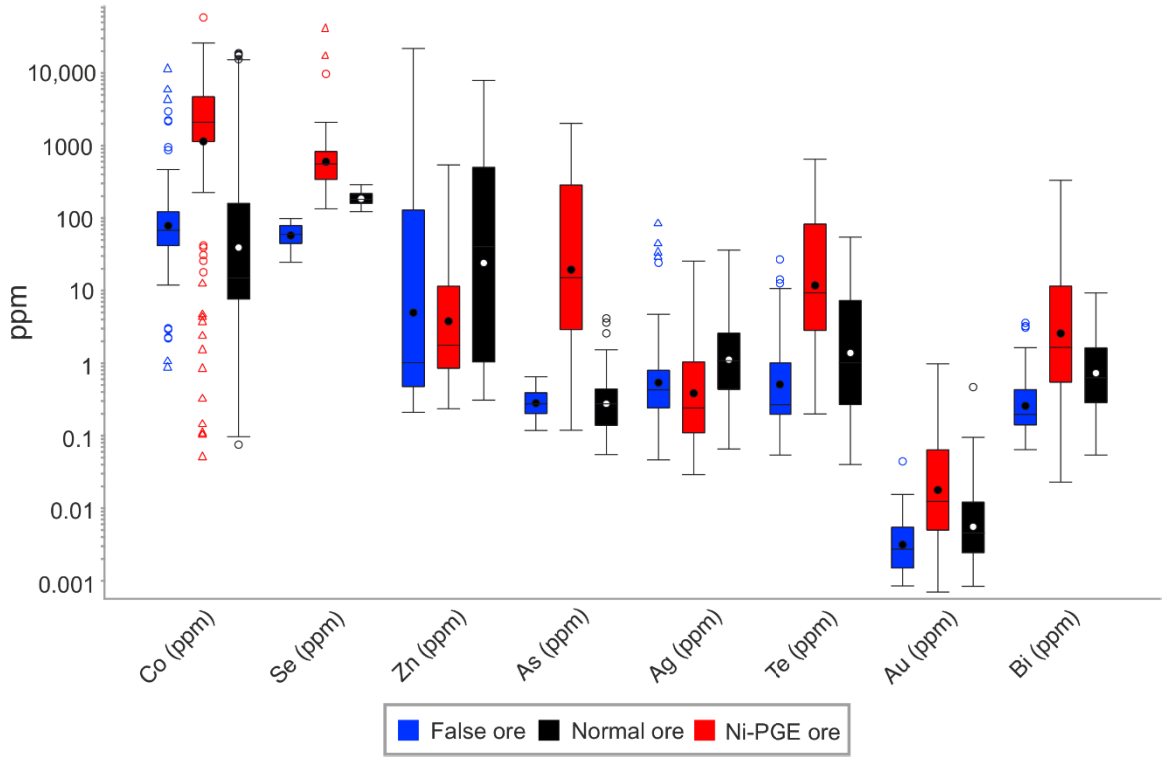

Figure 4-9: Box plot showing the spread of data for chalcophile elements around the mean for different ore types at Kevitsa. The box corresponds to the middle 50% of the data, with the bottom of the box representing the 25th percentile (Q1) and the top of the box representing the 75th percentile (Q3). The black circle and the line inside of the box represents the mean and median, respectively. Outliers (circles) are further than 1.5*(Q3-Q1) and far outliers (triangles) are further than 3*(Q3-Q1). Whiskers represent extreme values.

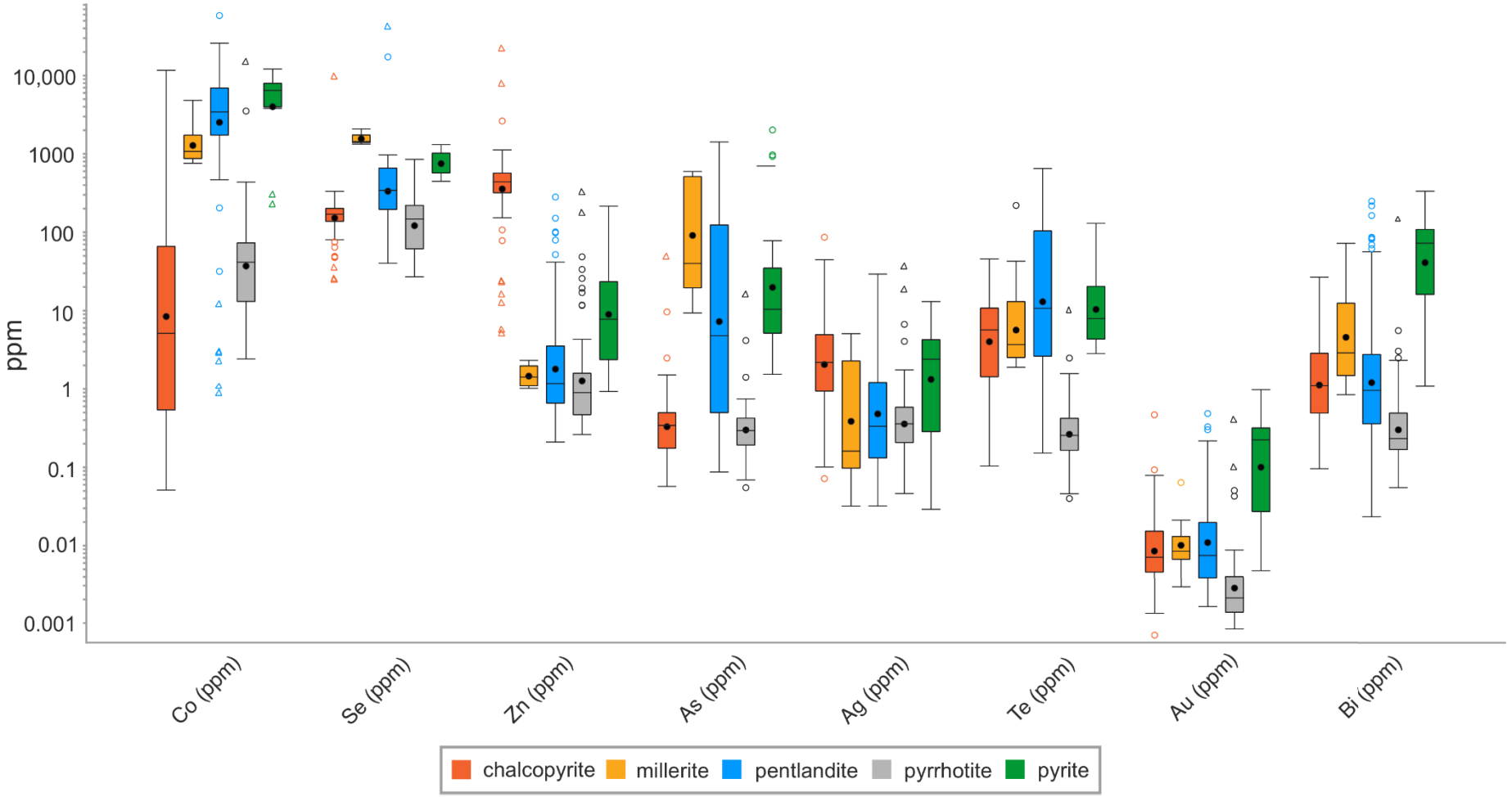

Figure 4-10: Box plot showing the spread of data for chalcophile elements around the mean for different BMS phases at Kevitsa. See *Fig. 4-9* for explanation.

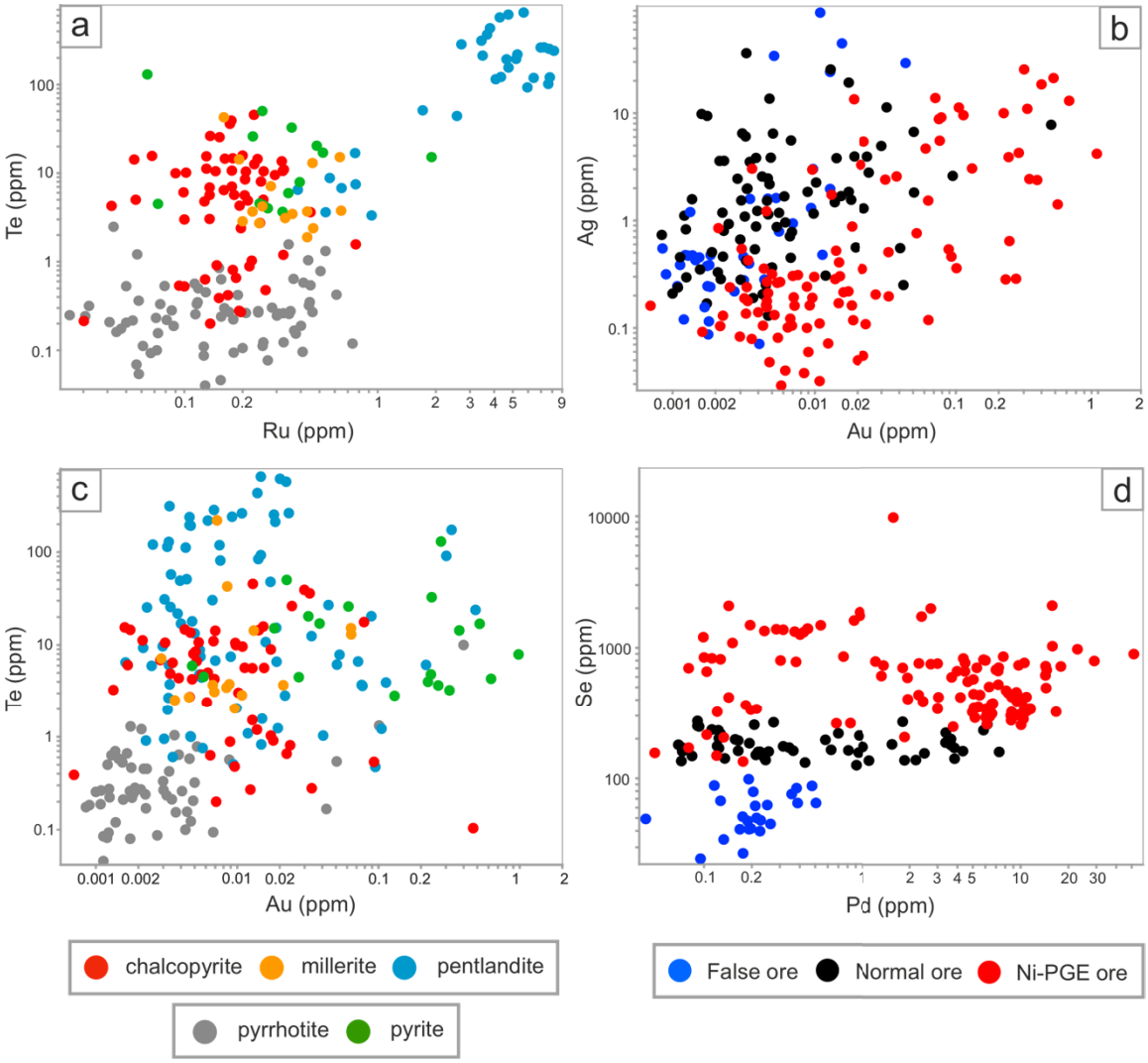

Figure 4-11: Variation of chalcophile element concentrations in different base metal sulphide phases (**a, c**) and ore types (**b, d**).

4.4 Mass Balance

Results of the 100% sulphide calculations are given in *Table 3-1* and in the *Appendix 8.2*. Ni, Cu, Pd and Pt tenor in 100% sulphide is also presented in *Figure 4-12*. The Ni-PGE ore samples have been separated into *KV* and *R* samples for comparison, as *R* samples appear to represent extremely high metal tenor (~40% Ni) end-members. The high Ni content was calculated for in the *R* samples but some inaccuracies remain and these calculations must be taken with caution.

Due to a lack of whole rock PGE data for false ore, the proportion of PGE hosted in BMS are only calculated for normal and Ni-PGE ore. Results from these mass balance calculations are summarised in *Table 4-3*. In addition, most normal and Ni-PGE ore samples did not have whole rock data for Os, Ir, Ru and Rh. Only *R* samples possessed data for all PGEs, which when used, produced values in excess of 100%. The whole rock data for Os, Ir, Ru and Rh is quite dated and may have produced large uncertainties in the mass balance calculation, whereas Pd and Pt are more thoroughly analysed in the mine and are more reliable. Therefore, Os, Ir, Ru and Rh in the mass balance calculation must be regarded as an approximation.

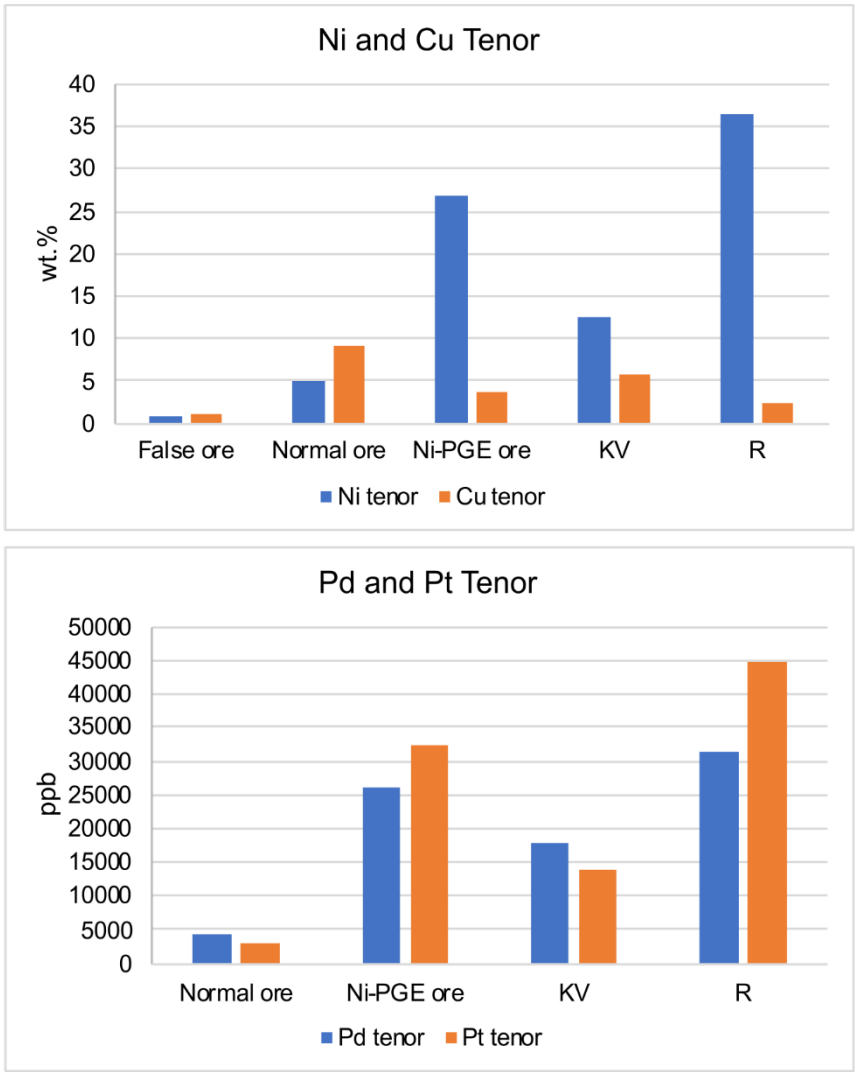

Figure 4-12: Ni, Cu, Pd and Pt tenors in 100% sulphide for false ore, normal ore and Ni-PGE ore. Ni-PGE ore is divided into KV and R samples for comparison.

Table 4-3: Proportion (%) of each PGE hosted in base metal sulphide for normal and Ni-PGE ore.

Sulphide	Fraction BMS	Element	Pd	Pt	Ru	Rh	Os	Ir
Normal ore								
Po	59.55	*n=56*	3.74	1.644				
Pn	13.98	*n=25*	10.03	0.05				
Cpy	26.47	*n=44*	0.51	0.86				
Sum BMS			14.27	2.554				
Ni-PGE ore								
KV45-63								
Po	41.26	*n=5*	0.59	0.017				
Pn	31.97	*n=14*	17.04	0.022				
Cpy	11.74	*n=0*	n/d	n/d				
Py	15.04	*n=3*	8.34	0.007				
Sum BMS			25.98	0.046				
KV45-75								
Po	19.42	*n=5*	2.02	0.007				
Pn	43.36	*n=15*	15.55	0.026				
Cpy	23.06	*n=1*	1.65	0.002				
Py	14.16	*n=10*	2.13	0.003				
Sum BMS			21.35	0.039				
R695 68.1								
Pn	46.68	*n=20*	10.29	0.563	83.53	85.69	118.8	56.83
Cpy	7.49	*n=3*	0.17	0.015	0.54	n/d	0.06	0.06
Py	20.15	*n=5*	2.93	0.002	3.43	4.8	8.9	4.11
Mill	25.7	*n=12*	0.39	0.003	5.47	0.55	9.09	0.89
Sum BMS			13.78	0.581	92.96	91.04	136.85	61.88
R695 69								
Pn	91.61	*n=17*	17.9	0.008	279.64	3.54	231.33	0.263
Cpy	7.89	*n=7*	0.03	0.001	1.04	n/d	0.08	0.06
Py	0.50	*n=1*	0.02	n/d	0.1	n/d	0.1	n/d
Sum BMS			17.94	0.009	280.77	3.54	231.51	0.32
R713 37.3								
Pn	60.60	*n=13*	25.45	0.137	122.51	67.73	96.84	73.48
Cpy	6.06	*n=0*	n/d	n/d	n/d	n/d	n/d	n/d
Mill	33.3	*n=7*	3.29	0.008	2.42	7.66	13.43	5.26
Sum BMS			28.74	0.145	124.93	75.4	110.27	78.74

Po pyrrhotite, *Pn* pentlandite, *Cpy* chalcopyrite, *Py* pyrite, *Mill* millerite, *BMS* base metal sulphide, *n/d* not determined, *n* number of lasered spots.

The mass balance calculations indicate, that with the exception of Ru and Os, little of the whole rock PGE is hosted within BMS. The elements with the smallest proportion within BMS are Pd and Pt, despite Pd being the most abundant PGE within BMS. In the normal ore, BMS host around 13% of Pd, mostly in pentlandite (~10%) (*Fig. 4-13 a*). BMS host much less Pt, with only 2.5% hosted in all BMS. A similar trend is seen for the Ni-PGE ore, where pentlandite dominates the budget with 10-25% of Pd and an overall share of 14-28% hosted in BMS.

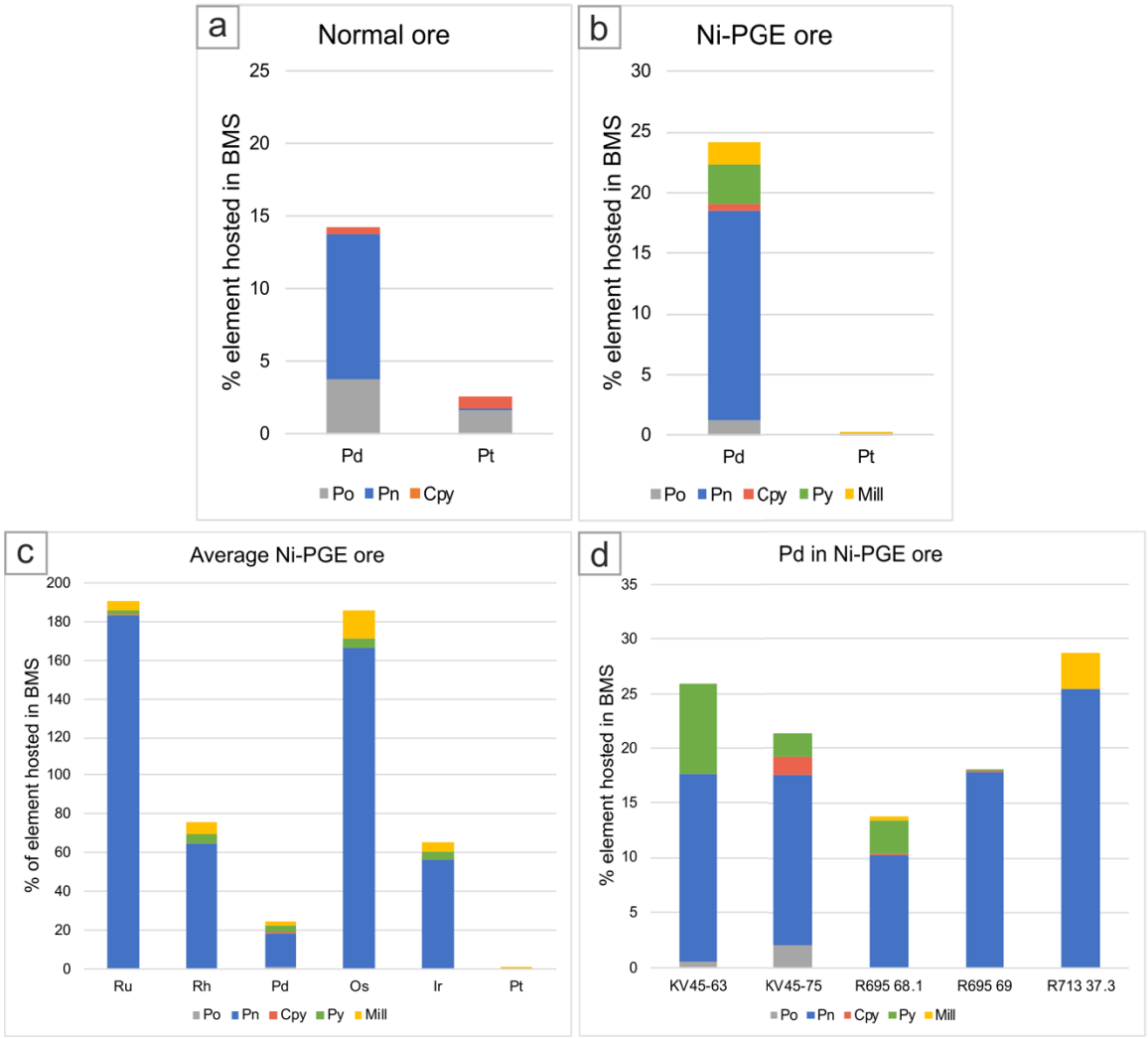

Figure 4-13: Mass balance of PGE in BMS from normal and Ni-PGE ore. **a** Average % Pd and Pt hosted by normal ore, **b** Average % Pd and Pt hosted by Ni-PGE ore, **c** Average % PGE hosted by Ni-PGE ore, **d** Pd hosted in different samples of Ni-PGE ore.

The Ni-PGE ore sulphides host even less Pt than the normal ore sulphides (<0.2% in all BMS). In the normal ore pyrrhotite hosts most of this Pt (1.644%), whereas pentlandite hosts more Pd (10.027%). As reflected in the LA-ICP-MS results, chalcopyrite and pyrrhotite host the lowest proportion of PGE in Ni-PGE ore whereas pentlandite hosts the majority (*Fig. 4-13 c*). Ru and Os are particularly high, with averages of 190% and 185% hosted within BMS respectively. Although this clearly demonstrates a large margin of error, it is plausible that these elements are predominantly hosted within BMS as IPGE partition into *mss* during sulphide liquid fractionation, rather than into *iss.*

This is supported by the majority of Ru and Os being hosted within pentlandite, with a small proportion hosted in pyrite (up to 3.53% Ru, 9.1% Os) and millerite (up to 5.6% Ru, 20.1% Os), all likely products of *mss*. Similarly, a large proportion of Rh (~75%) and Ir (~65%) are hosted within BMS, with pyrite and millerite combined making up around 10%.

There are some variations in Pd between the different Ni-PGE samples, particularly the *KV* and the *R* samples, shown in *Figure 4-13 d.* Although the sulphides in these samples contain similar proportions of Pd (13-28%), the role of other phases than pentlandite between the samples is quite different. Pyrite hosts a negligible amount of Pd in most samples but reaches 8.3% in *KV45-63* and seems to host more PGE in the *KV* samples than *R* samples. The sample hosting the least Pd is *R695-68.1* with 13% of Pd hosted in all BMS, whereas *R713-37.3* hosts the largest proportion (28.7%). Interestingly, *R695-68.1* is the sample with the largest proportions of Ru and Os (>200%), which may indicate underestimations in the whole rock data for these elements. Sample *R713-37.3* hosts almost double the Pd than *R695-68.1* in pentlandite alone, with a small proportion hosted by millerite (3.3%). *KV* samples also host small amounts of PGE in pyrrhotite (0.5-2%), while *R* samples are largely devoid of this phase. The absence of pyrrhotite may contribute to higher proportions of PGE being hosted in pentlandite, effectively reducing the amount of 'dilution' by mostly barren BMS phases like pyrrhotite and chalcopyrite. The *KV* samples share similar proportions of Pd hosted by pentlandite, whereas the *R* samples show much more variation, from 13-28%.

The mass balance results are in agreement with the whole rock metal tenors, where the *R* samples contain higher Pd tenor in 100% sulphide than *KV* samples (*Fig. 4-12*), although the difference is much less than expected. The *R* samples, and indeed Ni-PGE ore as a whole, has much higher Pt tenor than Pd, which is not reflected in the LA-ICP-MS data nor the mass balance results. This can be explained by platinum group minerals (PGMs) taking up the bulk of the Pt budget. The elevated proportion of PGE in pentlandite in the *R* samples may also have a relationship with high Ni tenor (*Fig. 4-12)*, as these samples feature extreme Ni tenors of 40% and Ni has been shown to positively correlate with Pd and Os (*Fig. 4-6 a, e*). The difference in proportions of sulphide-hosted Pd, Pt and IPGEs may be related to the role of PGMs, arsenides and sulpharsenides found within *R* samples.

5 DISCUSSION

This section attempts to amalgamate the findings of this study and compare them with previous studies of the Kevitsa Ni-Cu-(PGE) deposit in addition to studies from other PGE-rich deposits elsewhere. Aspects of the genesis for the Ni-PGE ore are derived from these comparisons and the evidence for magmatic *vs.* hydrothermal processes can be considered.

5.1 Comparison with Previous Studies on Kevitsa Ni-PGE Ore

There are two studies in the literature considering the sulphide trace-elements of the Kevitsa Ni-Cu-(PGE) deposit, namely by Gervilla and Kojonen (2002) and Cabri, et al. (2017). Cabri, et al. (2017) used LA-ICP-MS to analyse trace element concentrations of heavy mineral concentrate, typical run-of-mine samples with elevated levels of PGE. They analysed sulphides, sulpharsenides and arsenides as potential carriers of PGE, including pentlandite, pyrite, gersdorffite (NiAsS), maucherite ($Ni_{11}As_8$) and nickeline (NiAs). Their findings are quite different from those from this study, including a much higher concentration of Pd found in pentlandite (up to 256 ppm, avg. 21 ppm) compared to this study (up to 51 ppm), although the concentration of Pt is similar (0.14 ppm). They also measured much lower concentrations of Os, Ir and Rh (0.74 ppm, 0.21 ppm and 0.3 ppm respectively), which more resemble the results for normal ore in this study. The average results from this study for Ni-PGE ore sulphides are much higher (1.3 ppm Os, 1.1 ppm Ir and 1.06 ppm Rh). In contrast, Cabri, et al. (2017) measured higher IPGE and Rh concentrations for pyrite, with variable concentrations of Rh (1.62 ppm), Os (1.39 ppm) and Ir (1.95 ppm), over 1 ppm higher than the averages found in this study. Cabri, et al.'s study also found pyrite to be almost barren in Pd (0.01 ppm) and Pt (0.07 ppm), whilst our results show much higher Pd of 4 ppm on average. Cabri, et al. (2017) found that the principal carriers of Pd were gersdorffite (up to 1563 ppm, avg. 128 ppm), and maucherite (up to 1183 ppm, avg. 151 ppm), while nickeline was a significant carrier of Au (up to 74.1 ppm). However, as is the nature with any comparison, one must consider the critical differences between the studies – analysis of upgraded run-of-mine samples are not as representative of the deposit as *in-situ* samples, which make up this paper.

Gervilla and Kojonen (2002) conducted a detailed study of polished sections from two drill holes also used in this study, *R695* and *R713,* to assess the main carrier minerals of PGE for the purpose of exploration. Similar caution should be taken when comparing these results due to their use of electron probe micro-analyser (EPMA) with a much higher limit of detection and smaller excitation volume than LA-ICP-MS (Cabri, et al., 2003). Nonetheless, Gervilla and Kojonen's results share some similarities to those found in this study, with an average of 51.6 ppm Pd found in pentlandite and up to 30 ppm in pyrite. In contrast, they found higher concentrations of Pt in pentlandite with pyrite intergrowths (42 ppm) and chalcopyrite (34-54 ppm), and Rh was only found in gersdorffite. No data was provided on Ir and Os. The results for arsenides and sulpharsenides are in agreement with Cabri et al. (2017), with the main carriers of PGE (especially Pd) being gersdorffite, maucherite and nickeline.

5.2 Comparison With Other Deposits

Barnes, et al. (2008) compared the sulphide mass balances (*Fig. 5-1*) and mantle normalised metal patterns (*Fig. 5-2*) for PGE-rich sulphides from deposits in different geological settings. They proposed that the distribution of PGE among BMS and PGM depends on the rate of cooling, interaction of BMS with deuteric fluids, and metamorphism. Deposits that cooled relatively quickly, such as the sulphides from a sub-volcanic sill at Noril'sk (Barnes, et al., 2006) contain 80-120% of PGE in solid solution with BMS (*Fig. 5-1 c*) with the exception of Pt, which forms discrete PGMs. Deposits within large layered intrusions such as the *Platreef* (Holwell & McDonald, 2007) and *Merensky Reef* (Godel, et al., 2007; Barnes, et al., 2008) of the Bushveld Complex, which cooled relatively slowly, contain a much smaller proportion of PGE in BMS (20-70%) (*Fig. 5-1 b*). Barnes, et al. (2008) attributes this to the possible interaction of BMS with late magmatic fluids, allowing PGM to exsolve or crystallise from BMS at a greater degree than in fast cooling sub-volcanic sills (Shelley, 1992). Barnes, et al. (2008) also interpret Pt-bearing PGMs to be exsolutions from BMS, explaining the presence of Pt mineral inclusions in BMS at Noril'sk.

The Penikat intrusion, like the Kevitsa intrusion, has undergone greenschist facies metamorphism (Alapieti & Lahtinen, 1986) and feature textural relationships that indicate extensive low temperature recrystallisation of BMS, such as ragged, irregular sulphide grain boundaries (*Fig. 5-3*) (Barnes, et al., 2008). As a consequence, the proportion of PGE hosted within BMS is more variable than in unmetamorphosed reefs, and also features a higher abundance of PGM grains (over 100 grains per thin section, as opposed to 40-60 in unmetamorphosed samples) (Barnes, et al., 2008).

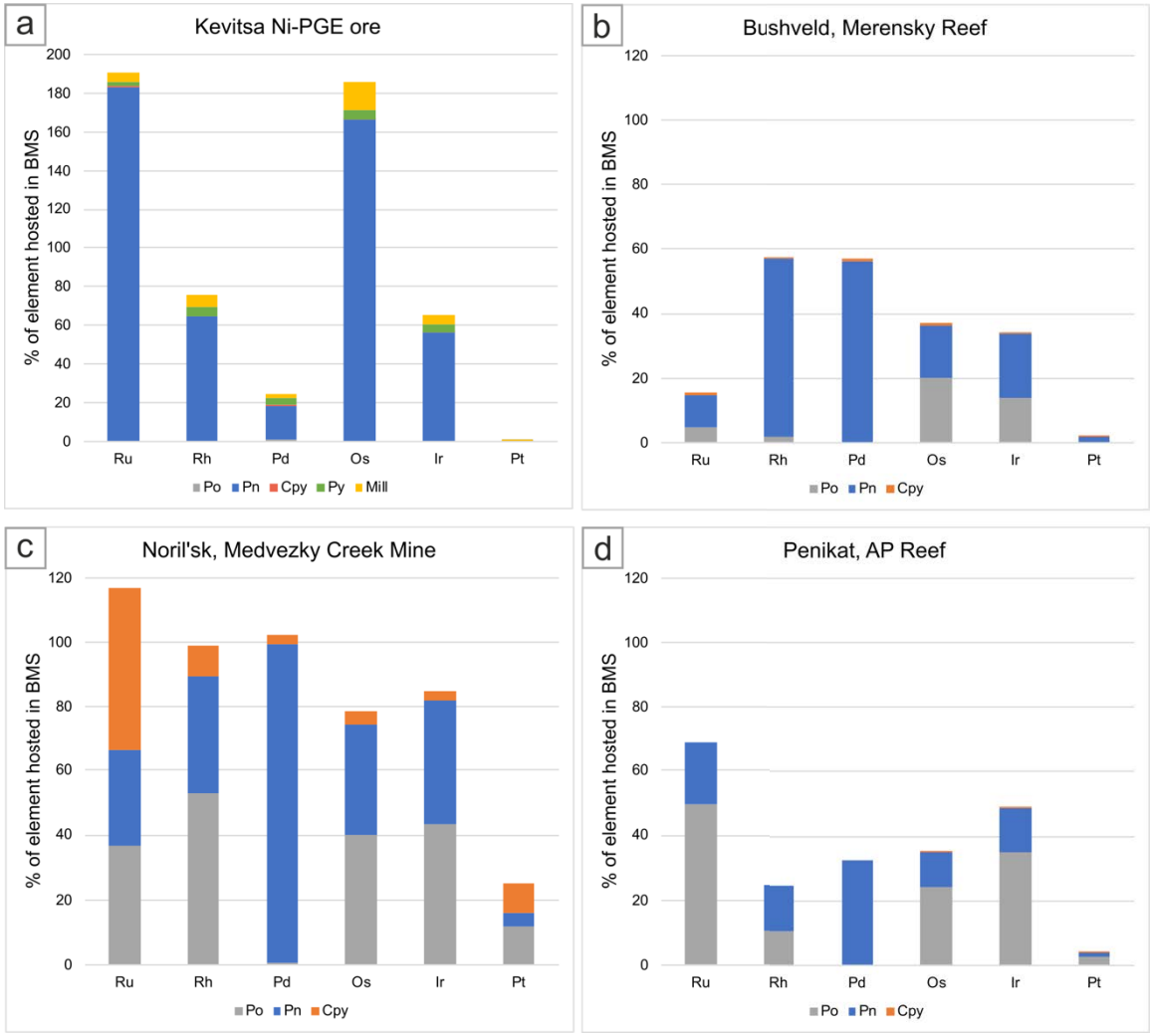

Figure 5-1: Mass balances of PGE in base metal sulphides (BMS) from different PGE-rich deposits. *Po* pyrrhotite, *Pn* pentlandite, *Cpy* chalcopyrite, *Py* pyrite, *Mill* millerite. **a** Disseminated sulphides from Ni-PGE ore, Kevitsa (this study). **b** Disseminated sulphides from the Merensky Reef, Bushveld (Godel, et al., 2007; Barnes, et al., 2008). **c** Sulphide droplets from a subvolcanic sill, Noril'sk (Barnes, et al., 2006; Barnes, et al., 2008). **d** Disseminated sulphides from AP Reef, Penikat intrusion (Barnes, et al., 2008).

Barnes, et al. (2008) suggest that this is a result of PGM exsolving from BMS before growing in size during metamorphism due to recrystallisation of BMS and the presence of metamorphic fluids, which would enhance the diffusion of PGE. The Penikat reefs also contain a large proportion of PGM that are not in contact with BMS, but isolated within silicates (50-70%, Halkoaho 1994; Huhtelin, et al. 1990) as does Kevitsa (54%, Gervilla and Kojonen, 2002). Barnes, et al. (2008) interpret these isolated PGMs a number of ways: BMS could have been dissolved leaving Pd-bismuthotellurides behind, bismuthotellurides could have been locally redistributed to surrounding grains during metamorphism, and/or Pd could have been added to the AP-reef rocks, being precipitated as isolated PGM (Boudreau & Meurer, 1999).

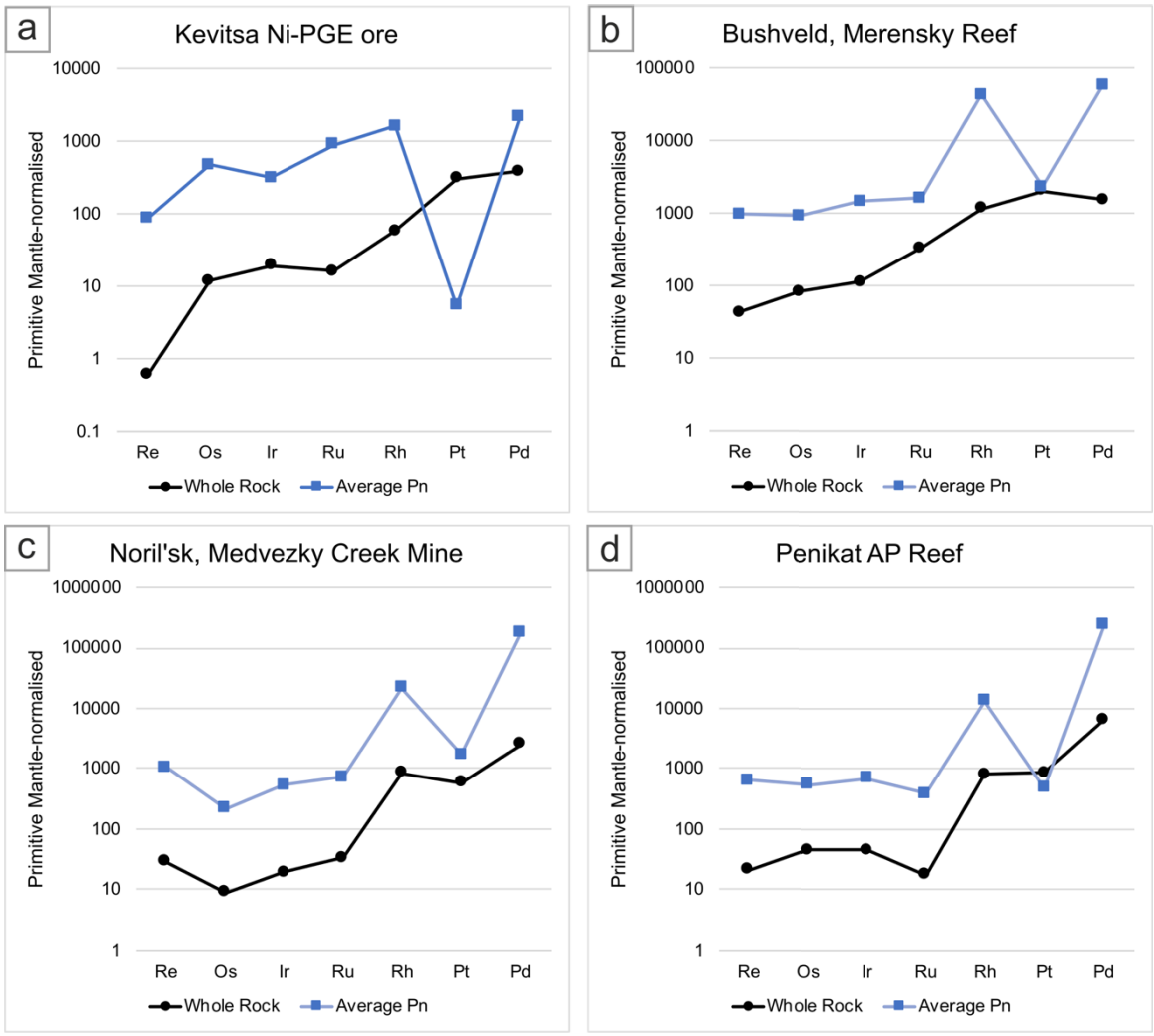

Figure 5-2: Mantle-normalised PGE patterns for pentlandite (blue) and whole rock compositions (black) of Kevitsa and other PGE-rich deposits. **a** Ni-PGE ore, Kevitsa (this study). **b** Merensky Reef, Bushveld (Godel, et al., 2007; Barnes, et al., 2008). **c** Medvezky Creek Mine, Noril'sk (Barnes, et al., 2006; Barnes, et al., 2008). **d** AP Reef, Penikat intrusion (Barnes, et al., 2008)**.** Normalisation values from Mcdonough and Sun (1995).

In contrast, Hutchinson and McDonald (2008) propose that at the Platreef, the amount of semimetals (As, Bi, Te) present in the sulphide melt may have a significant effect on whether PGM crystallise early from the melt at high temperatures or that PGE are hosted by the BMS and later exsolved as discrete PGMs.

Mantle normalised PGE patterns in whole rock and pentlandite for different deposits are shown in *Figure 5-2*. Generally, the patterns are flat from Re to Ru, with a sharp increase in Rh for all the compared deposits, but not Kevitsa. In comparison to whole rock Pt content, pentlandite in all the deposits show strong negative Pt anomaly, consistent with Pt being present as discrete PGM phases. IPGE are shown to be present in solid solution with pentlandite, with an enrichment in Pd (*Fig. 5-2 a-d*). The patterns for Merensky Reef (*Fig. 5-2 b*), both whole rock and pentlandite, show similarities to Kevitsa's (*Fig. 5-2 a*), which may indicate similarities between their relative cooling histories.

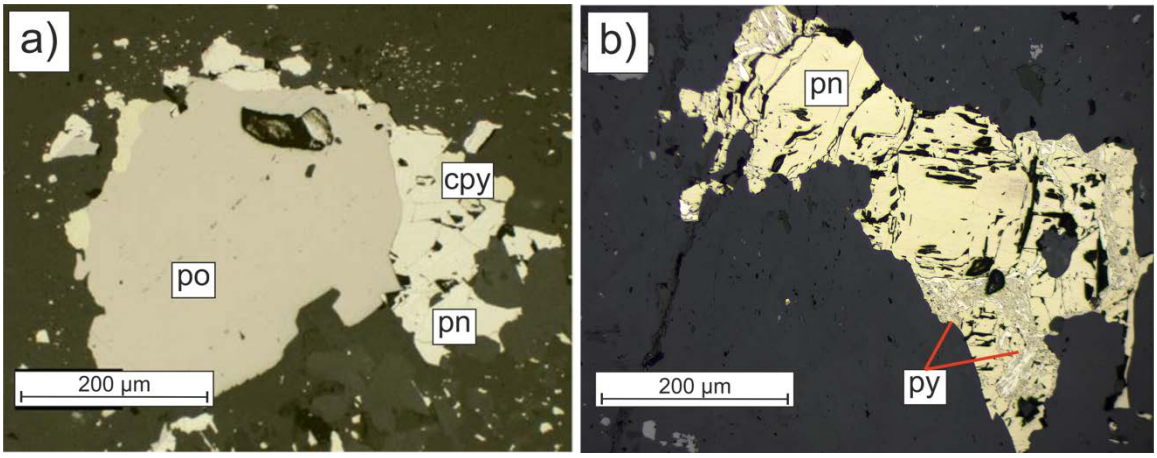

Figure 5-3: Photomicrographs of base metal sulphides (BMS). *po* pyrrhotite, *pn* pentlandite, *py* pyrite, *cpy* chalcopyrite. **a)** *After Barnes, et al. (2008)*. Penikat AP-reef, showing irregular grain boundaries, which suggests that the sulphides are not in textural equilibrium, **b)** Sample *R695 69* from the Kevitsa Ni-PGE ore.

5.3 Processes That Control the Distribution of PGE in BMS in the Ni-PGE Ore

5.3.1 Magmatic Processes

5.3.1.1 Diffusion of Pd into Pentlandite

There have been many experimental and empirical studies of the Fe-Ni-Cu-S system, which also investigate the fractionation of chalcophile elements during the crystallisation of monosulphide solid solution (*mss*) from a sulphide melt at 1,180-950°C (Fleet, et al., 1993; Li, et al., 1996; Barnes, et al., 1997; Ballhaus, et al., 2001; Mungall, et al., 2005; Naldrett, 2004). IPGE, Re and Co partition into *mss*, whereas PPGE, Au, Ag, As, Bi, Cd, Sb, Sn, Te, Pb and Zn are incompatible and concentrate in the residual Cu-rich liquid, from which intermediate solid solution (*iss*) crystallises at 950-840°C (Dare, et al., 2010). The partition coefficient for Ni into *mss* is slightly below 1 at high temperatures and increases as temperatures falls (Li, et al., 1996; Barnes, et al., 2001). *Mss* cools to exsolve Fe-rich and Ni-rich portions, which in turn exsolves to pyrrhotite and pentlandite at temperatures of 650°C and below, whilst chalcopyrite exsolves from *iss* (Barnes, et al., 2006). It is this late stage of crystallisation that is preserved as trace element compositions within BMS that we observe with LA-ICP-MS analysis.

According to the LA-ICP-MS results (*Table 4-1, 4-2*) and the mass balance calculations (*Fig. 4-13*) pentlandite is the principal BMS phase that hosts PGEs, particularly Pd. However, this is counterintuitive as Pd is incompatible in *mss*, from which pentlandite exsolves, and should thus partition into the Cu-rich liquid before partitioning into either *iss* or into a late stage melt upon cooling (Dare, et al., 2010). Therefore, Pd is expected to be present in chalcopyrite, which is not observed here. A similar enigma has been observed at the *Creighton Deposit*, Sudbury, where Dare, et al. (2010) found that the amount of Pd in pentlandite varied according to texture and the amount of chalcopyrite in the sample. Most of the Pd diffused into pentlandite at high temperature when the cores of coarse granular pentlandite formed, at temperatures of 650-400°C. Pd diffused from both the *mss*/pyrrhotite and the Cu-rich liquid, depleting the nearby *mss*/pyrrhotite in Pd. This study supports this theory as pyrrhotite is very depleted in PGE. Furthermore, *Figure 4-8 A* shows some zonation in pentlandite with Pd being enriched at the core, possibly indicating diffusion at an early stage. A similar approach may be applied to IPGE, whereby pyrrhotite is depleted

of these elements as they diffuse into nearby pentlandite. This would explain the increase of Os, Ir, and Rh towards the rim of pentlandite (*Fig. 4-8 A, B*). Similarly with this study, pentlandites at Creighton did not deplete pyrrhotite in Co because the *mss* contained larger concentrations of Co than Pd, resulting in high concentrations of Co in solid solution with pyrrhotite (avg. 1,519 ppm in Ni-PGE ore). In contrast, samples at Creighton with >10% chalcopyrite have higher concentrations of Pd (Dare, et al., 2010), whereas samples from Kevitsa, particularly the *R* samples, have higher Pd contents whilst being Cu-poor.

Other studies have also found pyrrhotite to be enriched in IPGE (Platreef: Holwell and Mcdonald, 2007; Merensky Reef: Ballhaus and Sylvester, 2000; Sandsloot: Barnes et al 2006) whereas this is not seen at Kevitsa. In particular, the *R* samples have very low fractions of chalcopyrite (up to 7.4% of total sulphide) and an absence of pyrrhotite altogether. As a consequence, the absence of a large Cu-rich portion and pyrrhotite may have caused the PGE to partition into whatever was available – Ni-rich *mss* and exsolving PGM, arsenides and sulpharsenides.

5.3.1.2 Formation of the Pentlandite-Pyrite-Millerite Assemblage in the Ni-PGE Ore

Experimental studies in regard to phase relations in the Fe-Ni-S system at 725°C have shown that Ni-rich pyrite forms slightly above 725°C in equilibrium with *mss* (Karup-Møller & Makovicky, 1995). As temperature falls, Ni-rich *mss* decomposes, forming pyrite and pentlandite at 230°C, which explains the existence of pyrite-pentlandite intergrowths in many of the samples in this study (*Fig. 2-9, Appendix 8.1*) and those studied by Gervilla and Kojonen (2002). Millerite can form as an oxidation product of BMS during hydrothermal alteration (Nickel, et al., 1974; Nickel, et al., 1977). This is seen in the Vaara Ni sulphide deposit, in which both silicates and sulphide minerals have been intensively altered, shown in millerite as clear replacement textures over BMS (Konnunaho, et al., 2013). The well preserved texture of millerite in this study indicates that the oxidation of BMS cannot account for the formation of millerite in Kevitsa. Barnes, et al. (2011) explains the presence of this sulphide assemblage in the context of *Betheno*, Western Australia, which features extremely high Ni tenor within komatiitic dunites. They explain the Ni-rich assemblage as either a product of a very Ni-rich magma, and/or by low temperature unmixing of an originally Ni-rich *mss* phase, which also explains the high PGE tenor of the deposit.

This study has shown that at Kevitsa, the Ni-PGE ore has much higher metal tenor (Ni, Pd and Pt) in 100% sulphide than the other ore types (*Fig. 4-12*), and pentlandites in the Ni-PGE ore also display a higher PGE content (Pd, Ir, Os, Ru) than those of the normal ore (*Fig. 4-6*). These features indicate that the Ni-PGE ore formed from a sulphide melt with a higher metal content than the normal ore. The high Ni also observed in olivines and pyroxenes in the Ni-PGE ore (Yang, et al., 2013) also suggest that the silicate melt with which the sulphide melt equilibrated was also metal-rich. Therefore, similarly to Betheno, the pentlandite-pyrite-millerite assemblage present in the Ni-PGE ore at Kevitsa may have formed primarily by magmatic processes.

5.3.1.3 Sulphide Fractionation and Crystallisation of a Semimetal-rich Residual Liquid

The formation of arsenide-rich sulphides of the Ni-PGE ore is more complex than simply sulphide liquid fractionation. During experiments on the partitioning behaviour of PGE in the Fe-Ni-Cu-S system in the presence of minor amounts of Bi, Te and As, Fleet, et al. (1993) found that during quenching, these elements segregate as a residual liquid, into which Pt partitions preferentially over Pd. Experiments of sulphide-telluride systems by Helmy, et al. (2006) also indicate that telluride and bismuthide (and antimonide) melts remain immiscible in a sulphide melt when temperatures fall below 1000°C, and remain liquid at temperatures where sulphide reaches its solidus. This forms a residual liquid that Pt and Pd both strongly partition into, and since Pt and Pd are more strongly complexed with Te and Bi than S, Pd will only enter *mss* when the Pd/semimetal ratio is sufficiently high to produce an excess of Pd that cannot be fully accommodated by this residual semi-metal melt (Helmy, et al., 2006). There are a number of studies that suggest that Pt, Pd and Au, along with semimetals, are concentrated in a late-stage residual liquid after the crystallisation of *iss,* which is then expelled to sulphide grain boundaries (Cabri & LaFlamme, 1976; Prichard, et al., 2004; Barnes, et al., 2008; Holwell & McDonald, 2006; Holwell & McDonald, 2007; Dare, et al., 2010). This residual liquid crystallises to form PGMs around the margins of sulphide grains, which is the case with 39% of PGMs at Kevitsa (Gervilla, et al., 2004). Later hydrothermal alteration of sulphide blebs at a local scale may expel PGMs and isolate them within secondary silicates (as seen in the Platreef, Holwell and Mcdonald 2007). This is also observed at Kevitsa, with 54% of PGMs as isolated grains within secondary silicates (Gervilla, et al., 2004).

The presence of a semimetal-rich residual liquid is supported by this study in that there is a marked increase in abundance of Bi, Te and As within pentlandite, pyrite and millerite in Ni-PGE ore, particularly in the *R* samples, indicating the high availability of these elements during sulphide fractionation. Arsenic appears to have been accommodated in *R* samples by arsenides, sulpharsenides and BMS, alongside a semimetal-rich residual liquid which later crystallised into PGMs such as sperrylite. Textural relationships between nickeline, maucherite and sulphides (e.g., gersdorffite coronae around Ni arsenides) indicates the formation of these minerals at a late stage of sulphide fractionation (Gervilla and Kojonen, 2002).

5.3.2 Hydrothermal Processes

5.3.2.1 Isolated PGMs Within Silicates

Gervilla and Kojonen (2002) noted that PGMs in the Kevitsa Ni-PGE ore are commonly associated with hydrous silicates or occur at the contacts between sulphides and silicates, which led them to attribute the origin of the Ni-PGE ore to hydrothermal and metamorphic processes. Based on experimental data by Kim, et al. (1990) and Shunk (1969), they suggested that moncheite ($PtTe_2$) and merenskyite ($PdTe_2$) crystallised at below magmatic temperatures due to the substitution of Te for Bi and of Pt for Pd. Michenerite (PdTeBi) is only stable below 500°C (Hoffman & MacLean, 1976), although this mineral may have exsolved from BMS, as is the case for the Merensky Reef (Barnes, et al., 2008) and/or crystallised from small volumes of late stage melt, as is the case at Sudbury (Cabri & LaFlamme, 1976).

The presence of Pd and Pt sulphides, such as cooperite (PtS) and braggite [(Pt,Pd)S] in the Ni-PGE ore support the theory of hydrothermal ore-forming processes, as they are metastable phases which result from the loss of Pd during hydrothermal alteration (Verryn & Merkle, 2002). Isolated PGM grains within silicates may have formed as more soluble BMS are dissolved, leaving behind insoluble grains of michenerite, as is the case at Great Dyke (Oberthür, et al., 2003), Raglan (Seabrook, et al., 2004) and the Merensky Reef (Li, et al., 2004). However, samples from Kevitsa do not seem to have suffered such severe

hydrothermal alteration that would completely dissolve sulphides, even in 'high alteration' samples, such as *R695-69* (*Fig. 5-3*).

5.3.2.2 Metamorphism and Serpentinisation

Gervilla and Kojonen (2002) suggest that metamorphism-related hydrothermal alteration may have remobilised PGE in the form of Cl-complexes and precipitate them in discrete horizons. They observed that the Ni-PGE ore does not form continuous horizons, as is the case with other PGE-rich deposits (e.g. Bushveld; Maier & Groves, 2011), but instead forms discontinuous bands at variable depths. There have been many studies of late magmatic and/or hydrothermal activity with low temperature (540-130°C) aqueous fluids in the context of footwall-style deposits at Sudbury (Farrow, 1994; Farrow & Watkinson, 1999; Hanley, 2005). These studies suggested that these highly saline, chlorie-rich fluids were responsible for remobilising PGE. However, Wood (2002) demonstrated that this is not possible, as the reduced and neutral pH conditions present in Ni-Cu-(PGE) deposits cause Pt and Pd to be insoluble in Cl-rich fluids. Furthermore, the presence of S, Se, Fe, As, Te, Sn, Sb, Cu, Bi and Ag will further limit the solubility of PGE in hydrothermal fluids (Wood, 2002). Therefore, it is unlikely that hydrothermal fluids remobilised PGE to form PGE-rich horizons at Kevitsa.

Gervilla and Kojonen (2002) also stated that serpentinisation could have liberated As, stabilising maucherite-bearing (Ni-rich) assemblages. This stabilisation of pentlandite and maucherite may have preserved and enriched the Pd content of these minerals (Gervilla, et al., 1994; Makovicky, et al., 1986). However, in a study by LeVaillant, et al. (2016), they showed that hydrothermal alteration (serpentinisation, amphibolitisation and epidotisation) has only had an effect on the distribution of PGE at Kevitsa at a centimetre to decimetre scale. Evidence for this includes the absence of decoupling in Pd and Pt concentrations, which would be expected with hydrothermal alteration, since Pd is more soluble than Pt (Wood, 2002; Hanley, 2005; Barnes & Liu, 2012). There is also a tight correlation between IPGE and PPGE, of which Pd and Pt are significantly more mobile. Hydrothermal enrichment of Pd in other deposits is commonly accompanied by an enrichment in Cu and Au, yet the opposite is true for the Ni-PGE ore (Le Vaillant, et al., 2016). In this study, the presence of PGE in solid solution within all the BMS and the high proportion of PGE

hosted by BMS (*Fig. 4-13*) favour a magmatic rather than hydrothermal origin for Ni-PGE ore in Kevitsa, although hydrothermal processes may have redistributed PGE at a local scale and expelled PGMs from sulphides into secondary hydrous silicates.

The high metal tenor of the Ni-PGE ore is explained by Gervilla and Kojonen (2002) as a result of post-magmatic serpentinisation of olivine followed by greenschist metamorphism, resulting in the release of Ni from olivine which was consequently collected by sulphides. They suggested that this favoured the formation of Ni-rich assemblages containing pentlandite and millerite (Eckstrand, 1975; Barnes & Hill, 2000). Metamorphism also partly dissolved sulphides, arsenides and PGM, redistributing them in association with hydrous silicates. This process recrystallised disseminated sulphides, allowing them to re-equilibrate with olivine, enriching sulphides in Ni (Barnes & Hill, 2000; Mancini & Papunen, 2000). This theory is refuted by Yang, et al. (2013), who found that the olivine, orthopyroxene and clinopyroxene in the Ni-PGE ore at Kevitsa all show unusually high Ni contents, with olivines containing up to 14,000 ppm Ni. This indicates that there has been no Ni depletion of olivine as a result of diffusion to the nearby sulphides. Anomalously high Ni content in the core of olivine grains and in grains without any contact with sulphides also argue against diffusion in the opposite direction, from sulphides to olivine. Equilibration of olivine with sulphides can generate zonation in olivine, with the highest contents occurring adjacent to sulphide blebs (Barnes, et al., 2011).

5.3.3 Implications for the Formation of the Ni-PGE Ore

Upon evaluation of the role of magmatic *vs.* hydrothermal processes, this study can conclude that hydrothermal processes did not play a significant role in the distribution of PGE in BMS from Kevitsa ores.

The vast difference in trace element content of the Ni-PGE ore compared with the normal ore, including elevated contents of As, Bi, Te and Se, strongly suggest a component of contamination or enrichment of the magma. According to the results of this study, it is possible that the Kevitsa magma encountered a source of metals that upgraded the sulphide droplets present in the Ni-PGE ore, and the surrounding olivine, allowing the formation of

high tenor ore through primary magmatic processes. Sulphide liquid from previous magma surges may have become trapped in a preceding magma chamber, for example in dense sulphide pools at constriction or stagnation points (Barnes, et al., 2016).

The previous comparisons, observations and processes regarding the evolution of sulphide liquids during fractionation can be amalgamated and applied to explain the possible formation of the Ni-PGE ore. *Figure 5-4* shows a proposed model to explain the distribution of PGE and other chalcophile elements in the BMS in the Ni-PGE ore at Kevitsa.

1. **>1200°C**: At the highest temperatures, the sulphide liquid is enriched with dissolved PGEs, semimetals, Fe, Ni and Cu.
2. **>1000°C**: Crystallisation of monosulphide solid solution (*mss*) begins upon cooling to 1000°C, into which IPGE (Ru, Rh, Os, Ir) partition preferentially, which is visible in the mantle normalised PGE pattern of *Figure 5-2 a*. Meanwhile, the Cu-rich residual liquid becomes enriched in Pd, Pt and semimetals after *mss* crystallises. At this stage, some PGE arsenides and sulpharsenides, including sperrylite and kotulskite, crystallise directly from the sulphide melt (Hutchinson & McDonald, 2008). Some PGE prefer As-bearing PGM than sulphide phases, depleting *mss* slightly in Ir and Rh, but enriching it in Os, Ru, Co and Ni.
3. **950-840°C**: Intermediate solid solution (*iss*) crystallises from the Cu-rich residual liquid. As Pd and Pt are incompatible into *iss* at this temperature relative to the sulphide melt (Peregoedova, 1998), they are concentrated in an immiscible semimetal-rich (As, Se, Bi, Te) melt which scavenges Pt and Pd from the *iss* and *mss*. Some of this liquid may become trapped in *mss*, creating microinclusions within sulphide (Holwell & McDonald, 2007). However, due to a high Pd:semimetal ratio, some Pd is still accommodated in pentlandite. Ni-rich arsenides (nickeline, maucherite) may form at this stage and Pd partitions into them. Ni-rich pyrite forms in equilibrium with *mss* (Holwell & McDonald, 2010).
4. **650-400°C**: *Iss* crystallises to chalcopyrite with low PGE in solid solution. *Mss* recrystallises to pentlandite and pyrrhotite with IPGE in solid solution. Pd diffuses from the Cu-rich portion into the cores of granular pentlandite (Dare, et al., 2010) and into gersdorffite which crystallises from *mss* at around 500°C (Gervilla, et al., 2004). Although gersdorffite receives more Pd, some is left behind in pentlandite,

whereas nearby pyrrhotite is depleted. Crystallisation of the semimetal-rich residual melt forms discrete PGMs around the margins of sulphide blebs (Holwell & McDonald, 2007).

5. **<300°C**: Ni-rich *mss* decomposes, forming a pentlandite-pyrite-millerite assemblage (Barnes, et al., 2011). Later hydrothermal alteration may have redistributed PGE at a centimetre to decimetre scale (Le Vaillant et al., 2016), isolating PGMs as satellite grains in secondary silicates (Holwell & McDonald, 2007).

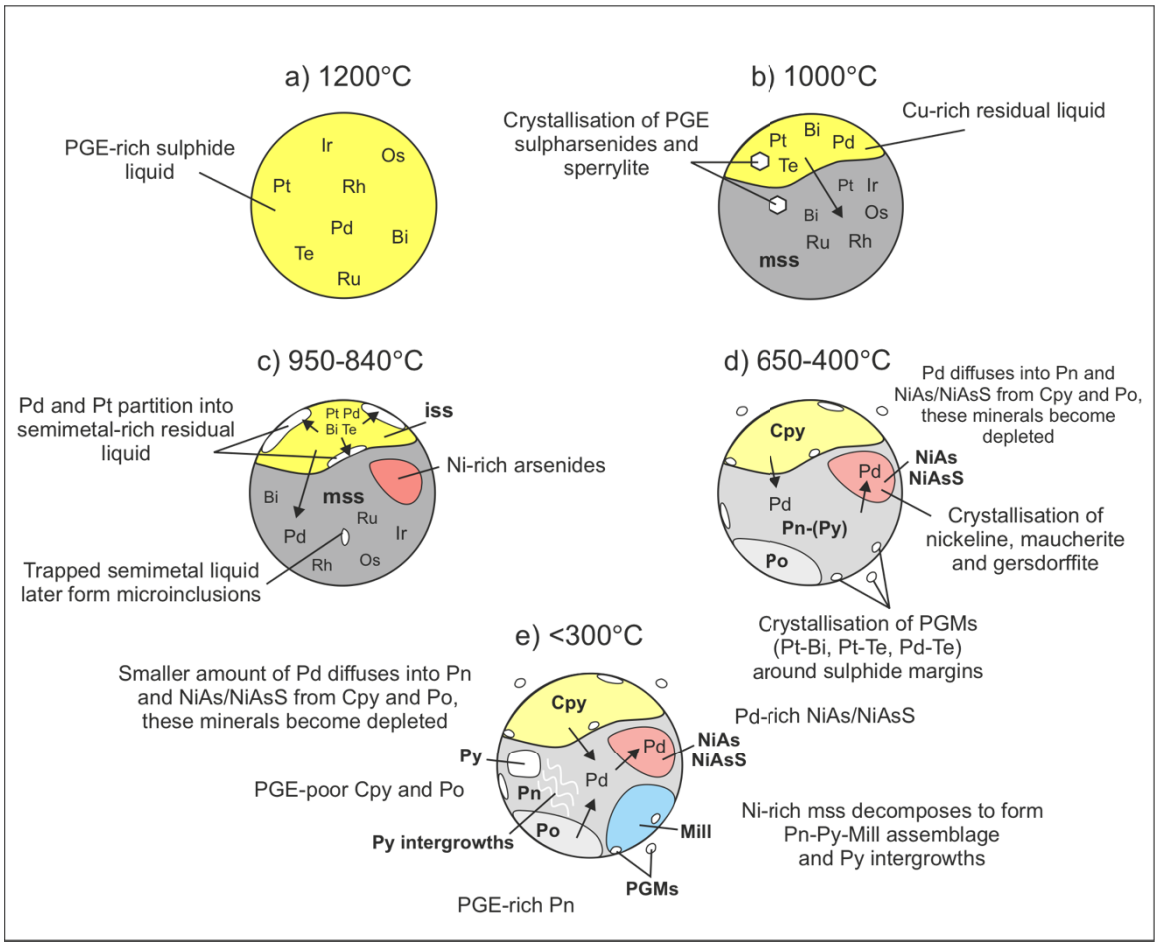

Figure 5-4: Schematic model of a fractionating sulphide droplet, highlighting processes that control the distribution of PGE and other chalcophile elements in base metal sulphides, PGMs and Ni-rich arsenides. **a** PGE-rich sulphide droplet. **b** Crystallisation of PGE sulpharsenides and sperrylite ($PtAs_2$), IPGE and Rh partition into *mss* while the Cu-rich residual liquid remains Pd, Pt, Bi and Te-enriched. **c** *Iss* crystallises, Pd and Pt partition into a semimetal-rich residual liquid. Ni-rich arsenides form. **d** Exsolution of pyrrhotite (*Po*), pentlandite (*Pn*) and Ni arsenides/sulpharsenides from *mss* and chalcopyrite from *iss*. Pd diffuses into pentlandite and Ni arsenides/sulpharsenides. PGMs crystallise at sulphide margins. **e** Pd diffuses into pentlandite and Ni arsenides/sulpharsenides from pyrrhotite and chalcopyrite. Ni-rich *mss* decomposes to form pentlandite, pyrite (*Py*) and millerite (*Mill*) assemblage and pyrite intergrowths.

6 CONCLUSIONS

The main aim of this study was to investigate the origin of the high tenor Ni-PGE ore, particularly in regard to the roles of primary magmatic processes and post-magmatic hydrothermal alteration. The use of LA-ICP-MS allowed the examination of conditions present during sulphide liquid fractionation and thus the magmatic conditions that formed the deposit.

The main results of this study are as follows:

- Pyrite and millerite in Ni-rich systems such as that in the Kevitsa intrusion can be minor carriers of PGE.
- Out of all the BMS, pentlandite is the principal carrier of PGE with Pd up to 51 ppm in Ni-PGE ores.
- The trace element characteristics of the Ni-PGE ore sulphides differ greatly from the other ore types with higher concentrations of both PGEs and semimetals.
- The presence of Bi, Te and As, together with results from other studies of Ni arsenides, sulpharsenides and PGMs, indicate that a semimetal-rich residual melt was critical in the distribution of PGE within BMS.
- The majority of Pt is not hosted within BMS, but can be accounted for in the form of discrete PGMs, arsenides and sulpharsenides, but considerable amount of Pd is hosted in BMS (~20%).
- BMS host a large proportion of Ru, Rh, Os and Ir, with much higher concentrations that can be accurately accounted for in the mass balance.
- The Kevitsa Ni-Cu-(PGE) deposit shares similarities with some other PGE-rich deposits, as shown by similar mantle-normalised PGE patterns of both whole rock and pentlandite.
- This study can provide insight into the primary magmatic processes that form high tenor Ni-Cu-(PGE) deposits, and how these processes are recorded within Ni-rich base metal sulphide assemblages at a trace element level.
- The origin of the Ni-PGE ore is still ambiguous, although it is very likely that the formation is dominated by magmatic processes and hydrothermal processes have not played a significant role.

- The high PGE and semimetal content of the Ni-PGE ore suggests introduction of an external source of metals, perhaps from interaction with sulphide liquid from previous magma surges at depth, although the mechanism for this is still unclear.

In general, the base metal sulphides from the Kevitsa Ni-Cu-(PGE) deposit are important indicators of conditions present in the magma chamber during the formation of the ore-bearing area of the intrusion. Future study of this deposit could involve resampling and reanalysing Ni-PGE ore samples to provide more representative data that can be used in a mass balance calculation. The *in-situ* analysis of arsenides, sulpharsenides and other nickel-bearing phases such as heazlewoodite were beyond the scope of this study, and could prove useful to investigate in the future.

7 REFERENCES

Ahtola, T., Eilu, P., Kärkkäinen, N., Tiainen, M., Tontti, M., Äikäs, O., Halkoaho, T., Kontinen, A., Kuivasaari, T., Nikander, J., Pohjolainen, E., Sorjonen-Ward, P., Torppa, A., Västi, K., Kontoniemi, O., Heikura, P., Hulkki, H., Iljina, M., Juopperi, H., Perdahl, J.-A. (2012). Metallogenic areas in Finland: Special paper. *Geological Survey of Finland*, 207-342.

Alapieti, T.T., Lahtinen, J.J. (1986). Stratigraphy, petrology, and platinum-group element mineralization of the early Proterozoic Penikat layered intrusion, Northern Finland. *Economic Geology, 81*, 1126-1136.

Ballhaus, C., Tredoux, M., & Spath, A. (2001). Phase relations in the Fe-Ni-Cu-PGE-S system at magmatic temperature and application to massive sulphide ores of the Sudbury Igneous Complex. *Journal of Petrology, 42*, 1911-1926.

Barnes, S., & Hill, R. (2000). Metamorphism of komatiite-hosted nickel sulfide deposits. *Rev. Economic Geology, 11*, 203-215.

Barnes, S., & Liu, W. (2012). Pt and Pd mobility in hydrothermal fluids: evidence from komatiites and from thermodynamic modelling. *Ore Geology Reviews, 44*, 49-58.

Barnes, S., & Maier, W. (1999). The fractionation of Ni, Cu, and the noble metals in silicate and sulphide liquids. *Geological Association of Canada Short Course Notes, 13*, 69-106.

Barnes, S., Acterberg, E., Makovicky, E., & Li, C. (2001). Proton probe results for partitioning of platinum group elements between monosulphide solid solution and sulphide liquid. *South African Journal of Geology, 104*, 337-351.

Barnes, S., Cruden, A., Arndt, N., & Saumur, B. (2016). The mineral system approach applied to magmatic Ni-Cu-PGE sulphide deposits. *Ore Geology Reviews, 76*, 296-316.

Barnes, S., Godel, B., Locmelis, M., Fiorentini, M., & Ryan, C. (2011). Extremely Ni-rich Fe-Ni sulfide assemblages in komatiitic dunite at Betheno, Western Australia: results from synchrotron X-ray fluorescence mapping. *Australian Journal of Geosciences, 58*, 691-709.

Barnes, S., Makovicky, E., Karup-Moller, S., Makovicky, M., & Rose-Hansen, J. (1997). Partition coefficients for Ni, Cu, Pd, Pt, Rh and Ir between monosulfide solid solution and sulfide liquid and the implications for the formation of

compositionally zoned Ni-Cu sulfide bodies by fractional crystallization of sulfide liquid. *Canadian Journal of Earth Science, 34*, 366-374.

Barnes, S., Osborne, G., Cook, D., Barnes, L., Maier, W., & Godel, B. (2011). The Santa Rita Nickel Sulfide Deposit in the Fazenda Mirabela Intrusion, Bahia, Brazil: Geology, Sulfide Geochemistry, and Genesis. *Economic Geology, 106*, 1053-1110.

Barnes, S.-J., & Lightfoot, P. (2005). Formation of magmatic nickel-sulfide deposits and processes affecting their copper and platinum-group element contents. (J. Hedenquist, J. Thompson, R. Goldfarb, & J. Richards, Eds.) *Economic Geology 100th Anniversary Volume*, 179-213.

Barnes, S.-J., Cox, R., & Zientek, M. (2006). Platinum-group element, gold, silver and base metal distribution in compositionally zoned sulfide droplets from the Medvezky Creek Mine, Noril'sk, Russia. *Contributions to Mineral Petrology, 152*, 187-200.

Barnes, S.-J., Prichard, H., Cox, R., Fisher, P., & Godel, B. (2008). The location of the chalcophile and siderophile elements in platinum-group element ore deposits (a textural, microbeam and whole rock geochemical study): Implications for the formation of the deposits. *Chemical Geology, 248*, 295-317.

Becker, H., Horan, M., Walker, R., & et al. (2006). Higher siderophile element composition of the Earth's primitive mantle: Contraints from new data on peridotite massifs and xenoliths. *Geochimica Cosmochimica Acta, 70*, 4528-4550.

Begg, G., Hronsky, J., Arndt, N., & et al. (2010). Lithospheric, Cratonic and geodynamic setting of Ni-Cu-PGE sulfide deposits. *Economic Geology, 105*, 1057-1070.

Boudreau, A., & Meurer, W. (1999). Concentration of platinum-group elements by magmatic fluids in layered intrusions. *Economic Geology, 87*, 1830-1848.

Brownscombe, W.; Ihlenfeld, C.; Hartshorne, C.; Coppard, J.; Klatt, S. (2015). The Sakatti Cu-Ni-PGE sulphide deposit, northern Finland. . In: W. Maier, H. O'Brien, & R. Lahtinen (Eds.), *Mineral Deposits of Finland* (pp. 211-251). Elsevier.

Brügmann, G., Naldrett, A., Asif, M., Lightfoot, P., Gorbachev, N., & Fedorenko, V. (1993). Siderophile and chalcophile metals as tracers of the evolution of the Siberian trap in the Noril'sk Region, Russia. *Geochimica et Cosmochimica Acta, 57*, 2001-2018.

Cabri, L., & LaFlamme, J. (1976). The mineralogy of the platinum-group elements from some copper-nickel deposits of the Sudbury area, Ontario. *Economic Geology, 71*, 1159-1195.

Cabri, L., Sylvester, P., Tubrett, M., Perogoedova, A., & Laflamme, J. (2003). Comparison of micro-PIXE and LAM-ICP-MS analyses for Pd and Rh. *Canadian Mineralogist, 41*, 321-329.

Campbell, I., & Naldrett, A. (1979). The influence of silicate:sulfide ratios on the geochemistry of magmatic sulfides. *Economic Geology, 74*, 1503-1506.

Capitrant, P., Hitzman, M., Wood, D., Kelly, N., Williams, G., Zimba, M., Stein, H. (2015). Geology of the Enterprise hydrothermal Nickel Deposit, North-Western Province, Zambia. *Economic Geology, 110*, 9-38.

Coppard, J., Klatt, S., & Ihlenfeld, C. (2013). The Sakatti Ni-Cu-PGE deposit in northern Finland. In E. Hanski, & W. Maier (Eds.), *Excursion Guidebook FINRUS, Ni-Cr-PGE deposits of Finland and Kola Peninsula. 12th SGA Biennial Meeting, Mineral Deposit Research for a High-tech World* (pp. 10-11). Uppsala, Sweden: Geological Survey of Sweden.

Cox, K., & Hawkesworth, C. (1985). Geochemical stratigraphy of the Deccan Traps at Mahabaleshwar, Western Ghats, India, with implications for open system magmatic processes. *Journal of Petrology, 26*, 355-377.

Dare, S., Barnes, S.-J., & Prichard, H. (2010). The distribution of platium group elements (PGE) and other chalcophile elements among sulfides from the Creighton Ni-Cu-PGE sulfide deposit, Sudbury, Canada, and the origin palladium in pentlandite. *MIneralium Deposita, 45*, 765-793.

Depaolo, D. (1985). Isotopic studies of processes in mafic magma chambers: I. The Kiglapait intrusion, Labrador. *Journal of Petrology, 26*, 925-951.

Eales, H., De Klerk, W., Butcher, A., & Kruger, F. (1990). The cyclic unit beneath the UG1 chromitite (UG1FW unit) at RPM Union Section Platinum Mine - Rosetta stone of the Bushveld Upper Critical Zone. *Mineral Mag, 54*, 23-43.

Eales, H., Marsh, J., Mitchell, A., De Klerk, W., Kruger, F., & Field, M. (1986). Some geochemical contraints upon models for the crystallization of the upper critical zone-main zone interval, northwestern Bushveld Complex. *Mineral Mag, 50*, 567-582.

Eckstrand, O. (1975). The Dumont serpentinite: a model for control of nickeliferous opaque assemblages by alteration products in ultramafic rocks. *Economic Geology, 70*, 183-201.

Eckstrand, O., & Hulbert, L. (2007). Magmatic Nickel-Copper-Platinum Group Element Deposits. In W. Goodfellow (Ed.), *Mineral Deposits of Canada: A Synthesis of Major Deposit Types, District Metallogeny, the Evolution of Geological Provinces and Exploration Methods* (Vol. 102, pp. 205-222). Geological Association of Canada.

Farrow, C. (1994). *Geology, alteration, and the role of fluids in Cu-Ni-PGE mineralization of the footwall rocks to the Sudbury Igneous Complex, Levack and Morgan townships, Sudbury district, Ontario.* Ottowa, Ontario, Carleton University: Unpublished Ph.D. thesis.

Farrow, C., & Watkinson, D. (1997). Diversity of precious-metal mineralization in footwall Cu-Ni-PGE deposits, Ontario: implications for hydrothermal models of formation. *Can. Mineral., 35*, 817-839.

Farrow, C., & Watkinson, D. (1999). An evaluation of the role of fluids in Ni-Ce-PGE-bearing, mafic-ultramafic systems. *Geological Association of Canada Short Course, 13*, 31-98.

First Quantum Minerals Ltd. (2011). Press Release 30 March 2011. Retrieved March 2020. From: https://www.first-quantum.com/Media-Centre/Press-Releases/Press-Release-Details/2011/First-Quantum-Minerals-Issues-Updated-Resource-and-Reserve-Estimates-and-Progress-Report-for-Kevitsa-Project/default.aspx

Fleet, M., Chryssoulis, S., Stone, W., & Weisner, C. (1993). Partitioning of platinum-group elements and Au in the Fe-Ni-Cu-S system: experiments on the fractional crystallization of sulfide melt. *Contrib. Miner. Petrol, 115*, 36-44.

Franchuk, A., Lightfoot, P., & Kontak, D. (2015). High tenor Ni-PGE sulfide mineralization in the South Manasan Ultramafic Intrusion, Paleoproterozoic Thompson Nickel Belt, Manitoba, Canada. *Ore Geology Reviews, 72*, 434-458.

Garde-Schönberg, D., & Müller, S. (2014). Nano-particulate pressed powder tablets for LA-ICP-MS. *J. Anal. At. Spectrom, 29*, 990-1000.

Gervilla, F., & Kojonen, K. (2002). The platinum-group minerals in the upper section of the Keivitsansarvi Ni-Cu-PGE deposit, northern Finland. *The Canadian Mineralogist, 40*, 377-394.

Gervilla, F., Kojonen, K., Parkkinen, J., & Välimaa, J. (2004). Platinum-group element mineralogy, geochemistry and 3-D modelling of the Keivitsa Ni-Cu-PGE sulfide deposit, northern Finland. In E. e. al. (Ed.), *Mineral Exploration and Sustainable Development* (pp. 583-586). Rotterdam: Millpress.

Gervilla, F., Makovicky, E., Makovicky, M., & Rose-Hansen, J. (1994). The system Pd-Ni-As at 790°C and 450°C. *Economic Geology, 89*, 1630-1639.

Godel, B., Barnes, S.-J., & Maier, W. (2007). Platinum-Group Elements in Sulphide Minerals, Platinum-Group Minerals. and Whole-Rocks of the Merensky Reef (Bushveld Complex, South Africa): Implications for the Formation of the Reef. *Journal of Petrology, 48*(8), 1569-1604.

Gregory, J., Journet, N., White, G., & Lappalainen, M. (2011). *Kevitsa copper nickel project in Finland: technical report for the mineral resources and reserves of the Kevitsa project.* First Quantum Minerals Ltd.

Grinenko, L., Hanski, E., & Grinenko, V. (2003). Formation conditions of the Keivitsa Cu-Ni deposit, Northern Finland: evidence from S and C isotopes. *Geochemistry International, 41*, 154-167.

Hackman, V. (1927). Studien über den Gesteinsaufbau der Kittilä-Lappmark. *Comm. géol. Finlande, Bull., 79*, 1-105.

Hanley, J. (2005). The aqueous geochemistry of the platinum-group elements (PGE) in surficial, low T hydrothermal and high-T magmatic hydrothermal environments. *Mineralogical Association of Canada Short Course, 35*, 35-56.

Hanski, E. (2015). Synthesis of the Geological Evolution and Metallogeny of Finland. In W. Maier, R. Lahtinen, & H. O'Brien (Eds.), *Mineral Deposits of Finland* (pp. 39-68). Amsterdam: Elsevier.

Hanski, E., & Huhma, H. (2005). Central Lapland Greenstone Belt. In M. Lehtinen, P. Nurmi, & O. Rämö (Eds.), *Precambrian Geology of Finland - Key to the Evolution of the Fennoscandian Shield* (pp. 139-194). Amsterdam: Elsevier.

Hanski, E., Huhma, H., Rastas, P., & Kamenetsky, V. (2011). The Palaeoproterozoic komatiite-picrite association of Finnish Lapland. *Journal of Petrology, 42*, 855-876.

Hanski, E., Huhma, H., Suominen, I., & Walker, R. (1997). Geochemical and isotopic (Os, Nd) study of the early Proterozoic Keivitsa intrusion and its Cu-Ni deposit, northern Finland. *Mineral Deposits*, 435-438.

Hanski, E., Walker, R., Huhma, H., & Suominen, I. (2001b). The Os and Nd isotopic signatures of the 2.44 Ga Akanvaara and Koitelainen mafic layered intrusions in northern Finland. *Precambrian Research, 109*, 73-102.

Heath, C., Lahaye, Y., Stone, W., & Lambert, D. (2001). Origin of variations in nickel tenor along the strike of the Edwards lode nickel sulfide orebody, Kambalda, Western Australia. *The Canadian Mineralogist, 39*, 655-671.

Helmy, H., Ballhaus, C., Berndt, J., Bockrath, C., & Wohlgemuth-Ueberwasser, C. (2006). Formation of Pt, Pd and Ni tellurides: experiments in sulfide-telluride systems. *Contributions to Mineralogy and Petrology, 153*, 577-591.

Helmy, H., Ballhaus, C., Berndt, J., Bockrath, C., & Wohlgemuth-Ueberwasser, C. (2007). Formation of Pt, Pd and Ni tellurides: experiments in sulfide-telluride systems. *Contributions to Mineralogy and Petrology, 153*, 577-591.

Hoffman, E., & MacLean, W. (1976). Phase relations of michenerite and merenskyite in the Pd-Bi-Te system. *Economic Geology, 71*, 1461-1468.

Holwell, D., & McDonald, I. (2006). Petrology, geochemistry and the mechanisms determining the distribution of platinum-group element and base metal sulfide mineralization in the Platreef and Overysel, northern Bushveld Complex, South Africa. *Mineralium Deposita, 41*, 575-598.

Holwell, D., & McDonald, I. (2007). Distribution of platinum-group elements in the Platreef at Overysel, northern Bushveld Complex: a combined PGM and LA-ICP-MS study. *Contributions to Mineralogy and Petrology, 154*, 171-190.

Holwell, D., & McDonald, I. (2010). A Review of the Behaviour of Platinum Group Elements within Natural Magmatic Sulfide Ore Systems. *Platinum Metals Rev., 54*, 26-36.

Hutchinson, D., & McDonald, I. (2008). Laser ablation ICP-MS study of platinum-group elements in sulphides from the Platreef at Turkspruit, northern limb of the Bushveld Complex, South Africa. *Mineralium Deposita, 43*, 695-711.

Hölttä, P., Heilimo, E., Huhma, H., & et al. (2012b). The Archaean of the Karelia Province in Finland . *Geological Survey of Finland, Special Paper, 54*, 21-73.

Iljina, M., & Hanski, E. (2005). Layered mafic intrusions of the Tornio-Näränkävaara belt. In M. Lehtinen, P. Nurmi, & O. Rämö (Eds.), *Precambrian Geology of Finland - Key to the Evolution of the Fennoscandian Shield* (pp. 103-138). Amsterdam: Elsevier.

Irvine, T. (1975). Crystallization sequences in the Muskox-II. Origin of chromitite layers and similar deposits of other magmatic ores. *Geochimica Cosmochimica Acta, 39*, 1009-1020.

Jugo, P., Luth, R., & Richards, J. (2005). An experimental study of the sulfur content in basaltic melts saturated with immiscible sulfide of sulfate liquids at 1300 C and 1.0 GPa. *Journal of Petrology, 46*, 783-798.

Karup-Møller, S., & Makovicky, E. (1995). The phase system Fe-Ni-S at 725°C. *Neues Jahrb. Mineral.*, 1-10.

Keays, R. (1995). The role of komatiitic and picritic magmatism and S-saturation in the formation of ore deposits. *Lithos, 34*, 1-18.

Keays, R., & Jowitt, S. (2013). The Avebury Ni deposit, Tasmania: a case study of an unconventional nickel deposit. *Ore Geology Reviews, 52*, 4-17.

Keays, R., & Lightfoot, P. (2007). Siderophile and chalcophile metal variations in Tertiary picrites and basalts from West Greenland with implications for the sulphide saturation history of continental flood basalt magmas. *Mineralium Deposita, 42*, 319-336.

Kim, W.-S., Chao, G., & Cabri, L. (1990). Phase relations in the Pd-Te system. *J. Less-Common Metals, 162*, 61-74.

Koivisto, E., Malehmir, A., Hellqvist, N., Voipio, T., & Wijns, C. (2015). Building a 3D model of lithological contacts and near-mine structures in the Kevitsa mining and exploration site, Northern Finland: constraints from 2D and 3D reflection seismic data. *Geophysical Prospecting, 63*, 754-773.

Kojonen, K., Laukkanen, J., & Gervilla, F. (2008). Applied mineralogy of the Kevitsa nickel-copper-PGE deposit, Sodankylä, Northern Finland. *Ninth International Congress for Applied Mineralogy, Brisbane*, 605-613.

Konnunaho, J.P., Hanski, E.J., Bekker, A., Halkoaho, T.A.A., Hiebert, R.S. & Wing, B.A. (2013). The Archaean komatiite-hosted, PGE-bearing Ni-Cu sulphide deposit at Vaara, eastern Finland: evidence for assimilation of external sulphur and post-depositional desulphurization. *Mineralium Deposita* 48, 967–989.

Kontinen, A., Käpyaho, A., Huhma, H., Karhu, J., & et al. (2007). Nurmes paragneisses in eastern Finland, Karelian craton: Provenance, tectonic setting and implications for Neoarchaean craton correlation. *Precambrian Research, 152*, 119-148.

Kortelainen, V. (1983). *Sirkka-konglomeraatin ja Levitunturin kvartsiitin sedimentologia Kittilässä.* University of Helsinki, Finland.

Kruger, F. (1994). The Sr-isotopic stratigraphy of the western Bushveld Complex. *South African Journal of Geology, 97*, 393-398.

Kähkönen, Y. (2005). Svecofennian supracrustal rocks. In M. Lehtinen, P. Nurmi, & O. Rämö (Eds.), *Precambrian Geology of Finland - Key to the Evolution of the Fennoscandian Shield* (pp. 343-406). Amsterdam: Elsevier.

Köykkä, J., Lahtinen, R., Huhma, H. (2019). Provenance evolution of the Paleoproterozoic metasedimentary cover sequences in northern Fennoscandia: Age distribution, geochemistry, and zircon morphology. *Precambrian Research, 331,* 1-21.

Lahtinen, R. (2012). Main geological features of Fennoscandia. *Geological Survey of Finland, Special Paper, 53*, 13-18.

Lahtinen, R., Korja , A., & Nironen, M. (2005). Palaeoproterozoic tectonic evolution. In M. Lehtinen, P. Nurmi, & O. Rämö (Eds.), *Precambrian Geology of Finland - Key to the Evolution of the Fennoscandian Shield* (pp. 481-532). Amsterdam: Elsevier.

Lappalainen, M., & White, G. (2010). *43-101 Technical Report on Mineral Resources of the Kevitsa Ni-Cu-PGE Deposit, Finland.*

Lauri, L., Andersen, T., Hölttä, P., & et al. (2011). Evolution of the Archaean Karelian Province in the Fennoscandian Shield in the light of U-Pb zircon ages and Sm-Nd and Lu-Hf isotope systematics. *Journal of the Geological Society, 168*, 201-218.

Le Vaillant, M., Barnes, S., Fiorentini, M., Santaguida, F., & Törmänen, T. (2016). Effects of hydrous alteration on the distribution of base metals and platinum group elements within the Kevitsa magmatic nickel sulphide deposit. *Ore Geology Reviews, 72*, 128-148.

Le Vaillant, M., Hill, J., & Barnes, S. (2017). Simplifying drill-hole domains for 3D geochemical modelling: an example from the Kevitsa Ni-Cu-(PGE) deposit. *Ore Geology Reviews, 90*, 388-398.

Lehtinen, M., Nurmi, P., & Rämö, O. (2005). *Precambrian Bedrock of Finland - Key to the Evolution of the Fennoscandian Shield.* Amsterdam: Elsevier.

Lehtonen, M., Airo, M.-L., Eilu, P., Hanski, E., Kortelainen, V., Lanne, E., Manninen, T., Rastas, P., Räsänen, J., Virransalo, P. (1998). Kittilän vihreäkivialueen geologia.

Lapin vulkaniittiprojektin raportti. Summary: The stratigraphy, petrology and geochemistry of the Kittilä greenstone area, northern Finland. *A report of the Lapland Volcanite Project, 140*, 1-144.

Lesher, C., & Keays, R. (1984). Metamorphically and hydrothermally mobilized Fe-Ni-Cu sulphides at Kambalda, Western Australia. In D. Buchanan, & M. Jones (Eds.), *Sulphide Deposits in Mafic and Ultramafic Rocks* (pp. 62-69). London: Institute of Mineralogy and Metallogeny.

Li, C., Barnes, S., Makovicky, E., Karup-Moller, S., Makovicky, M., & Rose-Hansen, J. (1996). Partitioning of Ni, Cu, Ir, Rh, Pt and Pd between monosulfide solid solution and sulfide liquid: Effects of composition and temperature. *Geochimica et Cosmochimica Acta, 60*, 1231-1238.

Li, C., Ripley, E., & Naldrett, A. (2009). A new genetic model for the giant Ni-Cu-PGE sulfide deposits associated with the Siberian Flood Basalts. *Economic Geology, 104*, 291-301.

Li, C., Ripley, E., Merino, E., & Maier, W. (2004). Replacement of base metal sulfides by actinolite, epidote, calcite and magnetite in the UG2 and Merensky Reef of the Bushveld Complex, South Africa. *Economic Geology, 99*, 173-184.

Lightfoot, P. (2017). *Nickel Sulfide Ores and Impact Melts: Origin of the Sudbury Igneous Complex.* Amsterdam: Elsevier.

Lightfoot, P., & Keays, R. (2005). Siderophile and chalcophile metal variations in flood basalts from the Siberan trap, Noril'sk region: Implication for the origin of Ni-Cu-PGE sulfide ores. *Economic Geology, 100*, 439-462.

Lightfoot, P., Keays, R., Evans-Lamswood, D., & Wheeler, R. (2011a). S-saturation history of the Nain Plutonic Suite mafic intrusions: origin of the Voisey's Bay Ni-Cu-Co sulfide deposit, Labrador . *Min. Dep., 47*, 23-50.

Lightfoot, P., Stewart, R., Gribbin, G., & Mooney, S. (2011b). Relative contributions of magmatic and post-magmatic processes in the genesis of the Thompson Belt Ni-Co sulfide ore deposits, Manitoba, Canada. *12th International Ni-Cu-(PGE) Symposium, Guiyang, China*.

Lorand, J., & Keays, R. (1993). Copper and Noble Metal Enrichments Across the Lithosphere - Asthenosphere Boundary of Mantle Diapirs: Evidence from the Lanzo Lherzolite Massif. *Journal of Petrology, 34*(6), 1111-1140.

Luolavirta, K., Hanski, E., Maier, W., & Santaguida, F. (2018a). Characterization and origin of dunitic rocks in the Ni-Cu-(PGE) sulfide ore-bearing Kevitsa intrusion, northern Finland: whole-rock and mineral chemical constraints. *Bulletin of the Geological Society of Finland, 90*, 5-32.

Luolavirta, K., Hanski, E., Maier, W., & Santaguida, F. (2018b). Whole-rock and mineral compositional constraints on the magmatic evoution of the Ni-Cu-(PGE) sulfide ore bearing Kevitsa intrusion, northern Finland. *Lithos, 296-299*, 37-53.

Luolavirta, K., Hanski, E., Maier, W., Lahaye, Y., O'Brien, H., & Santaguida, F. (2018c). In situ strontium and sulfur isotope investigation of the Ni-Cu-(PGE) sulfide ore bearing Kevitsa intrusion, northern Finland. *Mineralium Deposita, 53*, 1019–1038.

Maier, W. (2015). Geology and Petrogenesis of Magmatic Ni-Cu-PGE-Cr-V Deposits: An Introduction and Overview. In W. G. Maier, R. Lahtinen, & H. O'Brien (Eds.), *Mineral Deposits of Finland.* Elsevier Inc.

Maier, W., & Barnes, S.-J. (2010). The Kabanga Ni sulfide deposits, Tanzania: II. Chalcophile and siderophile element geochemistry. *Miner Deposita, 45*, 443-460.

Maier, W., & Groves, D. (2011). Temporal and spatial controls on the formation of magmatic PGE and Ni-Cu deposits. *Mineralium Deposita, 46*, 841-857.

Maier, W., Barnes, S., & De Waal, S. (1998). Exploration for magmatic Ni-Cu-PGE sulphide deposits: A review of recent advances in the use of geochemical tools and their applications to some South African ores. *South African Journal of Geology, 101*, 237-253.

Makovicky, M., Makovicky, E., & Rose-Hansen, J. (1986). Experimental studies on the solubility and distribution of platinum-group elements in base-metal sulfides in platinum deposits. In M. Gallagher, R. Ixer, C. Neary, & H. Prichard (Eds.), *Metallogeny of Basic and Ultrabasic Rocks* (pp. 415-425). London: Inst. Mining Metallurgy.

Mancini, F., & Papunen, H. (2000). Metamorphism of Ni-Cu sulfides in mafic-ultramafic intrusions: the Svecofennian Sääksjärvi complex, southern Finland. *Rev. Economic Geology, 11*, 217-231.

Mavrogenes, J., & O'Neill, H. (1999). The relative effects of pressure, temperature and oxygen fugacity on the solubility of sulfide melts in mafic magmas. *Geochimica Cosmochimica Acta, 63*, 1173-1180.

Meyer, G., & Wilson, J. (1999). Olivine-rich units in the Fongen-Hyllingen intrusion, Norway: implications for magma chamber processes. *Lithos., 47*, 157-179.

Mikkola, P., Huhma, H., Heilimo, E., & Whitehouse, M. (2011). Archean crustal evolution of the Suomussalmi district as part of the Kianta complex, Karelia: Constraints from geochemistry and isotopes of granitoids. *Lithos, 125*, 287-307.

Mungall, J., & Su, S. (2005). Interfacial tension between magmatic sulfide and silicate liquids: Contraints on kinetics of sulfide liquidation and sulfide migration through silicate rocks. *Earth and Planetary Science Letters, 234*, 135-149.

Mungall, J., Andrews, R., Cabri, L., & Sylvester, P. (2005). Partitioning of Cu, Ni, Au and platinum-group elements between monosulfide solid solution and sulfide melt under controlled oxygen and sulfur fugacities. *Geochimica et Cosmochimica Acta, 69*, 4349-4360.

Mutanen, T. (1997). Geology and petrology of the Akanvaara and Koitelainen mafic layered intrusions and Keivitsa-Satovaara layered complex, northern Finland. *Geological Survey of Finland Bulletin, 395*, 233.

Mutanen, T., & Huhma, H. (2001). U-Pb geochronology of the Koitelainen, Akanvaara and Keivitsa layered intrusions and related rocks. In M. Vaasjoki (Ed.), *Radiometric age determindations from Finnish Lapland and their bearing on the timing of Precambrian volcano-sedimentary sequences* (pp. 229-246). Geological Survey of Finland, Special Paper 33.

Mutanen, T., & Huhma, H. (2003). The 3.5 Ga Siurua trondhjemite gneiss in the Archaean Pudasjärvi Granulite Belt, northern Finland. *Bulletin of the Geological Society of Finland, 75*, 51-68.

Naldrett, A. (1999). World-class Ni-Cu-PGE deposits: key factors in their genesis. *Mineralium Deposita, 34*, 227-240.

Naldrett, A. (2004). *Magmatic Sulfide Deposits: Geology, Geochemistry and Exploration.* Heidelberg: Springer.

Naldrett, A. (2010a). From the Mantle to the Bank: The Life of a Ni-Cu-(PGE) Sulfide Deposit. *South African Journal of Geology, 113*, 1-32.

Naldrett, A. (2010b). Secular Variation of Magmatic Sulfide Deposits and Their Source Magmas. *Economic Geology, 105*, 669-688.

Naldrett, A. (2011). Fundamentals of Magmatic Sulfide Deposits. *Reviews in Economic Geology, 17*, 1-50.

Naldrett, A., Fedorenko, V., Asif, M., Lin, S., Kunilov, V., Stekhin, A., Gorbachev, N. (1996a). Controls on the composition of Ni-Cu sulfide deposits as illustrated by those of the Noril'sk Region, Siberia. *Economic Geology, 91*, 751-753.

Naldrett, A., Fedorenko, V., Lightfoot, P., Kunilov, V., Gorbachev, N., Doherty, W., & Johan, Z. (1995). Ni-Cu-PGE deposits of the Noril'sk region Siberia: their formation in conduits for flood basalt volcanism . *Trans. Inst. Mining Metall. , 104*, B18-B36.

Naldrett, A., Keats, H., Sparkes, K., & Moore, R. (1996b). Geology of the Voisey's Bay Ni-Cu-Co Deposit, Labrador, Canada. *Explor. Min. Geol., 5*, 169-179.

Namur, O., Charlier, B., Toplis, M., Higgins, M., Liégeois, J., & van der Auwera, J. (2010). Crystallization sequence and magma chamber processes in the ferrobasaltic Sept Iles layered intrusion, Canada. *Journal of Petrology, 51*, 1203-1236.

Nickel, E., Allchurch, P., Mason, M., & Rutland, R. (1977). Supergene alteration at the Perseverence nickel deposit, Agnew, Western Australia. *Economic Geology, 72*, 184-203.

Nickel, E., Ross, J., & Thornber, M. (1974). The supergene alteration of pyrrhotite-pentlandite ore at Kambalda, Western Australia. *Economic Geology, 69*, 93-107.

Nikula, R. (1988). Palaeosedimentology of Precambrian tidal Virttiövaara and fluvial Virttiövaara quartzite formations in Sodankylä, northern Finland. In K. Laajoki, & J. Paakkola (Eds.), *Sedimentology of the Precambrian formations in eastern and northern Finland. Proceedings of IGCP 160 Symposium at Oulu, January 21-22, 1986.* (Vol. 5, pp. 177-188). Geological Survey of Finland, Special Paper.

Oberthür, T., Weiser, T., Gast, L., & Kojonen, K. (2003). Geochemistry and mineralogy of platinum-group elements at Hartley platinum mine, Zimbabwe: Part 1. Primary distribution patterns in pristine ores of the Main sulfide zone of the Great Dyke. *Mineralium Deposita, 38*, 327-343.

Peltonen, P. (2005b). Svecofennian mafic-ultramafic intrusions. In M. Lehtinen, P. Nurmi, & O. Rämö (Eds.), *Precambrian Geology of Finland - Key to the Evolution of the Fennoscandian Shield* (pp. 407-442). Amsterdam: Elsevier.

Peregoedova, A. (1998). 'The Experimental Study of the Pt-Pd-Partitioning between Monosulfide Solid Solution and Cu-Ni-Sulfide Melt at 900-840C. In "The 8th International Platinum Symposium (1998)". *Symposium Series S18*, 325-373.

Prichard, H., Hutchinson, D., & Fisher, P. (2004). Petrology and Crystallization History of Multiphase Sulfide Droplets in a Mafic Dyke from Uruguay: Implications for the Origin of Cu-Ni-PGE Sulfide Deposits. *Economic Geology, 99*, 365-376.

Rastas, P., Huhma, H., Lehtonen, M., Paakkola, J., Mänttäri, I., & Härkönen, I. (2001). U-Pb isotopic studies on the Kittilä greenstone area, Central Lapland, Finland. In M. Vaasjoki (Ed.), *Radiometric Age determinations from Finnish Lapland and their bearing on the timing of Precambrian volcano-sedimentary sequences* (Vol. 33, pp. 95-141). Geological Survey of Finland, Special Paper.

Ripley, E., & Li, C. (2013). Sulfide saturation in mafic magmas: Is external Sulfur required for magmatic Ni-Cu-(PGE) ore genesis? *Economic Geology, 108*, 45-58.

Rollinson, H. (1993). *Using Geochemical Data: Evaluation, Presentation, Interpretation.* Pearson Education Limited.

Räsänen, J., Hanski, E., Juopperi, H., Kortelainen, V., Lanne, E., Lehtonen, M., Manninen, T., Rastas, P., Väänänen, J. (1995). New stratigraphical map of Central Finnish Lapland. *22nd Nordic Geological Winter Meeting, January 8-11, 1996, Turku, Abstracts*, 182.

Santaguida, F., Luolavirta, K., Lappalainen, M., Ylinen, J., Voipio, T., & Jones, S. (2015). Chapter 3.6 - The Kevitsa Ni-Cu-PGE Deposit in the Central Lapland Greenstone Belt in Finland. In W. Maier, H. O'Brien, & R. Lahtinen (Eds.), *Mineral Deposits of Finland* (pp. 195-210). Elsevier.

Seabrook, C., Prichard, H., & Fisher, P. (2004). Platinum-group minerals in the Raglan Ni-Cu-(PGE) sulphide deposit, Cape Smith, Quebec, Canada. *Canadian Mineralogist, 42*, 485-497.

Shelley, D. (1992). *Igneous and Metamorphic Rocks Under the Microscope.* Chapman Hall, London.

Shunk, F. (1969). *Constitution of Binary Alloys (2nd Supplement)*. McGraw-Hill, New York, N.Y.

Sorjonen-Ward, P., & Luukkonen, E. (2005). Archean rocks. In M. Lehtinen, P. Nurmi, & O. Rämö (Eds.), *Precambrian Geology of Finland - Key to the Evolution of the Fennoscandian Shield* (pp. 19-99). Amsterdam: Elsevier.

Sorjonen-Ward, P., Nironen, M., & Luukkonen, E. (1997). Greenstone associations in Finland. *Greenstone belts. Oxford monographs on geology and geophysics, 35*, 677-698.

Standing, J., De Luca, K., Outhwaite, M., Neilson, I., Lappalainen, M., Wijns, C., & et al. (2009). *Report and Recommendations from the Kevitsa Campaign.* Jigsaw Geoscience Pty Ltd, Finland.

Taylor, S., & McLennan, S. (1985). *The continental crust: Its composition and evolution.* Oxford: Blackwell.

Vaasjoki, M., Korsman, K., & Koistinen, T. (2005). Overview. In M. Lehtinen, P. Nurmi, & O. Rämö (Eds.), *The Precambrian Geology of Finland - Key to the Evolution of the Fennoscandian Shield* (pp. 1-18). Amsterdam: Elsevier.

Verryn, S., & Merkle, R. (2002). The system PtS-PdS-NiS between 1200°C and 900°C. *Canadian Mineralogy, 40*, 571-584.

Vuollo, J., & Huhma, H. (2005). Paleoproterozoic mafic dikes in NE Finland. In M. Lehtinen, P. Nurmi, & O. Rämö (Eds.), *Precambrian Geology of Finland - Key to the Evolution of the Fennoscandian Shield* (pp. 195-278). Amsterdam: Elsevier.

Weihed, P., Arndt, N., Billström, K., & et al. (2005). Precambrian geodynamics and ore formation: The Fennoscandian Shield. *Ore Geology Reviews, 27*, 273-322.

Wilson, S., Ridley, W., & Koenig, A. (2002). Development of sulfide calibration standards for the laser ablation inductively coupled plasma mass spectrometry technique. *J. Anal. As. Spectrom, 17*, 406-409.

Wood, S. (2002). The aqueous geochemistry of the platinum-group elements with applications to ore deposits. In L. Cabri (Ed.), *The geology, geochemistry, mineralogy and mineral beneficiation of platinum-group elements* (pp. 211-249). Montreal: Canadian Institute of Mining, Metallurgy and Petroleum.

Yang, S.-H., Maier, W., Hanski, E., Markku, L., Santaguida, F., & Määttä, S. (2013). Origin of ultra-nickeliferous olivine in the Kevitsa Ni-Cu-PGE-mineralized intrusion, northern Finland. *Contributions to Mineralogy and Petrology, 166*, 81-95.

7.1 URLs

URL01: http://tupa.gtk.fi/paikkatieto/meta/suomen_kalliopera_5m.html - accessed 21.01.2020

URL02: http://tupa.gtk.fi/paikkatieto/meta/bedrock_of_finland_200k.html - accessed 21.01.2020

8 APPENDICES

8.1 Additional Photomicrographs of Noteworthy Features From Thick Sections

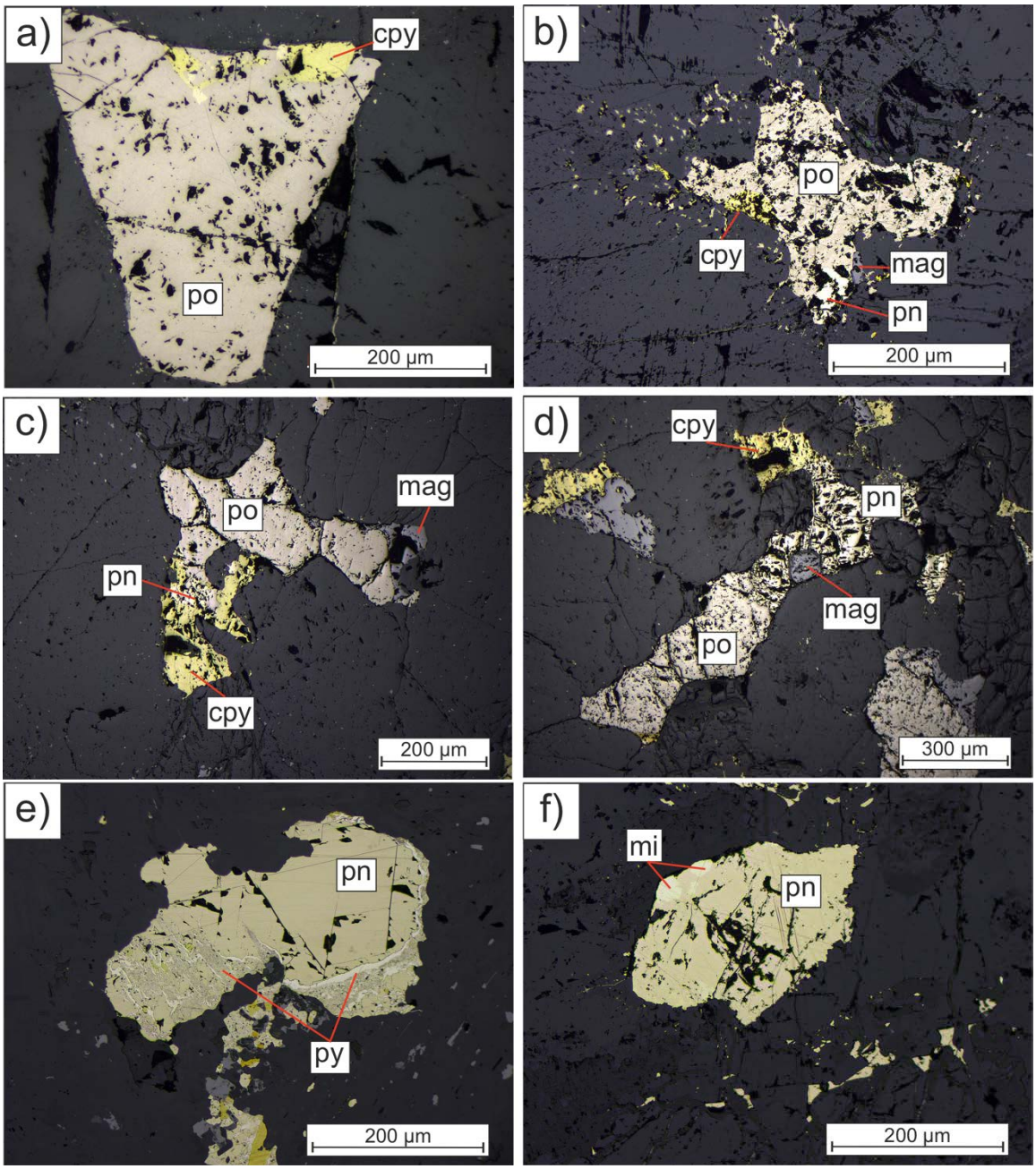

Figure 8-1: Photomicrographs of sulphide blebs under reflected light from different ore types of the Kevitsa deposit. **a)**, **b)** False ore, **c)**, **d)** Normal ore, and **e)**, **f)** Ni-PGE ore. *cpy* = chalcopyrite, *mag* = magnetite, *mi* = millerite, *pn* = pentlandite, *po* = pyrrhotite, *py* = pyrite.

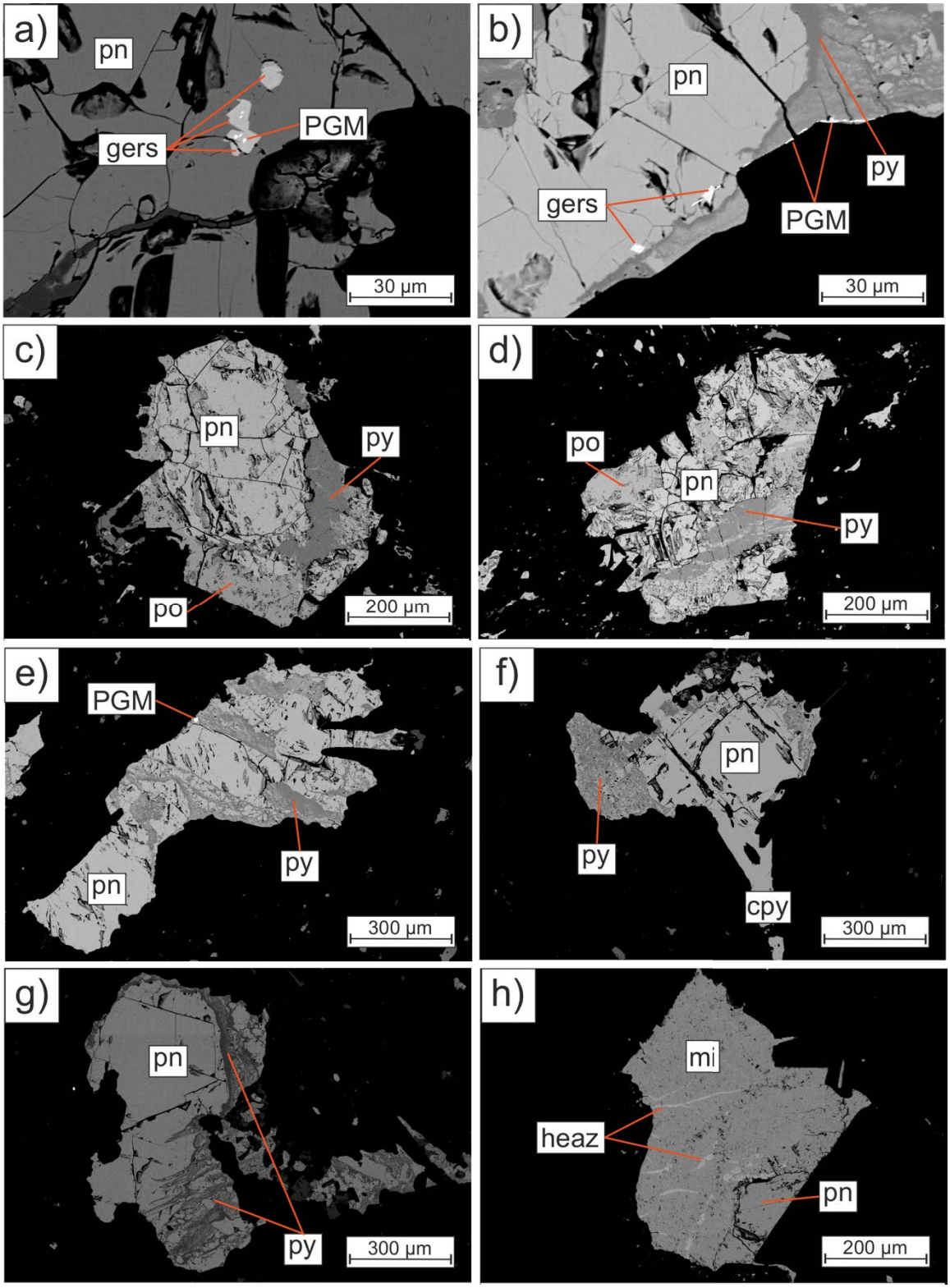

Figure 8-2: Backscattered electron image of sulphide grains from Ni-PGE ore showing noteworthy features: **a)** PGMs surrounded by grains of gersdorffite (*gers*) within pentlandite (*pn*). **b)** Grains of gersdorffite and elongated PGM at the margin of a pentlandite grain, also showing pyrite (*py*) intergrowths. **c-g)** Grains of pentlandite, pyrrhotite (*po*) and chalcopyrite (*cpy*) showing pyrite intergrowths. **f)** Grain of millerite (*mi*) with intergrowths of heazlewoodite (*heaz*).

8.2 Results of 100% Sulphide Calculations

Table 8-1: Whole rock concentrations for samples from Kevitsa Ni-Cu-(PGE) deposit and results of 100% sulphide calculations including mineral proportions, BMS weight fractions and metal tenors.

Sample No.	**KV280 574.95**	**KV280 620.4**	**R688 65.7**	**R802 81.4**	**KV34B 327.73**	**KV34B 554.48**	**KV45-32**	**KV45-35**	**KV103 421.2**	**KV45-63**	**KV45-75**	**R695 68.1**	**R695 69**	**R713 37.3**
Ore Type	False	False	False	False	Normal	Normal	Normal	Normal	Normal	Ni-PGE	Ni-PGE	Ni-PGE	Ni-PGE	Ni-PGE
Whole rock														
S (wt%)	1.870	0.786	3.090	2.170	3.670	3.540	2.730	2.740	1.960	1.530	1.820	2.904	1.79	0.679
Ni (wt%)	0.040	0.039	0.026	0.019	0.403	0.706	0.375	0.377	0.174	0.565	0.747	2.240	1.740	0.546
Cu(wt%)	0.037	0.040	0.055	0.035	0.637	0.990	0.669	0.947	0.373	0.201	0.385	0.197	0.145	0.041
Pd (ppb)					410	482	421	458	55.3	578	1260	1880	1880	678
Pt (ppb)					352	299	306	299	39.9	397	1020	2850	2730	893
Ir (ppb)												103.150	53.48	25.6
Os (ppb)												69.695	34.78	17
Ru (ppb)												134.815	68.2	40.2
Rh (ppb)												81.305	49.62	26.5
Mineral proportions														
Cpy wt%	0.108	0.115	0.159	0.100	1.846	2.870	1.939	2.745	1.081	0.583	1.116	0.572	0.421	0.119
Pn wt%	0.113	0.110	0.072	0.054	1.132	1.983	1.053	1.059	0.489	1.587	2.098	3.146	4.886	0.767
Po wt%	4.601	1.818	7.719	5.428	6.796	4.823	4.370	3.672	3.644	2.986	0.940	0.000	0.018	0.000
Py wt%										0.746	0.685	1.955	0.013	
Mill wt%												1.731		0.422
Sulphide wt%	4.823	2.044	7.951	5.583	9.775	9.676	7.363	7.476	5.214	5.902	4.839	7.404	5.339	1.308
Weight fraction BMS														
Cpy	2.248	5.630	2.001	1.796	18.890	29.657	26.337	36.716	20.738	9.872	23.062	7.726	7.883	9.088
Po	95.405	88.969	97.091	97.233	69.529	49.847	59.356	49.118	69.887	50.588	19.418	0.000	0.344	0.000

Table 8-1 (continued)

Sample No.	KV280 574.95	KV280 620.4	R688 65.7	R802 81.4	KV34B 327.73	KV34B 554.48	KV45-32	KV45-35	KV103 421.2	KV45-63	KV45-75	R695 68.1	R695 69	R713 37.3
Pn	2.347	5.401	0.908	0.971	11.581	20.496	14.307	14.165	9.375	26.892	43.364	42.491	91.522	58.644
Py										12.649	14.156	26.404	0.251	
Mill												23.380		32.268
100% sulphide composition														
Ni tenor	0.84	1.92	0.32	0.35	4.12	7.30	5.09	5.04	3.34	9.57	15.44	30.25	32.58	41.75
Cu tenor	0.78	1.94	0.69	0.62	6.52	10.23	9.09	12.67	7.15	3.41	7.96	2.67	2.72	3.14
Cu + Ni tenor	1.61	3.87	1.01	0.97	10.64	17.53	14.18	17.71	10.49	12.98	23.39	32.92	35.30	44.89
Pd tenor (ppb)	228.07				4194.57	4981.50	5717.95	6126.25	1060.71	9793.67	26039.22	25392.79	35211.68	51849.05
Pt tenor (ppb)					3601.19	3090.18	4156.04	3999.45	765.32	6726.79	21079.37	38494.40	51131.86	68290.86
Ir tenor (ppb)												1393.23	1001.66	1957.72
Os tenor (ppb)												941.4	651.4	1300.1
Ru tenor (ppb)												1820.92	1277.36	3074.24
Rh tenor (ppb)												1098.17	929.36	2026.55

Po pyrrhotite, *pn* pentlandite, *cpy* chalcopyrite, *py* pyrite, *mill* millerite, *ppb* parts per billion, *wt.%* weight percent

8.3 Results of Mass Balance Calculations

Table 8-2: Proportion (%) of PGE hosted in BMS from the Kevitsa Ni-Cu-(PGE) deposit.

Sulphide	Fraction BMS	Element	Pd	Pt	Ru	Rh	Os	Ir
Normal ore								
KV34B 327.73								
Po	69.53	*n=9*	2.54	0.12				
Pn	11.58	*n=2*	11.28					
Cpy	18.89	*n=6*	1.06	0.023				
Sum BMS			14.88	0.143				
KV34B 554.48								
Po	49.85	*n=10*	1.66	6.824				
Pn	20.50	*n=9*	14.72	0.043				
Cpy	29.66	*n=6*	0.000	0.047				
Sum BMS			16.38	6.914				
KV45-32								
Po	59.36	*n=13*	2.13	0.302				
Pn	14.31	*n=6*	4.52	0.110				
Cpy	26.34	*n=8*	0.000	0.544				
Sum BMS			6.65	0.955				
KV45-35								
Po	49.12	*n=12*	0.97	0.633				
Pn	14.17	*n=3*	6.2	0.01				
Cpy	36.72	*n=14*	1.46	3.467				
Sum BMS			8.63	4.109				
KV103 421.2								
Po	69.89	*n=12*	11.39	0.341				
Pn	9.37	*n=5*	13.41	0.038				
Cpy	20.74	*n=10*	0.000	0.222				
Sum BMS			24.8	0.6				
Ni-PGE ore								
KV45-63								
Po	41.26	*n=5*	0.59	0.017				
Pn	31.97	*n=14*	17.04	0.022				
Cpy	11.74		n/d	n/d				
Py	15.04	*n=3*	8.34	0.007				
Sum BMS			25.98	0.046				
KV45-75								
Po	19.42	*n=5*	2.02	0.007				
Pn	43.36	*n=15*	15.55	0.026				
Cpy	23.06	*n=1*	1.65	0.002				
Py	14.16	*n=10*	2.13	0.003				

Table 8-2 (continued)

Sulphide	Fraction BMS	Element	Pd	Pt	Ru	Rh	Os	Ir
Sum BMS			21.35	0.039				
R695 68.1								
Pn	46.68	*n=20*	10.29	0.563	83.53	85.69	118.8	56.83
Cpy	7.49	*n=3*	0.17	0.015	0.54	n/d	0.06	0.06
Py	20.15	*n=5*	2.93	0.002	3.43	4.8	8.9	4.11
Mill	25.7	*n=12*	0.39	0.003	5.47	0.55	9.09	0.89
Sum BMS			13.78	0.581	92.96	91.04	136.85	61.88
R695 69								
Pn	91.61	*n=17*	17.9	0.008	279.64	3.54	231.33	0.26
Cpy	7.89	*n=7*	0.03	0.001	1.04	n/d	0.08	0.06
Py	0.50	*n=1*	0.02	n/d	0.1	n/d	0.1	n/d
Sum BMS			17.94	0.009	280.77	3.54	231.51	0.32
R713 37.3								
Pn	60.60	*n=13*	25.45	0.137	122.51	67.73	96.84	73.48
Cpy	6.06	*n=0*	n/d	n/d	n/d	n/d	n/d	n/d
Mill	33.3	*n=7*	3.29	0.008	2.42	7.66	13.43	5.26
Sum BMS			28.74	0.145	124.93	75.4	110.27	78.74
Normal ore								
Po	59.55	*n=56*	3.74	1.644				
Pn	13.98	*n=25*	10.03	0.050				
Cpy	26.47	*n=44*	0.51	0.860				
Sum BMS			14.27	2.554				
Ni-PGE ore								
Po	12.20	*n=10*	1.3	0.012				
Pn	53.60	*n=79*	15.1	0.132	158.08	49.03	144.39	41.03
Cpy	11.90	*n=11*	0.46	0.006	0.8		0.07	0.06
Py	13.96	*n=19*	3.5	0.004	2.27	6.28	5.85	5.38
Mill	13.91	*n=19*	1.22	0.004	3.66	3.96	10.64	2.95
Sum BMS			21.59	0.158	164.8	59.27	160.95	49.42

Po pyrrhotite, *Pn* pentlandite, *Cpy* chalcopyrite, *Py* pyrite, *Mill* millerite, *BMS* base metal sulphide, *n/d* not determined.

8.4 LA-ICP-MS Results

The full results of the LA-ICP-MS analysis are given on the next page. Gaps in the tables represent either below detection limit values or PGE values that could not be used due to interferences.

Table 8-3: LA-ICP-MS results for BMS in different ore types from Kevitsa. *po* pyrrhotite, *pn* pentlandite, *py* pyrite, *mill* millerite, *cpy* chalcopyrite. All values in ppm.

Slide	R802-81.4	R802-81.4	R802-81.4	R802-81.4	R802-81.4	R802-81.4	R802-81.4	R802-81.4	R802-81.4	R802-81.4	R802-81.4	R802-81.4	R802-81.4	R802-81.4	R802-81.4
Ore Type	**False ore**	**False ore**	**False ore**	**False ore**	**False ore**	**False ore**	**False ore**	**False ore**	**False ore**	**False ore**	**False ore**	**False ore**	**False ore**	**False ore**	**False ore**
Spot Name	802-81.4 gr1_pt1	802-81.4 gr1_pt2	802-81.4 gr1_pt3	802-81.4 gr2_pt1	802-81.4 gr2_pt2	802-81.4 gr2_pt3	802-81.4 gr2_pt4	802-81.4 gr3_pt1	802-81.4 gr3_pt2	802-81.4 gr3_pt3	802-81.4 gr3_pt4	802-81.4 gr4_pt1	802-81.4 gr4_pt2	802-81.4 gr5_pt1	802-81.4 gr5_pt2
Mineral	**po**	**po**	**cpy**	**po**	**po**	**pn**	**cpy**	**po**	**po**	**pn**	**cpy**	**po**	**po**	**po**	**po**
Ru				0.058	0.05						0.055		0.073	0.117	
Rh	0.041	0.01		0.025						0.116		0.015			0.012
Pd	0.262		0.227					0.175		0.506			0.214		
Os				0.007	0.005	0.008	0.005	0.006	0.009		0.01	0.009	0.003	0.01	
Ir			0.001	0.002			0.002		0.001				0.002		0.004
Pt		0.005	0.004	0.003						0.004		0.003	0.005	0.003	
S34	344073	356426	244363	351204	382959	262799	211308	350239	347547	326692	319580	348268	353100	312012	325627
Co59	61.2	57.0	2226.2	36.1	63.8	11.9	20.7	69.1	173.0	31.7	67.1	52.2	49.5	94.5	134.8
Ni61	8	50	5803	2	5	179159	74	31	620	226596	140	60	9	154	378
Cu65	17		208020		4	139	11263		8	14240	608	12	15		
Zn67		1.3	220.1			0.9	78.2		0.4	41.7	152.7		2.2	0.5	
Ge72	3.4	3.7	2.3	3.7	2.9	2.5	2.1	3.7	3.7	3.7	3.6	3.4	3.4	3.2	3.0
As75	0.39	0.14	0.50	0.59	0.38	0.23	0.13	0.27	0.23	0.16	0.58	0.24		0.16	0.51
Se78	45	58	48	52	58	43	35	51	61	65	64	62	50	59	58
Mo95	0.126	0.111		0.056	0.18	0.177	0.046	0.09	0.147	0.237	1.184		0.142	0.054	0.137
Ag107	0.47	0.60	1.20	0.40	0.45	4.71	0.50	0.37	0.46	1.60	0.94	0.39	0.28	0.71	0.43
Cd111	0.08		0.82	0.10		0.28	0.24		0.12		0.50				
Sn120	0.12	0.20	0.15	0.11	0.09		0.10	0.07	0.16	0.07	0.21		0.06	0.03	
Sb121				0.02	0.07	0.01	0.01			0.05	0.04		0.02		0.02
Te126	0.12	0.16	3.26	0.36	0.53	0.24	1.78	0.23	0.36	1.01	14.25	0.24	0.16	0.35	0.58
Re185	0.046	0.018		0.007	0.024	0.012	0.005		0.026	0.030	0.046	0.020	0.051		0.017
Au197	0.001		0.001		0.002					0.005	0.007	0.002	0.004		0.001
Pb208	0.38	0.22	6.19	0.34	0.52	1.48	4.84	0.20	0.37	7.80	2.55	0.24	0.18	0.75	0.29
Bi209	0.22	0.07	0.41	0.23	0.32	0.06	0.38	0.19	0.20	1.42	0.70	0.15	0.07	0.20	0.16

Slide	R802-81.4	R802-81.4	R802-81.4	R802-81.4	R802-81.4	R802-81.4	KV280-574.95	KV280-574.95	KV280-574.95	KV280-574.95	KV280-574.95	KV280-574.95	KV280-574.95	KV280-574.95	KV280-574.95	KV280-574.95
Ore Type	**False ore**	**False ore**	**False ore**	**False ore**	**False ore**	**False ore**	**False ore**	**False ore**	**False ore**	**False ore**	**False ore**	**False ore**	**False ore**	**False ore**	**False ore**	**False ore**
Spot Name	802-81.4 gr5_pt3	802-81.4 gr5_pt4	802-81.4 gr6_pt1	802-81.4 gr6_pt2	802-81.4 gr6_pt3	802-81.4 gr6_pt4	kv280-574 gr1_pt1	kv280-574 gr1_pt2	kv280-574 gr1_pt3	kv280-574 gr2_pt1	kv280-574 gr2_pt2	kv280-574 gr2_pt3	kv280-574 gr3_pt1	kv280-574 gr3_pt2	kv280-574 gr3_pt3	kv280-574 gr4_pt1
Mineral	**cpy**	**cpy**	**po**	**po**	**cpy**	**pn**	**po**	**po**	**cpy**	**po**	**po**	**pn**	**po**	**po**	**cpy**	**po**
Ru	0.1	0.03		0.155	0.257		0.0581	0.061	0.181				0.0255	0.0307	0.23	0.0445
Rh			0.025	0.013		0.011		0.027								
Pd		0.095				0.388					0.25	0.188				0.127
Os	0.009	0.006	0.011		0.007			0.004	0.003	0.005	0.008	0.015	0.012	0.003		
Ir			0.003			0.003		0.004		0.002	0.007		0.002	0.006		0.006
Pt		0.003		0.005	0.004		0.002					0.003				
S34	189533	158064	345593	366691	349948	285496	352649	370905	367347	383685	398217	287218	366881	360997	382885	368902
Co59	156.2	77.3	217.3	96.4	424.5	950.5	80.6	122.2	2.2	93.5	122.0	468.1	123.7	81.3	14.9	100.8
Ni61	285	117	851	71	168	176471	1392	2132	38	1352	2200	179066	1931	1734	64	1810
Cu65	11131	18998	5	43	5	34	6673	17871		9431	10741	50389	11068	2551		23801
Zn67	16.1	5.8	0.6	4.3	1124.4	1.4			254.0	0.3	0.6	0.3	1.5	0.5	299.2	0.3
Ge72	1.8	1.7	3.1	3.8	3.6	2.9	4.1	4.0	4.1	4.0	4.0	2.9	3.9	3.9	4.2	4.0
As75	0.34	0.24		0.14	0.39	0.17	0.31	0.27	0.21	0.35	0.34	0.24	0.38	0.61	0.12	0.42
Se78	26	25	52	60	87	65	54	60	92	63	63	48	59	65	80	68
Mo95			0.212	0.229		0.143	0.066	0.095	0.091	0.095	0.222	4.63	0.134	0.187	0.0725	
Ag107	0.42	0.24	0.19	0.47	0.80	2.82	0.31	0.32	0.48	0.39	0.12	29.27	0.28	0.24	2.35	1.51
Cd111	0.15			0.10	5.78	0.16			7.49			0.04	0.15	0.05	9.60	0.08
Sn120	0.05	0.05	0.14	0.09	0.30	0.05	0.08	0.10	0.18	0.11	0.08	0.16	0.13	0.12	0.15	0.09
Sb121				0.02	0.05				0.03	0.02		0.01	0.02		0.01	0.04
Te126	0.53	0.21	0.36	0.63	10.49	0.37	0.05	0.11	5.68	0.09	0.08	26.93	0.25	0.24	12.61	0.16
Re185		0.004	0.017			0.007	0.041	0.055	0.006	0.056	0.029	0.318	0.057	0.054		0.017
Au197				0.001					0.011	0.001	0.001	0.044		0.002		
Pb208	1.67	1.19	0.24	0.83	13.52	8.53	0.59	0.81	12.58	0.51	0.63	401.51	0.85	0.40	8.53	5.31
Bi209	0.49	0.11	0.10	0.26	0.84	0.22	0.11	0.18	0.50	0.14	0.18	1.64	0.21	0.13	0.32	0.47

Slide	KV280-574.95	KV280-574.95	KV280-574.95	KV280-574.95	KV280-574.95	KV280-574.95	KV280-574.95	KV280-574.95	KV280-574.95	KV280-574.95	KV280-574.95	KV280-574.95	KV280-620.4	KV280-620.4	KV280-620.4	KV280-620.4
Ore Type	**False ore**	**False ore**	**False ore**	**False ore**	**False ore**	**False ore**	**False ore**	**False ore**	**False ore**	**False ore**	**False ore**	**False ore**	**False ore**	**False ore**	**False ore**	**False ore**
Spot Name	kv280-574 gr4_pt2	kv280-574 gr4_pt3	kv280-574 gr5_pt1	kv280-574 gr5_pt2	kv280-574 gr5_pt3	kv280-574 gr6_pt1	kv280-574 gr6_pt2	kv280-574 gr6_pt3	kv280-574 gr7_pt1	kv280-574 gr7_pt2	kv280-574 gr7_pt3	kv280-574 gr7_pt4	kv280-620 gr1_pt1	kv280-620 gr1_pt2	kv280-620 gr1_pt3	kv280-620 gr2_pt1
Mineral	**po**	**cpy**	**po**	**po**	**cpy**	**po**	**po**	**cpy**	**po**	**po**	**pn**	**cpy**	**po**	**po**	**pn**	**po**
Ru	0.114		0.0235			0.05	0.0372	0.176				0.145				0.088
Rh			0.031											0.012	0.007	0.007
Pd	0.21												0.191	0.116	0.356	
Os	0.006		0.002	0.004	0.003	0.008	0.004		0.007	0.002	0.004	0.002	0.005	0.006	0.002	0.008
Ir	0.002	0.002	0.002		0.002	0.003		0.001		0.001	0.007		0.008	0.005	0.008	0.009
Pt		0.003				0.002			0.003	0.002				0.006	0.007	
S34	371482	321316	381668	402680	348524	372600	377142	347453	375087	366480	363672	343926	389771	382867	301918	389437
Co59	96.7	6017.0	93.3	93.1	2150.2	116.0	104.9	241.5	79.6	108.9	2.9	41.4	43.3	40.0	2960.9	62.2
Ni61	1754	39788	1705	1309	11789	1711	1720	1028	990	1519	293034	206	1552	1352	217611	1917
Cu65	2976		12291	12749	5171440	6785	4934		62007	13920	1668339		4587	14206	22682	22969
Zn67	0.5	238.6			21822.3		0.9	268.0		1.1	0.8	583.7	0.7	0.3	0.2	
Ge72	3.9	3.4	4.3	4.0	4.2	4.1	3.7	3.7	3.9	4.2	3.8	3.7	4.0	4.4	2.9	4.3
As75	0.32	0.20		0.32	0.65	0.29	0.47	0.46	0.17	0.27	0.52	0.42	0.26	0.20	0.13	0.25
Se78	62	75	63	60	80	72	72	75	59	55	59	83	99	88	76	87
Mo95	0.0325	0.119	0.156	0.052	0.255	0.272	0.141		0.249	0.038	0.154		0.153	0.108	0.0488	0.103
Ag107	0.40	86.28	0.43	0.46	34.14	0.36	0.21	1.62	0.40	0.32	1.59	3.02	0.38	0.38	0.45	0.25
Cd111	0.10	6.27			349.55			8.43	0.17		0.14	14.55		0.06		
Sn120	0.18	0.14	0.11	0.08	0.41	0.18	0.10	0.13	0.07	0.10		0.19	0.14	0.07	0.09	0.10
Sb121		0.04			0.09	0.02		0.01		0.02		0.01				
Te126		9.62			6.70	0.21		10.68	0.21	0.18	0.61	10.52	0.08	0.27		0.19
Re185	0.003		0.011	0.008	0.008	0.063	0.047	0.004	0.071	0.022	0.021	0.005		0.034	0.003	0.025
Au197		0.011		0.003	0.005	0.005		0.005	0.003	0.001	0.004	0.010	0.002			0.001
Pb208	0.72	104.45	2.14	0.51	269.94	0.82	0.45	6.43	1.73	1.37	22.40	23.73	3.67	1.13	207.09	2.57
Bi209	0.09	0.51	0.26	0.10	0.45	0.17	0.08	0.14	0.20	0.17	3.59	0.40	0.18	0.20	1.33	0.14

Slide	KV280-620.4	KV280-620.4	KV280-620.4	KV280-620.4	KV280-620.4	KV280-620.4	KV280-620.4	KV280-620.4	KV280-620.4	KV280-620.4	KV280-620.4	KV280-620.4	R688-65.7	R688-65.7	R688-65.7	R688-65.7
Ore Type	**False ore**	**False ore**	**False ore**	**False ore**	**False ore**	**False ore**	**False ore**	**False ore**	**False ore**	**False ore**	**False ore**	**False ore**	**False ore**	**False ore**	**False ore**	**False ore**
Spot Name	kv280-620 gr2_pt2	kv280-620 gr2_pt3	kv280-620 gr3_pt1	kv280-620 gr3_pt2	kv280-620 gr3_pt3	kv280-620 gr4_pt1	kv280-620 gr4_pt2	kv280-620 gr4_pt3	kv280-620 gr5_pt1	kv280-620 gr5_pt2	kv280-620 gr6_pt1	kv280-620 gr6_pt2	R688-65 gr1_pt2	R688-65 gr1_pt3	R688-65 gr1_pt4	R688-65 gr2_pt1
Mineral	**po**	**cpy**	**po**	**po**	**pn**	**po**	**po**	**cpy**	**po**	**po**	**po**	**po**	**po**	**pn**	**cpy**	**po**
Ru	0.067					0.047		0.135	0.0713	0.0565		0.126	0.081		0.099	
Rh	0.007		0.015			0.015			0.008	0.013			0.012			
Pd							0.478				0.204	0.382	0.192		0.043	
Os	0.012			0.005		0.003	0.008	0.006	0.004		0.015	0.006	0.005		0.006	0.007
Ir	0.011		0.004	0.013	0.007	0.006	0.004		0.007	0.007	0.014	0.009	0.003			0.001
Pt					0.005		0.002	0.004					0.007			
S34	351084	330997	379499	391247	357256	379659	388737	325510	376416	362380	366953	396604	372349	338640	313216	386530
Co59	39.6	11537.2	63.6	71.1	204.3	32.4	36.7	863.5	50.8	32.8	41.9	64.6	54.5	1.1	65.7	22.5
Ni61	635	128220	1758	2214	309610	1385	1755	8383	1554	831	806	1700	5	189531	74	3
Cu65	11246	3422660	5975	19628	47839	3923	11204		9885	16371	43654	25188	26451	113771	87513008	3017289
Zn67		439.2	0.9			0.4		281.3	0.9	0.5				2.0	390.8	0.4
Ge72	4.2	3.6	4.3	4.3	3.5	4.0	4.2	3.8	4.1	3.9	4.1	4.9	4.2	4.0	3.7	4.1
As75		0.40	0.23	0.34	0.18	0.27	0.18	0.50	0.17	0.23	0.27		0.18	0.45	0.20	0.35
Se78	84	82	88	96	87	79	88	89	95	84	79	84	41	48	49	35
Mo95	0.076		0.05	0.122	0.054		0.162	0.0384	0.046	0.081	0.153	0.042	0.17	0.139	0.49	
Ag107	0.48	24.21	0.28	0.21	0.79	0.55	0.58	44.66	0.43	0.70	0.48	0.22	0.07	0.10	0.16	0.12
Cd111	0.05	26.21		0.09		0.23	0.07	14.41			0.28			0.03	0.72	
Sn120	0.08	0.18	0.10	0.10	0.08	0.09	0.07	0.26	0.08	0.11	0.10	0.06	0.10	0.04	1.02	0.11
Sb121	0.04	0.06			0.03		0.01	0.04					0.02	0.03	0.08	0.01
Te126	0.09	1.52	0.23	0.20	4.46	0.18	0.25	5.66	0.23	0.07		0.09	0.22	0.24	6.07	0.32
Re185	0.010		0.020	0.012	0.012	0.007	0.289	0.007	0.015	0.031	0.036	0.036	0.017	0.031	0.025	
Au197	0.001	0.013	0.003		0.006	0.001		0.016			0.002	0.003			0.002	
Pb208	1.18	363.74	1.31	0.86	15.42	2.13	2.18	51.86	0.99	2.58	1.67	1.78	0.20	3.37	5.33	0.63
Bi209	0.17	3.24	0.20	0.10	0.59	0.18	0.66	0.28	0.18	0.12	0.14	0.18	0.14	0.17	1.49	0.28

Slide	R688-65.7	R688-65.7	R688-65.7	R688-65.7	R688-65.7	R688-65.7	R688-65.7	R688-65.7	R688-65.7	R688-65.7	R688-65.7	R688-65.7	R688-65.7	KV103-421.2	KV103-421.2	KV103-421.2
Ore Type	**False ore**	**False ore**	**False ore**	**False ore**	**False ore**	**False ore**	**False ore**	**False ore**	**False ore**	**False ore**	**False ore**	**False ore**	**False ore**	**Normal ore**	**Normal ore**	**Normal ore**
Spot Name	R688-65 gr2_pt2	R688-65 gr2_pt3	R688-65 gr3_pt1	R688-65 gr3_pt2	R688-65 gr3_pt3	R688-65 gr4_pt1	R688-65 gr4_pt2	R688-65 gr4_pt3	R688-65 gr5_pt1	R688-65 gr5_pt2	R688-65 gr5_pt3	R688-65 gr6_pt1	R688-65 gr6_pt2	kv103-421 gr1_pt1	kv103-421 gr1_pt2	kv103-421 gr1_pt3
Mineral	**po**	**pn**	**po**	**po**	**pn**	**po**	**po**	**pn**	**po**	**po**	**cpy**	**po**	**po**	**pn**	**po**	**po**
Ru						0.0321				0.054	0.205		0.041		0.161	
Rh			0.024	0.028		0.027						0.027				0.022
Pd							0.133	0.168		0.225		0.176			0.212	0.255
Os	0.007	0.012		0.010	0.011	0.003	0.001		0.005	0.001	0.008	0.004	0.004	0.014	0.029	0.030
Ir		0.011		0.002			0.002		0.001				0.002			0.004
Pt						0.003	0.003						0.005		0.003	
S34	377945	281825	375545	395501	352793	357780	368263	336331	353698	365047	328254	348634	392588	278404	361023	407284
Co59	45.4	0.9	57.8	41.2	2.3	65.6	74.1	3.0	68.5	68.0	4371.3	437.3	51.6	8766.0	8.5	3521.9
Ni61		170354	26	7	196527	34	16	174348	9	10	6847	999	6	252227	1031	82246
Cu65	4562	654153	18968	5727	1798531	3988	9289	587585	14448		2195133	15438	10996	5371	1189	28940
Zn67		4.8	0.3	0.4	6.9		0.3	0.5			2629.3		1.0		1.2	0.4
Ge72	4.3	3.0	4.2	4.2	3.9	3.6	4.4	3.7	3.9	4.5	3.7	4.0	4.2	3.2	4.0	4.1
As75	0.30	0.28	0.13	0.43	0.19	0.47	0.23	0.22	0.39	0.41	0.28	0.38		0.11	0.16	0.13
Se78	41	40	38	44	43	30	34	41	31	40	47	27	37	123	151	160
Mo95	0.034	0.084		0.148	0.172			0.337	0.078	0.059	1.27			0.179	0.246	
Ag107	0.15	0.61	0.09	0.05	1.03	0.09	0.25	1.31	0.12	0.10	1.97	0.07	0.08	6.95	0.59	4.05
Cd111	0.13		0.10						0.07		7.93		0.18			0.26
Sn120	0.07	0.10	0.08	0.15	0.16	0.06	0.07	0.10	0.11	0.10	0.80	0.02	0.12	0.06	0.08	0.18
Sb121	0.02	0.07	0.03		0.20			0.19			0.24	0.01	0.05		0.02	
Te126	0.19	0.30	0.47	0.12	0.46	0.32	1.29	0.50	0.22	0.22	5.62	0.26	0.21	0.17	0.30	0.46
Re185	0.013	0.021	0.019	0.067	0.011	0.038	0.023	0.015	0.023	0.009	0.373	0.005	0.028	0.030	0.031	0.017
Au197			0.002				0.002	0.009	0.002		0.013	0.004				
Pb208	0.27	5.52	0.45	0.28	10.54	0.20	2.08	8.98	0.23	0.26	28.99	0.72	0.61	1.39	1.84	36.81
Bi209	0.17	0.21	0.11	0.24	0.76	0.17	0.16	1.58	0.11	0.11	3.09	0.13	0.19	0.28	0.49	2.45

Slide	KV103-421.2	KV103-421.2	KV103-421.2	KV103-421.2	KV103-421.2	KV103-421.2	KV103-421.2	KV103-421.2	KV103-421.2	KV103-421.2	KV103-421.2	KV103-421.2	KV103-421.2	KV103-421.2	KV103-421.2	KV103-421.2
Ore Type	**Normal ore**	**Normal ore**	**Normal ore**	**Normal ore**	**Normal ore**	**Normal ore**	**Normal ore**	**Normal ore**	**Normal ore**	**Normal ore**	**Normal ore**	**Normal ore**	**Normal ore**	**Normal ore**	**Normal ore**	**Normal ore**
Spot Name	kv103-421 gr1_pt4	kv103-421 gr1_pt5	kv103-421 gr2_pt1	kv103-421 gr2_pt2	kv103-421 gr2_pt3	kv103-421 gr3_pt1	kv103-421 gr3_pt2	kv103-421 gr3_pt3	kv103-421 gr3_pt4	kv103-421 gr3_pt5	kv103-421 gr4_pt1	kv103-421 gr4_pt2	kv103-421 gr4_pt3	kv103-421 gr4_pt4	kv103-421 gr4_pt5	kv103-421 gr5_pt1
Mineral	**cpy**	**cpy**	**po**	**po**	**po**	**pn**	**pn**	**cpy**	**cpy**	**po**	**po**	**po**	**cpy**	**cpy**	**pn**	**po**
Ru	0.176	0.13	0.079	0.126				0.09	0.254	0.154	0.117		0.175	0.136		0.24
Rh			0.038				0.089					0.031				
Pd					0.135	1.86	2.19					0.124			0.91	0.239
Os	0.002	0.002	0.055	0.040	0.044	0.017	0.023			0.049	0.017	0.006	0.001	0.005	0.018	0.051
Ir		0.002	0.002								0.003	0.001	0.002			0.003
Pt	0.004	0.004	0.003							0.002	0.005	0.002			0.003	0.006
S34	335376	359570	367668	400452	378172	307478	319174	361613	325188	353963	355026	346189	336148	327316	294563	385396
Co59	32.4	6.4	21.7	12.1	10.7	18807.6	18085.8	0.4	157.7	13.7	9.8	9.9	0.1	1.5	14228.5	17.5
Ni61	1119	108	2448	1587	1002	300971	316839	12	3374	1016	439	349	13	26	263990	2359
Cu65			5075	1853	681	3975	1036			1221	28316	1626			30803	1650
Zn67	461.6	538.2	0.8	1.0	33.6			379.4	425.8	0.3	1.0		557.6	183.2	1.8	1.1
Ge72	3.7	3.8	4.0	4.1	4.0	4.0	3.4	3.9	3.7	4.0	4.3	3.7	3.6	3.6	3.2	4.2
As75	0.08	0.06	0.07	0.11	0.24	0.59	1.50	0.08	0.21	0.16	0.38	0.33	0.15	0.35	0.30	0.26
Se78	159	161	149	135	142	139	139	174	144	140	168	169	194	188	126	144
Mo95		0.139		0.142	0.149	0.209				0.237	0.113				0.051	0.129
Ag107	2.45	3.59	0.09	0.39	0.46	0.93	1.00	1.16	3.83	0.46	0.85	1.58	4.94	2.79	1.09	0.25
Cd111	8.02	9.64			0.10	0.21		5.61	7.10		0.19	0.15	7.08	4.79		
Sn120	1.63	1.60	0.12	0.07	0.06	0.09	0.12	1.69	1.57	0.12	0.10		2.45	2.22	0.15	0.02
Sb121		0.03	0.01	0.02	0.02	0.03		0.05	0.05	0.03			0.06	0.02	0.03	
Te126	7.06	11.23	0.53	0.11	0.17	5.96	9.54	9.97	4.39	0.05		0.70	39.25	26.30	1.97	
Re185		0.004	0.033	0.047	0.036	0.026	0.007	0.009		0.050	0.041			0.004	0.030	0.020
Au197		0.002			0.002	0.002		0.010	0.004	0.001		0.001	0.030	0.024	0.003	0.005
Pb208	16.83	18.73	0.71	0.12	0.28	4.38	0.90	4.32	24.69	2.52	0.23	0.78	0.93	3.79	9.49	0.20
Bi209	0.68	1.10	0.34	0.25	0.30	0.92	0.61	0.90	1.20	0.49	0.41	0.96	7.88	5.13	1.12	0.35

Slide	KV103-421.2	KV103-421.2	KV103-421.2	KV103-421.2	KV103-421.2	KV103-421.2	KV103-421.2	KV103-421.2	KV34B-327.73	KV34B-327.73	KV34B-327.73	KV34B-327.73	KV34B-327.73	KV34B-327.73	KV34B-327.73	KV34B-327.73
Ore Type	**Normal ore**	**Normal ore**	**Normal ore**	**Normal ore**	**Normal ore**	**Normal ore**	**Normal ore**	**Normal ore**	**Normal ore**	**Normal ore**	**Normal ore**	**Normal ore**	**Normal ore**	**Normal ore**	**Normal ore**	**Normal ore**
Spot Name	kv103-421 gr5_pt2	kv103-421 gr5_pt3	kv103-421 gr5_pt4	kv103-421 gr6_pt1	kv103-421 gr6_pt2	kv103-421 gr6_pt3	kv103-421 gr6_pt4	kv103-421 gr6_pt5	kv34b-327 gr1_pt1	kv34b-327 gr1_pt2	kv34b-327 gr1_pt3	kv34b-327 gr1_pt4	kv34b-327 gr1_pt5	kv34b-327 gr3_pt1	kv34b-327 gr3_pt2	kv34b-327 gr3_pt3
Mineral	**po**	**cpy**	**cpy**	**po**	**cpy**	**cpy**	**pn**	**po**	**po**	**cpy**	**cpy**	**po**	**po**	**po**	**po**	**cpy**
Ru	0.189	0.178	0.327	0.053	0.229	0.172			0.326	0.056	0.042	0.114	0.401	0.072		0.256
Rh							0.010		0.015				0.052			
Pd	0.072						1.11		0.225	0.157	0.121			0.164	0.073	0.069
Os	0.054	0.004	0.003	0.041	0.002	0.004	0.072	0.057	0.077			0.068	0.090		0.005	0.002
Ir		0.001			0.002	0.002						0.012	0.003	0.036		0.007
Pt	0.004	0.007	0.004	0.004	0.018	0.012				0.004		0.009	0.006	0.008		
S34	375729	345681	359573	319346	343107	327915	289968	356954	361802	392446	362433	356755	333608	357596	367794	368910
Co59	18.6	0.9	45.3	7.8	2.1	0.1	14215.4	13.2	15.0	3.1	25.3	10.6	11.2	14.7	8.1	3.3
Ni61	2294	37	1394	284	36	14	283825	519	1944	122	1033	734	850	492	135	78
Cu65	1767			3928			66119	13318	388	1904	15671	15991	1230	524	248	
Zn67		391.6	429.0	2.2	408.7	335.9	1.0	2.6		455.8	564.3	0.8	11.8		0.4	726.7
Ge72	4.2	4.3	3.8	4.5	3.8	3.8	2.8	4.4	3.3	4.0	3.8	3.5	3.1	3.7	4.0	3.7
As75				0.67	0.36	0.14	0.36		0.17	0.11	0.41	0.25	0.35	0.10	0.23	0.12
Se78	135	155	161	143	191	181	138	146	159	198	176	147	153	162	160	180
Mo95	0.141			0.056	0.067		0.273	0.202		0.119		0.047			0.121	0.073
Ag107	0.14	2.57	5.57	1.08	25.54	11.30	3.95	0.80	0.13	0.74	2.18	0.21	0.34	0.21	0.35	0.96
Cd111		7.16	9.81		7.08	5.47				2.56	3.59			0.09		4.58
Sn120	0.12	1.83	1.66	0.29	2.75	3.00	0.13	0.29	0.04	9.61	8.43	0.14	0.08	0.04	0.04	12.87
Sb121	0.01	0.03	0.03	0.05	0.04	0.03	0.04	0.01		0.01	0.19	0.02	0.04	0.01		
Te126	0.42	14.71	11.00		45.55	36.05	6.61	0.45	0.12	5.01	4.27	0.26	0.19	0.10	0.21	5.02
Re185	0.033			0.062		0.006	0.204	0.101	0.008			0.014	0.058			
Au197		0.004	0.007		0.013	0.033	0.019	0.002	0.005		0.005	0.001		0.004	0.002	0.006
Pb208	0.34	2.22	8.11	3.82	14.31	1.46	3.87	9.77	0.24	1.89	6.49	0.33	0.78	0.21	0.32	1.90
Bi209	0.36	2.74	1.76	0.52	8.30	9.31	2.10	1.09	0.09	0.16	0.14	0.09	0.30	0.17	0.05	0.10

Slide	KV34B-327.73	KV34B-327.73	KV34b-327.73	KV34b-327.73	KV34B-327.73	KV34B-327.73	KV34B-327.73	KV34B-327.73	KV34B-327.73	KV34B-554.48	KV34B-554.48	KV34B-554.48	KV34B-554.48	KV34b-554.48	KV34b-554.48	KV34B-554.48
Ore Type	**Normal ore**	**Normal ore**	**Normal ore**	**Normal ore**	**Normal ore**	**Normal ore**	**Normal ore**	**Normal ore**	**Normal ore**	**Normal ore**	**Normal ore**	**Normal ore**	**Normal ore**	**Normal ore**	**Normal ore**	**Normal ore**
Spot Name	kv34b-327 gr3_pt4	kv34b-327 gr4_pt1	kv34b-327 gr4_pt2	kv34b-327 gr4_pt3	kv34b-327 gr4_pt4	kv34b-327 gr4_pt5	kv34b-327 gr4_pt6	kv34b-327 gr5_pt1	kv34b-327 gr5_pt2	kv34b-554 gr1_pt1	kv34b-554 gr1_pt2	kv34b-554 gr1_pt3	kv34b-554 gr1_pt4	kv34b-554 gr1_pt5	kv34b-554 gr1_pt6	kv34b-554 gr2_pt1
Mineral	**cpy**	**cpy**	**pn**	**pn**	**po**	**po**	**cpy**	**po**	**po**	**cpy**	**cpy**	**po**	**po**	**pn**	**pn**	**po**
Ru	0.196	0.208			0.241	0.086	0.193	0.179	0.208	0.223	0.178	0.306	0.449			0.348
Rh					0.021			0.022	0.009							0.013
Pd	0.364	0.63	3.84	4.33		0.084	0.073	0.219					0.274	3.37	3.64	0.207
Os	0.013	0.002	0.130	0.068	0.073	0.092	0.008	0.056	0.053		0.013	0.172	0.176	0.063	0.119	0.140
Ir	0.021	0.003	0.004	0.002	0.003		0.017		0.001			0.011			0.001	
Pt	0.006	0.002					0.006		0.002	0.012	0.004	0.003				
S34	337553	340152	297741	302777	395150	366875	359314	347518	366286	338815	353155	397433	397311	347822	353028	381373
Co59	35.9		17925.9	17436.0	16.7	10.1	0.2	12.5	12.8	3.7	2.3	54.8	160.5	10958.4	10223.6	60.4
Ni61	911	5	280142	297046	960	489	10	1201	1373	15	272	2033	8331	373031	371071	3071
Cu65			746	1044	464		16324		153				2834322		9254	3654
Zn67	391.0	452.2			0.7		356.5		0.4	512.6	743.3	0.7	176.0		1.0	
Ge72	3.9	3.4	3.4	3.2	3.4	3.6	3.5	3.4	3.8	3.9	3.7	4.0	4.1	3.4	3.4	4.1
As75	0.27	0.12	0.09			0.09		0.13	0.15	0.31	0.37	0.15	0.40	0.28	0.11	0.27
Se78	162	165	143	163	166	148	171	159	167	164	160	248	267	189	202	256
Mo95								0.146		0.065	0.072					0.061
Ag107	1.68	0.54	0.31	1.14	0.28	0.51	0.78	0.30	0.24	1.85	3.93	0.17	6.68	0.55	0.56	0.19
Cd111	3.07	2.81		0.07			2.60	0.18	0.14	12.30	14.36		2.96		0.14	
Sn120	11.24	8.96	0.12	0.11	0.04	0.13	10.25	0.14	0.15	2.31	2.65	0.06		0.14	0.07	0.10
Sb121	0.03	0.03	0.01	0.06	0.01	0.01	0.02				0.02			0.06		0.02
Te126	2.39	10.43	1.09	1.00	0.27	0.28	4.29	0.22	0.26	1.03	0.81	0.26	0.54	1.03	1.24	0.26
Re185		0.003	0.003	0.006	0.010	0.021		0.006	0.013	0.001	0.002	0.007	0.009	0.002	0.004	0.006
Au197	0.006		0.012	0.005	0.003	0.002	0.007	0.001	0.001	0.017	0.024	0.002	0.051	0.041	0.019	
Pb208	8.04	0.82	1.66	2.61	0.59	0.77	1.62	0.44	0.57	2.78	2.05	0.13	7.15	3.21		
Bi209	0.20	0.73	0.27	0.36	0.18	0.25	0.18	0.20	0.17	0.82	0.59	0.30	3.00	1.25	0.82	0.26

Slide	KV34b-554.48	KV34b-554.48	KV34B-554.48	KV34B-554.48	KV34B-554.48	KV34b-554.48	KV34B-554.48	KV34B-554.48	KV34b-554.48	KV34b-554.48	KV34B-554.48	KV34B-554.48	KV34B-554.48	KV34B-554.48	KV34B-554.48	KV34B-554.48
Ore Type	**Normal ore**	**Normal ore**	**Normal ore**	**Normal ore**	**Normal ore**	**Normal ore**	**Normal ore**	**Normal ore**	**Normal ore**	**Normal ore**	**Normal ore**	**Normal ore**	**Normal ore**	**Normal ore**	**Normal ore**	**Normal ore**
Spot Name	kv34b-554 gr2_pt2	kv34b-554 gr2_pt3	kv34b-554 gr2_pt4	kv34b-554 gr2_pt5	kv34b-554 gr2_pt6	kv34b-554 gr2_pt7	kv34b-554 gr3_pt1	kv34b-554 gr3_pt2	kv34b-554 gr3_pt3	kv34b-554 gr3_pt4	kv34b-554 gr4_pt1	kv34b-554 gr4_pt2	kv34b-554 gr4_pt3	kv34b-554 gr4_pt4	kv34b-554 gr5_pt1	kv34b-554 gr5_pt2
Mineral	**pn**	**pn**	**po**	**cpy**	**cpy**	**pn**	**po**	**po**	**pn**	**pn**	**po**	**po**	**cpy**	**cpy**	**po**	**po**
Ru			0.116	0.217	0.147		0.37	0.18			0.241	0.612	0.325	0.185	0.409	0.301
Rh		0.044				0.739	0.027	0.019	0.205	0.226					0.026	0.042
Pd	0.95	0.7				5.84			7.33	6.17					0.093	0.091
Os	0.041	0.039	0.140	0.004	0.004	0.064	0.185	0.123	0.220	0.232	0.086	0.870		0.002	0.173	0.160
Ir	0.002	0.002	0.002			0.013	0.038	0.002	0.009	0.011	0.004	1.890	0.002			0.002
Pt	0.002			0.002						0.002		1.680	0.001		0.004	0.006
S34	330956	348909	415385	377332	351962	395865	397900	375571	324097	306052	377056	396080	347952	353857	403170	383781
Co59	10732.7	10515.0	70.3	0.3	0.1	9385.6	73.5	67.8	11194.6	11307.9	72.4	309.6	0.1	0.2	91.1	73.0
Ni61	372335	365906	3108	185	10	400514	4406	4235	370125	337757	3813	7570	18	12	5321	4046
Cu65	32997	2079	46060			18757	1103	3268	12936	5463	4140221	10574677			1593	17789
Zn67	0.4			573.1	600.0		0.4		79.5	1.6	48.6	328.1	569.6	504.9	1.5	1.0
Ge72	3.4	3.5	4.2	3.5	3.6	3.8	4.1	4.0	3.5	3.2	4.0	4.6	3.3	3.3	3.9	3.6
As75	0.09	0.30	0.14	0.19	0.10	3.62	0.26	0.06	1.32	1.53		4.15	0.21			
Se78	212	220	266	178	166	236	265	251	161	261	257	248	167	155	248	251
Mo95			0.088				0.099		0.09	0.12		0.259		0.092		0.039
Ag107	1.82	0.42	0.09	1.85	1.56	1.23	0.25	0.45	0.54	0.71	0.68	36.19	1.48	1.29	0.62	0.08
Cd111	0.38		0.29	9.63	10.30			0.15	0.12		0.68	5.40	10.53	10.32		0.35
Sn120	0.10	0.04	0.14	3.08	2.73	0.20	0.07	0.08	0.11	0.07	0.13	0.23	2.21	1.90	0.14	0.07
Sb121	0.05	0.03		0.03		0.12			0.02			0.02				0.01
Te126	6.15	6.08	0.33	0.89	0.91	49.31	0.17	0.09	21.80	30.44	0.28	0.42	1.20	0.66	0.10	0.25
Re185	0.004	0.005	0.009	0.002		0.014	0.013	0.009	0.018	0.013		0.026			0.003	0.010
Au197	0.051	0.003		0.009	0.018	0.004	0.043	0.007	0.004	0.007		0.003	0.014	0.022		
Pb208	7.62	1.63	0.25	2.51	2.30	5.86	0.44	0.77	0.71	1.76	1.19	16.12	2.26	2.12	0.97	0.08
Bi209	3.92	0.94	0.48	0.61	0.64	2.08	0.35	0.82	0.62	1.26	1.43	5.48	0.54	0.49	1.04	0.23

Slide	KV34b-554.48	KV34b-554.48	KV45-32	KV45-32	KV45-32	KV45-32	KV45-32	KV45-32	KV45-32	KV45-32	KV45-32	KV45-32	KV45-32	KV45-32	KV45-32	KV45-32
Ore Type	**Normal ore**	**Normal ore**	**Normal ore**	**Normal ore**	**Normal ore**	**Normal ore**	**Normal ore**	**Normal ore**	**Normal ore**	**Normal ore**	**Normal ore**	**Normal ore**	**Normal ore**	**Normal ore**	**Normal ore**	**Normal ore**
Spot Name	kv34b-554 gr5_pt3	kv34b-554 gr5_pt4	kv45-32 gr1_pt1	kv45-32 gr1_pt2	kv45-32 gr1_pt3	kv45-32 gr1_pt4	kv45-32 gr1_pt5	kv45-32 gr2_pt1	kv45-32 gr2_pt2	kv45-32 gr2_pt3	kv45-32 gr2_pt4	kv45-32 gr3_pt1	kv45-32 gr3_pt2	kv45-32 gr3_pt3	kv45-32 gr3_pt4	kv45-32 gr4_pt1
Mineral	**pn**	**pn**	**po**	**po**	**pn**	**pn**	**po**	**po**	**po**	**cpy**	**cpy**	**po**	**po**	**cpy**	**cpy**	**po**
Ru			0.129	0.2			0.17	0.284	0.445	0.294	0.319	0.128	0.24	0.249	0.152	0.254
Rh	0.010			0.008	0.077			0.041	0.054							
Pd	3.38	0.81	0.164	0.124	0.432	1.01	0.193	0.315				0.091				
Os	0.108	0.101	0.073	0.104	0.054	0.081	0.081	0.163	0.168	0.002	0.002	0.048	0.029	0.002		0.120
Ir	0.005	0.006		0.002	0.087		0.004	0.038	0.045	0.002	0.004		0.002	0.003	0.002	
Pt	0.016	0.007		0.006	0.147	0.003	0.009	0.055	0.041	0.066	0.103	0.012		0.020	0.181	0.004
S34	327607	250213	379203	379856	242811	318039	381188	401306	384158	402074	382082	386293	411477	409682	368748	375761
Co59	10108.4	2267.5	9.4	11.4	4754.2	12256.1	10.1	51.1	12.6	10.5	10.2	21.0	24.3	3.6	0.5	11.4
Ni61	325089	77204	1451	1921	149255	287033	2173	1935	1878	510	515	1652	2280	52	22	2044
Cu65	31236	9284	24392	28511	148274	504231	32954	3428	4279			2646	3007			11044
Zn67	1.2		1.4	0.7	2.6	1.6	1.4	1.1	19.3	750.5	477.6		25.7	7895.2	501.6	0.7
Ge72	3.6	2.4	3.4	3.6	2.5	3.1	3.9	3.7	3.7	4.0	3.9	3.5	4.3	3.8	3.7	3.6
As75	0.43	0.12	0.57	0.52	0.57	0.51	0.39	0.55	0.75	0.37	0.41	0.41	0.43	0.40	0.38	0.42
Se78	225	163	194	202	132	175	185	175	189	184	170	273	247	289	234	207
Mo95			0.097	0.091	0.0317	0.149	0.12	0.034	0.093	0.05	0.055	0.11				
Ag107	0.73	2.60	0.29	0.19	2.59	1.86	0.33	0.68	0.27	2.58	2.47	0.17	0.07	3.85	3.02	0.26
Cd111	0.09		0.06	0.06					0.28	12.16	6.92		0.07	143.16	13.10	0.11
Sn120	0.13	0.06	0.17	0.03	0.09	0.10	0.14	0.03	0.08	6.19	5.82	0.12	0.10	4.81	5.20	
Sb121	0.02	0.03	0.03		0.03	0.05							0.04	0.02		
Te126	2.44	0.47	0.45	0.11	0.31	0.15	0.27	0.30	0.35	9.52	13.61	0.04		8.04	25.47	0.11
Re185	0.010		0.019	0.041	0.003	0.034	0.018	0.037	0.044			0.036	0.022	0.006		0.010
Au197		0.095	0.002				0.002				0.005			0.005		
Pb208	5.99	15.69	0.21	0.55	17.56	12.56	1.79	1.27	0.25	5.20	4.44	0.27	0.16	27.10	8.71	0.22
Bi209	1.66	4.24	0.62	0.85	2.88	4.13	0.35	0.27	0.22	1.18	1.09	0.23	0.15	2.64	6.52	0.50

Slide	KV45-32	KV45-32	KV45-32	KV45-32	KV45-32	KV45-32	KV45-32	KV45-32	KV45-32	KV45-32	KV45-32	KV45-32	KV45-32	KV45-35	KV45-35	KV45-35
Ore Type	**Normal ore**	**Normal ore**	**Normal ore**	**Normal ore**	**Normal ore**	**Normal ore**	**Normal ore**	**Normal ore**	**Normal ore**	**Normal ore**	**Normal ore**	**Normal ore**	**Normal ore**	**Normal ore**	**Normal ore**	**Normal ore**
Spot Name	kv45-32 gr4_pt2	kv45-32 gr4_pt3	kv45-32 gr4_pt4	kv45-32 gr5_pt1	kv45-32 gr5_pt2	kv45-32 gr5_pt3	kv45-32 gr5_pt4	kv45-32 gr6_pt1	kv45-32 gr6_pt2	kv45-32 gr6_pt3	kv45-32 gr6_pt4	kv45-32 gr6_pt5	kv45-32 gr6_pt6	kv45-35 gr1_pt1	kv45-35 gr1_pt2	kv45-35 gr1_pt3
Mineral	**po**	**pn**	**pn**	**po**	**po**	**cpy**	**cpy**	**cpy**	**cpy**	**pn**	**pn**	**po**	**po**	**po**	**po**	**cpy**
Ru	0.256			0.155	0.075	0.213		0.206	0.13			0.72	0.741	0.325	0.367	0.323
Rh	0.016	0.024	0.540	0.007						0.086	0.014		0.024	0.036	0.076	
Pd		0.94	1.81							1.55	2.48		0.343	0.123	0.127	
Os	0.177	0.057	1.100	0.046	0.039		0.009	0.004		0.035	0.208	0.243	0.203	0.172	0.130	
Ir	0.351	0.005	0.005	0.022	0.010	0.002		0.003	0.003	0.003	0.001	0.003		0.111	0.274	
Pt						0.034	0.119	0.039	0.125		0.004			0.032	0.033	0.242
S34	402775	297215	324140	373783	383827	353280	407235	354385	343195	303988	329566	370027	345894	393847	367823	365717
Co59	11.9	11074.8	11953.8	163.5	13.9	14.3	130.1	0.2	2.4	12559.6	13043.5	7.6	62.7	27.8	18.5	221.6
Ni61	2097	271898	304395	6586	1787	736	6093	14	151	290372	301375	704	2336	2184	950	5408
Cu65	27310	19272	86383	69614	261356					2980969	3233660	8753	65234	1941		
Zn67	2.3		2.8		1.8	440.2	632.3	501.4	588.1	98.2	0.6	1.0		0.5	0.6	350.6
Ge72	3.5	2.9	3.0	3.9	3.7	3.6	3.8	3.3	3.4	3.0	3.3	3.2	3.7	4.2	4.0	3.6
As75		0.13	2.58	0.47	0.44	0.50	0.41	0.26	0.53	0.24	0.25		0.56	0.54	0.64	0.07
Se78	212	157	273	185	181	168	203	167	157	183	157	164	171	232	218	194
Mo95	0.073	0.075		0.223	0.159		0.082		0.107	0.116		0.122		0.313	0.931	0.094
Ag107	0.34	0.87	0.90	1.18	0.67	1.99	19.26	6.46	9.82	3.60	1.54	0.74	1.75	0.62	0.88	6.48
Cd111	0.25	0.11	0.25	0.05		7.62	11.90	11.47	12.06	4.16				0.07		9.49
Sn120	0.03	0.17	0.19	0.05	0.09	3.19	3.47	4.03	3.92	0.16	0.04		0.12	0.08	0.12	0.98
Sb121			0.07		0.02	0.03				0.02				0.02		0.02
Te126	0.12	4.80	54.69	0.24	0.33	4.90	8.96	8.50	15.49	25.39	0.95		0.12	0.26	0.64	10.58
Re185	0.027	0.006	0.065	0.052	0.039	0.004	0.005		0.005	0.004		0.038	0.017	0.195	0.660	0.007
Au197		0.005		0.002	0.003	0.003	0.017	0.005	0.002	0.002	0.003	0.001			0.004	0.003
Pb208	0.52	4.88	1.96	1.47	1.05	7.27	26.75	0.75	0.91	2.96	2.39	0.08	1.30	1.75	6.84	25.91
Bi209	0.57	4.22	0.43	0.59	0.53	1.25	5.17	1.58	2.85	2.54	0.63	0.26	0.93	0.92	1.20	2.60

Slide	KV45-35	KV45-35	KV45-35	KV45-35	KV45-35	KV45-35	KV45-35	KV45-35	KV45-35	KV45-35	KV45-35	KV45-35	KV45-35	KV45-35	KV45-35	KV45-35
Ore Type	**Normal ore**	**Normal ore**	**Normal ore**	**Normal ore**	**Normal ore**	**Normal ore**	**Normal ore**	**Normal ore**	**Normal ore**	**Normal ore**	**Normal ore**	**Normal ore**	**Normal ore**	**Normal ore**	**Normal ore**	**Normal ore**
Spot Name	kv45-35 gr1_pt4	kv45-35 gr1_pt5	kv45-35 gr2_pt1	kv45-35 gr2_pt2	kv45-35 gr2_pt3	kv45-35 gr2_pt4	kv45-35 gr2_pt5	kv45-35 gr3_pt1	kv45-35 gr3_pt2	kv45-35 gr3_pt3	kv45-35 gr3_pt4	kv45-35 gr4_pt1	kv45-35 gr4_pt2	kv45-35 gr4_pt3	kv45-35 gr4_pt4	kv45-35 gr4_pt5
Mineral	**cpy**	**pn**	**cpy**	**cpy**	**po**	**po**	**cpy**	**cpy**	**cpy**	**po**	**po**	**po**	**po**	**cpy**	**cpy**	**cpy**
Ru	0.162		0.068	0.135	0.354	0.46		0.16	0.135	0.241	0.292	0.228	0.441	0.1	0.102	0.449
Rh		0.236			0.062	0.014				0.027	0.037	0.043				
Pd		0.58				0.112	0.244									
Os		0.004		0.001	0.198	0.184	0.206	0.002	0.005	0.136	0.146	0.137	0.143			0.0045
Ir	0.001	0.005			0.052	0.055	0.501			0.150	0.172	0.052	0.015	0.010		
Pt	0.331	0.002	0.415	0.013	0.016	0.018	0.190	0.164	0.318	0.048	0.072	0.015		0.051	0.372	0.017
S34	385845	363673	408657	361098	388138	410501	214344	381650	391016	365405	389507	401033	412725	361453	399128	404640
Co59	4.1	17553.6	0.2	2.3	13.0	30.8	1919.0	8.4	0.5	9.4	11.1	16.5	17.9	65.4	2.1	21.9
Ni61	129	312562	19	78	780	2224	33680	193	14	486	42	1397	2130	3724	54	1109
Cu65		4926467			7691	2552	1355487				1102	2852	2414	675341	20665	11226
Zn67	552.6	151.1	530.1	505.4	1.2		23.9	721.0	727.6			1.5	0.7	896.8	319.4	859.7
Ge72	3.9	3.5	4.4	3.7	3.5	3.9	2.3	4.0	3.9	3.7	3.6	4.3	4.2	3.9	4.3	4.2
As75	0.12	0.14		0.21	0.21	0.20	1.46	0.06	0.26	0.50	0.10	0.50	0.28	0.50	0.27	1.10
Se78	212	196	228	207	218	235	138	190	196	188	227	221	256	180	217	230
Mo95		0.064			0.304	0.3				0.146	0.152	0.417	0.514		0.149	0.044
Ag107	9.43	6.07	5.34	2.26	0.76	0.19	7.78	3.52	2.45	0.83	0.54	0.69	0.37	16.39	3.95	6.32
Cd111	13.91	1.87	11.96	8.76		0.07	0.45	17.56	13.26	0.24		0.19	0.07	22.53	9.16	26.17
Sn120	1.22	0.08	1.46	1.02	0.09	0.17		0.94	1.02	0.12	0.14	0.11	0.13	1.30	1.56	1.49
Sb121	0.01	0.03		0.03				0.01	0.04			0.04				0.10
Te126	14.57	2.68	15.65	3.04	0.28	0.27	0.10	6.43	6.89	0.27			0.32	3.00	10.13	3.62
Re185			0.004	0.005	0.055	0.114	0.012	0.001		0.064	0.082	0.089	0.092	0.012		
Au197	0.002	0.003		0.010			0.468	0.003	0.003	0.001			0.005			
Pb208	6.59	23.20	10.65	10.33	0.28	0.23	18.47	9.39	7.97	0.21	0.18	1.46	0.28	39.10	11.50	18.77
Bi209	3.96	2.87	4.75	0.49	0.20	0.19	2.97	1.44	2.30	0.13	0.16	0.30	0.26	1.00	3.21	0.94

Slide	KV45-35	KV45-35	KV45-35	KV45-35	KV45-35	KV45-35	KV45-35	KV45-35	KV45-35	KV45-35	KV45-63	KV45-63	KV45-63	KV45-63	KV45-63	KV45-63
Ore Type	**Normal ore**	**Normal ore**	**Normal ore**	**Normal ore**	**Normal ore**	**Normal ore**	**Normal ore**	**Normal ore**	**Normal ore**	**Normal ore**	**Ni-PGE ore**	**Ni-PGE ore**	**Ni-PGE ore**	**Ni-PGE ore**	**Ni-PGE ore**	**Ni-PGE ore**
Spot Name	kv45-35 gr5_pt1	kv45-35 gr5_pt2	kv45-35 gr5_pt3	kv45-35 gr5_pt4	kv45-35 gr6_pt1	kv45-35 gr6_pt2	kv45-35 gr6_pt3	kv45-35 gr6_pt4	kv45-35 gr6_pt5	kv45-35 gr6_pt6	kv45-63 gr1_pt1	kv45-63 gr1_pt2	kv45-63 gr1_pt3	kv45-63 gr1_pt4	kv45-63 gr2_pt1	kv45-63 gr2_pt2
Mineral	**po**	**po**	**cpy**	**cpy**	**po**	**po**	**pn**	**pn**	**cpy**	**cpy**	**pn**	**pn**	**pn**	**pn**	**pn**	**pn**
Ru	0.043		0.239	0.2	0.27	0.377			0.127	0.246						
Rh	0.010	0.039				0.026	0.097	0.043				0.016				
Pd							3.64	3.83			10.42	10.07	8.72	8.68	6.4	6.03
Os			0.003	0.002	0.173	0.112	0.037		0.004	0.002	0.154	0.053	0.13	0.168	0.142	0.188
Ir	0.002		0.001	0.002	0.002	0.078			0.003							
Pt	0.222	0.063	1.660	1.350	0.004	0.043	0.004		0.155	0.010	0.008	0.011		0.003	0.009	
S34	377149	368366	347354	390849	372930	410639	327529	340748	401830	406534	327321	300587	310254	313493	311456	317039
Co59	10.2	4.0	0.1	7.3	15.0	16.6	15501.4	15225.3	1.3	2.6	5027.5	4954.4	5127.8	5353.9	4702.7	4996.5
Ni61	696	21	12	93	1733	2192	315293	315531	9	161	350000	335078	336222	334451	320092	342465
Cu65	44479	140397			461	4544	17326	34516		2902	424	1547	13942	5959	2210	10264
Zn67		0.3	466.6	690.6		1.9	0.3	0.8	329.1	504.1	0.7	1.5	2.2	1.2		1.3
Ge72	4.1	3.5	3.7	4.0	3.9	4.3	3.2	3.0	4.0	3.9	3.9	3.6	3.7	3.5	3.4	3.3
As75	0.25	0.30	0.30	0.13	0.19	0.53	0.52	0.18	0.44	0.11	3.31	2.34	4.16	2.25	0.77	0.63
Se78	198	189	189	202	231	231	181	173	212	223	287	259	280	305	299	295
Mo95				0.06	0.231	0.233	0.134		0.065		0.066		0.294		0.118	
Ag107	1.32	1.11	3.81	1.69	0.34	0.19	13.65	1.97	1.18	1.53	0.22	0.10	0.51	0.08	0.41	0.13
Cd111		0.09	9.55	13.88					10.83	15.58	0.09					
Sn120		0.08	1.39	1.37		0.10	0.10	0.11	1.46	1.84	0.10	0.11	0.07	0.02	0.14	0.06
Sb121	0.04		0.01		0.02			0.02				0.02	0.08			
Te126	2.48	0.50	14.45	15.81	0.08	0.15	18.00	3.75	4.79	2.74	10.76	9.33	12.47	7.50	0.83	0.91
Re185			0.005	0.003	0.098	0.035	0.035	0.007		0.004		0.002	0.021	0.007	0.006	0.005
Au197		0.001	0.014	0.015		0.004	0.005	0.003	0.006	0.005	0.016	0.002	0.034	0.006	0.015	0.002
Pb208	0.18	1.26	14.47	3.94	0.13	0.20	15.00	2.69	11.99	6.04	0.07	0.33	4.36	2.03	0.17	0.41
Bi209	0.97	0.31	4.51	4.15	0.17	0.23	0.22	0.37	1.58	0.29	0.91	0.49	3.13	0.94	1.73	0.40

Slide	KV45-63	KV45-63	KV45-63	KV45-63	KV45-63	KV45-63	KV45-63	KV45-63	KV45-63	KV45-63	KV45-63	KV45-63	KV45-63	KV45-63	KV45-63	KV45-63
Ore Type	**Ni-PGE ore**	**Ni-PGE ore**	**Ni-PGE ore**	**Ni-PGE ore**	**Ni-PGE ore**	**Ni-PGE ore**	**Ni-PGE ore**	**Ni-PGE ore**	**Ni-PGE ore**	**Ni-PGE ore**	**Ni-PGE ore**	**Ni-PGE ore**	**Ni-PGE ore**	**Ni-PGE ore**	**Ni-PGE ore**	**Ni-PGE ore**
Spot Name	kv45-63 gr2_pt3	kv45-63 gr2_pt4	kv45-63 gr2_pt5	kv45-63 gr2_pt6	kv45-63 gr2_pt7	kv45-63 gr3_pt1	kv45-63 gr3_pt2	kv45-63 gr3_pt3	kv45-63 gr3_pt4	kv45-63 gr3_pt5	kv45-63 gr4_pt1	kv45-63 gr4_pt2	kv45-63 gr4_pt3	kv45-63 gr4_pt4	kv45-63 gr5_pt1	kv45-63 gr5_pt2
Mineral	**pn**	**py**	**py**	**po**	**po**	**po**	**py**	**pn**	**pn**	**pn**	**pn**	**po**	**po**	**pn**	**pn**	**pn**
Ru			1.9	0.506	0.537	0.413						0.113	0.057			
Rh		0.023		0.022		0.008	0.134	0.037						0.014	0.028	0.012
Pd	5.16	6.34	8.39		0.214	0.121	4.65	3.76	6.13	6.15	0.68			4.18	5.09	5.42
Os	0.206	0.255	0.246	0.245	0.214	0.269	0.35	0.115	0.125	0.176	0.128	0.339	0.234	0.19	0.105	0.112
Ir									0.005		0.005		0.021			
Pt	0.003	0.004	0.003			0.005		0.002		0.007		0.002	0.003	0.003	0.004	
S34	297365	483386	503693	345800	353909	377119	499415	268345	308467	317128	264456	354273	363245	360066	342486	335192
Co59	4173.3	7588.7	7739.5	4.7	12.5	39.4	12094.0	2734.6	4927.3	5029.1	4810.1	25.7	251.0	18450.3	6622.3	5886.6
Ni61	312911	277325	393627	1691	1481	3349	79979	194040	311238	321115	213820	2221	11653	111314	238693	247192
Cu65	12832	1131349	1097747	871	1482	926	2271748	9598	15553	30806	2040	1094	1112	37501	63996	585961
Zn67	6.0	23.9	22.1	11.6		1.6	215.2	0.2	0.8	0.7	8.7	2.7		4.2	0.4	
Ge72	3.3	5.4	5.7	4.4	3.6	3.9	5.5	2.8	3.6	3.5	3.1	4.1	4.4	4.1	4.2	3.9
As75	0.83	7.66	5.15	0.37		0.58	3.11	0.30	4.32	1.13	0.30	0.51	0.12	4.51	0.84	4.41
Se78	294	500	447	346	340	322	548	251	262	321	263	336	328	415	348	353
Mo95					0.073	0.08					0.111			0.122		
Ag107	0.27	2.38	0.88	0.13	0.36	0.27	3.89	0.27	0.08	0.22	0.42	0.24	0.85	0.54	11.27	8.79
Cd111	0.12						0.93						0.18		0.49	
Sn120	0.18	0.08		0.15	0.10	0.12	0.04	0.07	0.13	0.05	0.03	0.06	0.06	0.05	0.04	0.05
Sb121		1.00	0.87			0.03	1.06	0.07	0.06	0.03	0.01	0.05		0.04	0.12	0.41
Te126	0.75	14.35	15.17	0.78	1.32	0.58	4.82	2.29	9.70	9.09	5.49	0.57	1.21	20.43	1.22	3.71
Re185		0.009	0.018		0.008	0.008	0.009		0.006	0.004		0.006	0.007			0.004
Au197	0.006	0.373	0.018	0.005	0.101	0.005	0.235		0.003			0.009	0.002	0.089	0.105	0.076
Pb208	2.00	25.93	3.27	0.46	0.28	2.89	38.56	15.34	0.07	5.69	3.44	0.23	0.42	17.64	7.01	14.73
Bi209	0.34	77.54	6.54	0.46	1.16	1.14	107.82	2.09	0.20	0.82	3.57	1.80	2.29	85.53	61.21	68.59

Slide	KV45-75	KV45-75	KV45-75	KV45-75	KV45-75	KV45-75	KV45-75	KV45-75	KV45-75	KV45-75	KV45-75	KV45-75	KV45-75	KV45-75	KV45-75	KV45-75
Ore Type	**Ni-PGE ore**	**Ni-PGE ore**	**Ni-PGE ore**	**Ni-PGE ore**	**Ni-PGE ore**	**Ni-PGE ore**	**Ni-PGE ore**	**Ni-PGE ore**	**Ni-PGE ore**	**Ni-PGE ore**	**Ni-PGE ore**	**Ni-PGE ore**	**Ni-PGE ore**	**Ni-PGE ore**	**Ni-PGE ore**	**Ni-PGE ore**
Spot Name	kv45-75 gr1_pt1	kv45-75 gr1_pt2	kv45-75 gr1_pt3	kv45-75 gr1_pt4	kv45-75 gr1_pt5	kv45-75 gr1_pt6	kv45-75 gr2_pt1	kv45-75 gr2_pt2	kv45-75 gr2_pt3	kv45-75 gr2_pt4	kv45-75 gr2_pt5	kv45-75 gr2_pt6	kv45-75 gr3_pt1	kv45-75 gr3_pt2	kv45-75 gr4_pt1	kv45-75 gr4_pt2
Mineral	**po**	**po**	**pn**	**pn**	**pn**	**py**	**pn**	**pn**	**py**	**py**	**po**	**cpy**	**pn**	**pn**	**py**	**py**
Ru	0.346	0.151				0.395			0.073	0.359	0.118	0.77			0.345	0.245
Rh	0.020			0.046			0.018	0.012	0.457	0.012	0.013		0.033	0.053	0.009	
Pd		0.183	8.78	9.28	4.97	1.94	9.61	10.95	0.08	2.29		1.86	10.45	10.58	0.127	
Os	0.109	0.086	0.073	0.086	0.181	0.099	0.006	0.006	0.006	0.021	0.016	0.006	0.096	0.183	0.145	0.124
Ir	0.005	0.001	0.005		0.001		0.004		0.001	0.002	0.011					0.001
Pt	0.013	0.003	0.017	0.005	0.005			0.004				0.002	0.005	0.009		0.003
S34	372636	378945	341970	310484	308209	491983	340444	319909	615785	575734	379753	218503	342410	112625	611966	575846
Co59	2.4	4.3	3587.5	2822.4	3431.9	7949.6	4002.6	3743.0	225.1	3977.6	30.9	1184.8	3687.9	4724.5	227.1	306.4
Ni61	4444	3783	294139	355365	334014	31182	362713	370210	3786	37154	8051	113822	381546	295884	1453	851
Cu65		1161	20582	2183	367	1754098	1063	351	4486517	159994	406	7726933	639	24002	1182	54
Zn67			10.4	0.3	0.4	11.2		3.5	13.0	1.6	0.3	107.2	1.9	3.8		2.3
Ge72	3.7	4.3	3.6	2.8	3.2	4.9	3.8	3.3	6.1	6.1	3.5	2.9	3.3	3.6	6.2	5.6
As75	0.39	1.41	3.93	0.86	135.69	6.16	1.30	0.87	3.62	10.38	0.16	1.51	0.30	12.15	34.87	32.90
Se78	362	364	326	305	325	587	309	330	700	757	373	209	328	348	818	689
Mo95	0.127	0.211		0.136		0.226	0.362					0.473	0.096	0.102	0.142	
Ag107	0.23	0.06	0.76	0.07	0.31	4.18	0.35	0.30	0.20	0.64	0.43	1.83	0.28	5.53	0.05	0.03
Cd111									0.10	0.10	0.38	0.29	0.23		0.15	0.12
Sn120	0.04	0.03	0.07	0.13	0.22	0.06	0.06	0.12	0.04	0.08	0.10	0.10	0.05	0.16	0.01	0.02
Sb121		0.03	0.27		0.06	0.27	0.05		0.04	0.68	0.01	0.06	0.04	0.62		0.12
Te126	1.57	0.85	7.86	1.11	81.26	7.92	2.84	2.06	4.50	32.70	0.50	1.57	0.75	3.63	5.95	4.55
Re185	0.018	0.022	0.021	0.083	0.061	0.039	0.018	0.004		0.005	0.008	0.036		0.011	0.006	0.011
Au197			0.053		0.008	0.980	0.022	0.010	0.027	0.238				0.077	0.005	0.006
Pb208	0.06	0.10	8.27	0.20	0.30	16.07	1.25	1.00	2.86	9.52	0.90	3.41	0.83	33.15	0.82	0.20
Bi209	0.13	0.48	12.65	0.02	0.60	87.53	1.65	0.65	15.91	107.95	0.51	0.92	0.04	20.69	1.07	2.07

Slide	KV45-75	KV45-75	KV45-75	KV45-75	KV45-75	KV45-75	KV45-75	KV45-75	KV45-75	KV45-75	KV45-75	KV45-75	KV45-75	KV45-75	KV45-75	R695-68.1
Ore Type	**Ni-PGE ore**	**Ni-PGE ore**	**Ni-PGE ore**	**Ni-PGE ore**	**Ni-PGE ore**	**Ni-PGE ore**	**Ni-PGE ore**	**Ni-PGE ore**	**Ni-PGE ore**	**Ni-PGE ore**	**Ni-PGE ore**	**Ni-PGE ore**	**Ni-PGE ore**	**Ni-PGE ore**	**Ni-PGE ore**	**Ni-PGE ore**
Spot Name	kv45-75 gr4_pt3	kv45-75 gr5_pt1	kv45-75 gr5_pt2	kv45-75 gr5_pt3	kv45-75 gr5_pt4	kv45-75 gr6_pt1	kv45-75 gr6_pt2	kv45-75 gr6_pt3	kv45-75 gr6_pt4	kv45-75 gr7_pt1	kv45-75 gr7_pt2	kv45-75 gr7_pt3	kv45-75 gr7_pt4	kv45-75 gr8_pt1	kv45-75 gr8_pt2	r695-68.1 gr1_ln1
Mineral	**pn**	**py**	**py**	**pn**	**pn**	**pn**	**pn**	**py**	**po**	**pn**	**pn**	**po**	**py**	**py**	**pn**	**pn**
Ru		0.27	0.322						0.437							5.69
Rh	0.521		0.038	0.037				0.028	0.013	0.022	0.014	0.170	0.085	0.216	0.030	3.450
Pd	9.48	0.1		9.41	8.92	9.48	10.44	7.24	0.143	6.69	6.57	7.78	5.04	14.59	14.46	4.47
Os	0.210	0.233	0.255	0.132	0.093	0.006	0.005	0.147	0.200	0.025	0.045	0.169	0.112	0.178	0.357	1.55
Ir	0.189		0.006	0.002	0.007	0.003	0.003	0.003	0.008	0.001	0.001	0.003	0.002	0.003		0.024
Pt	0.080	0.003	0.004	0.002	0.008	0.007	0.007						0.003	0.013	0.003	0.007
S34	366656	527265	558381	385465	346119	333889	339748	482035	376948	346209	335961	651948	482777	546383	363606	392190
Co59	4019.3	4330.5	4048.8	4245.1	4042.5	3152.1	2958.9	6896.1	3.8	3661.8	3765.4	14825.3	6462.1	5755.6	2641.6	1322.2
Ni61	362013	1662	2448	397136	376011	364724	352952	242535	4169	340752	368817	202022	250300	326544	379746	502281
Cu65	4912	113356	78420	784	454	320	110	261216	620	1067	2128	1265864	434559	2096090	3699	
Zn67	1.0	2.5	0.9		2.2			38.3	0.5	1.6	4.3	17.0	5.6	8.7	1.0	2.1
Ge72	4.0	5.6	5.8	3.8	3.2	3.5	3.6	4.4	3.8	3.6	3.2	7.0	4.4	5.4	3.8	4.0
As75	16.85	1.73	1.54	0.85	2.96	10.80	8.31	5.59	0.29	9.49	41.47	15.98	8.97	27.60	93.77	344.80
Se78	444	845	891	454	418	388	327	520	418	373	370	852	571	674	491	763
Mo95		0.12	0.193		0.122		0.057	0.207	0.086			0.305		0.093	0.067	0.116
Ag107	0.43	0.28	0.29	0.11	0.12	0.14	0.07	3.05	0.08	0.32	0.18	18.52	10.96	1.41	0.49	
Cd111	0.37				0.19							0.38		0.38		0.52
Sn120	0.09	0.01	0.05		0.15	0.10	0.09	0.03	0.11	0.13	0.13	0.05	0.34	0.11	0.18	1.11
Sb121	0.01	0.08	0.11	0.02				0.93	0.04		0.12	1.32	1.75	0.44		0.10
Te126	16.98	4.01	3.66	3.98	10.63	17.00	11.67	2.83	1.04	13.34	25.68	10.00	3.24	16.92	57.18	650.62
Re185	0.005	0.011	0.021		0.013		0.010	0.018	0.010	0.004	0.013	0.040			0.026	0.018
Au197		0.224	0.265			0.004		0.130	0.004	0.005	0.003	0.400	0.318	0.520		0.015
Pb208	2.97	2.34	2.27	0.11	0.62	0.10	0.09	21.10	0.21	1.80	2.67	108.48	75.38	24.67	2.99	0.04
Bi209	0.39	85.42	84.41	0.16	0.32	0.31	0.02	8.34	0.31	0.92	0.33	145.19	24.69	71.73	0.50	1.46

Slide	R695-68.1	R695-68.1	R695-68.1	R695-68.1	R695-68.1	R695-68.1	R695-68.1	R695-68.1	R695-68.1	R695-68.1	R695-68.1	R695-68.1	R695-68.1	R695-68.1	R695-68.1	R695-68.1
Ore Type	**Ni-PGE ore**	**Ni-PGE ore**	**Ni-PGE ore**	**Ni-PGE ore**	**Ni-PGE ore**	**Ni-PGE ore**	**Ni-PGE ore**	**Ni-PGE ore**	**Ni-PGE ore**	**Ni-PGE ore**	**Ni-PGE ore**	**Ni-PGE ore**	**Ni-PGE ore**	**Ni-PGE ore**	**Ni-PGE ore**	**Ni-PGE ore**
Spot Name	r695-68.1 gr1_pt1	r695-68.1 gr1_pt1	r695-68.1 gr1_pt2	r695-68.1 gr1_pt2	r695-68.1 gr1_pt3	r695-68.1 gr1_pt3	r695-68.1 gr1_pt4	r695-68.1 gr1_pt5	r695-68.1 gr1_pt6	r695-68.1 gr2_pt1	r695-68.1 gr2_pt1	r695-68.1 gr2_pt2	r695-68.1 gr2_pt2	r695-68.1 gr2_pt3	r695-68.1 gr2_pt4	r695-68.1 gr2_pt5
Mineral	**pn**	**mill**	**pn**	**mill**	**pn**	**mill**	**py**	**py**	**pn**	**pn**	**mill**	**pn**	**mill**	**pn**	**py**	**pn**
Ru	4.28	0.253	2.71	0.16	4.74	0.28	0.0643	0.226		3.49	0.432	0.386	0.192	0.93	0.253	
Rh	3.110	0.015	3.040	0.020	3.080		0.500	0.055	0.246	1.281		0.024	0.020	0.047	0.443	
Pd	2.72		4.46	0.24	3		15.85	0.099	1.22	0.104	0.45	0.112	0.195	1.37	0.151	0.303
Os	1.24	0.334	0.927	0.39	1.37	0.287	0.118	0.228	0.148	1.71	0.364	0.38	0.284	0.456	0.327	0.284
Ir	0.024		0.020	0.004	0.033	0.003		0.004		0.007		0.002		0.004		0.001
Pt		0.008			0.002	0.005	0.002			0.003			0.002			
S34	394963	655089	416425	623959	394984	652697	508743	553352	401216	431910	632459	405190	660443	414378	604700	390346
Co59	1292.6	935.1	1356.1	815.2	1290.0	808.1	7618.6	10689.1	12130.8	1579.3	1077.6	1473.6	948.8	1493.1	10837.6	10185.8
Ni61	490993	633214	494660	618433	508456	648915	9089	34549	223745	534129	660124	526306	630588	500887	30396	161928
Cu65	1356	28721	555	1200	1671		26099886	2663679	11032774	3069	1227	21954	160021	5936	17145698	16973048
Zn67		2.3					126.7	1.6	281.4		1.7	0.7		1.2	4.4	
Ge72	4.0	8.0	3.9	7.1	4.0	8.0	4.8	5.4	4.0	4.5	7.0	4.2	7.9	4.1	5.8	3.9
As75	326.42	512.49	336.21	500.59	365.11	507.84	972.39	928.42	970.33	405.63	562.98	155.92	596.20	120.33	2018.82	338.45
Se78	747	1394	657	1343	754	1420	1023	1205	782	659	1396	832	1488	729	1089	801
Mo95	0.198	0.09	0.157	0.354	0.207	0.319	0.0268	0.092	0.103		0.469	0.19	0.058	0.067	0.153	0.052
Ag107	0.05	0.78			0.05		4.26	4.67	21.20	0.12	0.12	0.09	1.74	0.05	5.43	13.47
Cd111					0.22	0.20	0.87		2.55		0.20	0.08		0.18		
Sn120	1.11	0.14	0.59	0.28	1.05	0.11	0.22	0.06	0.11	0.33	0.10	0.19		0.08	0.06	0.07
Sb121	0.03	0.03	0.14		0.12	0.14	0.25	0.05	0.37		0.07	0.05	0.12		0.04	0.08
Te126	573.61	4.22	284.69	42.74	616.45	7.13	130.31	25.99	23.88	212.34	3.69	6.49	14.31	3.33	50.25	15.32
Re185	0.022	0.002	0.020	0.007	0.015			0.003	0.010	0.022	0.006				0.004	0.002
Au197	0.022		0.007	0.009	0.020	0.003	0.277	0.061	0.486	0.019	0.007	0.002	0.013		0.022	0.019
Pb208	0.25	0.03	0.02	0.12	0.08	0.02	29.32	7.05	255.52	0.86	0.17	0.11	0.34	0.55	50.92	121.09
Bi209	2.41	1.48	0.20	72.28	1.74	2.66	332.13	61.64	162.07	4.01	12.42	0.95	28.31	0.23	204.45	49.33

Slide	R695-68.1	R695-68.1	R695-68.1	R695-68.1	R695-68.1	R695-68.1	R695-68.1	R695-68.1	R695-68.1	R695-68.1	R695-68.1	R695-68.1	R695-68.1	R695-68.1	R695-68.1	R695-68.1
Ore Type	**Ni-PGE ore**	**Ni-PGE ore**	**Ni-PGE ore**	**Ni-PGE ore**	**Ni-PGE ore**	**Ni-PGE ore**	**Ni-PGE ore**	**Ni-PGE ore**	**Ni-PGE ore**	**Ni-PGE ore**	**Ni-PGE ore**	**Ni-PGE ore**	**Ni-PGE ore**	**Ni-PGE ore**	**Ni-PGE ore**	**Ni-PGE ore**
Spot Name	r695-68.1 gr2_pt6	r695-68.1 gr3_pt1	r695-68.1 gr3_pt1	r695-68.1 gr3_pt2	r695-68.1 gr3_pt3	r695-68.1 gr3_pt4	r695-68.1 gr3_pt5	r695-68.1 gr4_pt1	r695-68.1 gr4_pt3	r695-68.1 gr5_pt1	r695-68.1 gr5_pt2	r695-68.1 gr6_pt1	r695-68.1 gr6_pt1	r695-68.1 gr6_pt2	r695-68.1 gr7_pt1	r695-68.1 gr7_pt2
Mineral	**cpy**	**pn**	**mill**	**pn**	**pn**	**py**	**py**	**pn**	**cpy**	**mill**	**mill**	**pn**	**mill**	**mill**	**pn**	**pn**
Ru	0.168	4.34	0.432	7.63	0.565	0.484	0.521		0.094	0.362	0.332	0.65	0.637	0.46	3.44	3.81
Rh		3.220		2.230	0.181		0.048						0.033	0.020	2.350	2.520
Pd	0.197	9.72	0.285	7.28	5.84	0.424	0.402		0.834			0.754	0.542	0.448		
Os	0.007	2.05	0.247	2.08	0.446	0.711	0.694	26.4		0.318	0.339	0.315	0.323	0.267	1.6	1.52
Ir	0.001	2.590	0.109	1.840	0.306	0.469	0.379	18.060	0.020			0.001	0.001		0.005	
Pt	0.002	0.006	0.003	0.011		0.005	0.002	1.840	0.150				0.003	0.004	0.003	
S34	374092	433417	628282	417191	439437	605358	592043	20247112	368048	634421	651172	429724	672208	623844	464973	436298
Co59	17.9	1642.5	948.8	1601.1	1578.8	8211.7	6231.4	58279.1	42.0	1164.0	1150.1	3021.3	1734.0	1659.6	1970.5	1984.3
Ni61	518	522442	631540	493849	506036	6075	2366	36522212	12115	627396	638474	557893	649949	631855	491837	540830
Cu65	22314		1392	3153	1945	555934	496750		127730			3991411	1389200	21135	1106	1692
Zn67	5.1			0.7	1.4			51.9	23.1	1.0		0.9			0.5	0.7
Ge72	3.8	4.7	7.8	3.8	4.7	5.7	6.1	187.6	4.1	8.2	7.7	4.6	8.7	8.0	4.1	4.9
As75	9.62	10.35	11.70	9.46	8.09	16.41	15.03	249.45	0.35	488.14	533.75	165.72	518.15	495.74	354.67	368.65
Se78	334	731	1384	702	808	1316	1261	41521	263	1438	1418	858	1484	1401	751	785
Mo95	0.249	0.118	0.223		0.141	0.468	0.12	6.1	0.109			0.253			0.078	0.098
Ag107	1.25	0.07	0.09	0.21	0.26	2.40	2.57	2.43	0.46	0.04	0.11	0.31	1.53	0.12	0.24	0.29
Cd111	0.31		0.25			0.08		13.65	0.27	0.11	0.19	0.18		0.50	0.13	0.22
Sn120	0.15	0.26	0.18	0.25	0.16	0.03	0.06	1.83	0.33	0.07	0.15	0.14		0.19	0.63	0.82
Sb121	0.10		0.06		0.02	0.03	0.13		0.02	0.03		0.15	0.15	0.12	0.05	
Te126	0.42	121.91	1.89	101.58	8.81	20.38	17.04	173.94	0.54	3.46	3.11	6.78	15.17	13.02	312.89	433.15
Re185		0.023	0.005	0.015		0.003		0.226	0.005	0.004	0.005	0.012			0.009	0.021
Au197					0.005	0.032	0.038	0.329	0.093	0.008	0.007	0.007	0.064	0.064	0.003	0.014
Pb208	20.92	0.09	0.02	0.10	0.14	0.44	0.21	3.35	10.02	0.00	0.02	7.30	0.57	0.23	0.09	0.07
Bi209	3.03	0.90	2.18	0.64	1.33	71.70	42.46	215.44	4.13	1.06	1.65	4.00	26.78	18.71	3.84	2.67

Slide	R695-68.1	R695-68.1	R695-68.1	R695-68.1	R695-68.1	R695-69	R695-69	R695-69	R695-69	R695-69	R695-69	R695-69	R695-69	R695-69	R695-69	R695-69
Ore Type	**Ni-PGE ore**	**Ni-PGE ore**	**Ni-PGE ore**	**Ni-PGE ore**	**Ni-PGE ore**	**Ni-PGE ore**	**Ni-PGE ore**	**Ni-PGE ore**	**Ni-PGE ore**	**Ni-PGE ore**	**Ni-PGE ore**	**Ni-PGE ore**	**Ni-PGE ore**	**Ni-PGE ore**	**Ni-PGE ore**	**Ni-PGE ore**
Spot Name	r695-68.1 gr7_pt3	r695-68.1 gr8_pt1	r695-68.1 gr8_pt1	r695-68.1 gr8_pt2	r695-68.1 gr8_pt2	r695-69 gr1_pt1	r695-69 gr1_pt2	r695-69 gr1_pt3	r695-69 gr2_pt1	r695-69 gr2_pt2	r695-69 gr2_pt3	r695-69 gr3_pt1	r695-69 gr3_pt2	r695-69 gr3_pt3	r695-69 gr3_pt4	r695-69 gr4_pt1
Mineral	**pn**	**pn**	**mill**	**pn**	**mill**	**pn**	**pn**	**pn**	**pn**	**pn**	**py**	**pn**	**pn**	**cpy**	**cpy**	**pn**
Ru	3.68	4.08	0.464	1.71	0.647	4.64	0.764	2.57			0.257			0.196	0.108	5.2
Rh	2.450	3.010	0.023		0.033	0.021			0.054	0.019		0.008	0.034			0.091
Pd	0.379	3.98	0.372	7.22	0.315	5.51	6.6	6.08	3	5.06	1.33	10.88	10.21	0.12	0.08	8.12
Os	1.6	1.2	0.448	0.241	0.398	2.01	0.094	0.994	0.269	3.22	0.129	1.9	1.71	0.004	0.003	2.46
Ir		2.390	0.116	1.830	0.057	0.001		0.001	0.003			0.003	0.001			0.007
Pt					0.002							0.002				0.005
S34	413477	412954	633107	418293	638812	336321	319705	316425	327433	325950	513270	332565	314098	349435	331798	350327
Co59	1942.5	1706.4	1078.4	1654.3	1077.1	1946.3	1792.6	1733.8	2209.1	2098.0	3803.1	2207.8	2134.0	0.3	0.1	1957.0
Ni61	500424	514820	629204	505540	656823	362413	349551	348643	367624	374052	70182	367861	338045	28	29	407879
Cu65	2851	1999	1265	41094784	1393	5990	1830		2120	3947	6856155	2751	576			639
Zn67		1.6		100.9	1.2			0.4	0.7		6.9	0.7		366.0	296.6	
Ge72	4.2	4.2	7.7	4.4	7.6	3.4	3.1	3.2	3.9	4.1	5.5	3.7	3.6	3.8	3.6	4.1
As75	342.49	15.76	19.69	13.80	19.56	1343.76	112.57	353.38	247.49	1420.86	77.95	853.47	914.47	2.48	0.33	1406.49
Se78	782	660	1328	662	1373	433	316	341	344	440	605	418	397	149	171	468
Mo95		0.32	0.425	0.162	0.238						0.436					
Ag107	0.10	0.11	0.10	0.36	0.10	0.21	0.12	0.10	0.22	0.16	13.03	0.14	0.19	0.07	0.16	0.09
Cd111	0.20	0.48		0.54	0.29			0.08			0.19	0.11		0.61	0.68	
Sn120	0.71	0.19	0.25	0.15		0.32	0.08	0.26	0.30	0.44	0.11	0.32	0.32	2.03	2.33	0.43
Sb121				0.07	0.11		0.01		0.01	0.02	0.39			0.10	0.06	0.03
Te126	367.06	114.94	2.39	51.18	3.77	192.95	16.84	44.22	47.91	238.48	4.32	129.03	114.33	0.27		194.65
Re185			0.007	0.014		0.041	0.006	0.032	0.011	0.097	0.009	0.040	0.057			0.027
Au197				0.004	0.009	0.005			0.017	0.005	0.626	0.003	0.003	0.012	0.005	
Pb208	0.16	0.17	0.01	17.75	0.02	0.12	0.05	0.03	0.25	0.06	7.82	0.14	0.02	0.34	0.38	0.09
Bi209	0.92	0.59	1.73	1.66	2.89	3.54	0.08	0.34	4.42	0.95	143.57	0.03	0.20	1.10	1.36	0.29

Slide	R695-69	R695-69	R695-69	R695-69	R695-69	R695-69	R695-69	R695-69	R695-69	R695-69	R695-69	R695-69	R695-69	R695-69	R713-37.3	R713-37.3
Ore Type	**Ni-PGE ore**	**Ni-PGE ore**	**Ni-PGE ore**	**Ni-PGE ore**	**Ni-PGE ore**	**Ni-PGE ore**	**Ni-PGE ore**	**Ni-PGE ore**	**Ni-PGE ore**	**Ni-PGE ore**	**Ni-PGE ore**	**Ni-PGE ore**	**Ni-PGE ore**	**Ni-PGE ore**	**Ni-PGE ore**	**Ni-PGE ore**
Spot Name	r695-69 gr4_pt2	r695-69 gr4_pt3	r695-69 gr4_pt4	r695-69 gr5_pt1	r695-69 gr5_pt2	r695-69 gr5_pt3	r695-69 gr6_pt1	r695-69 gr6_pt2	r695-69 gr6_pt3	r695-69 gr6_pt4	r695-69 gr7_pt1	r695-69 gr7_pt2	r695-69 gr7_pt3	r695-69 gr7_pt4	r713-37 gr1_pt1	r713-37 gr1_pt2
Mineral	**pn**	**pn**	**pn**	**cpy**	**cpy**	**cpy**	**cpy**	**cpy**	**pn**	**pn**	**pn**	**pn**	**pn**	**pn**	**mill**	**mill**
Ru	5.28	4.75	7.25	0.263	0.192	0.128	0.151	0.136		0.769						
Rh	0.061	0.026	0.105						0.008		0.009	0.018		0.014		
Pd	9.28	8.8	5.55		0.104	0.133	0.049	0.176	11.54	16.72	1.95	2.28	3.04	2.43	0.143	0.96
Os	2.4	2.72	3.36			0.004		0.014	0.622	0.099	1.320	2.230	2.540	0.044	0.005	0.003
Ir	0.004	0.001		0.002	0.003		0.002	0.021				0.003			0.075	0.087
Pt	0.006				0.002	0.005		0.020		0.004					0.010	
S34	331884	345491	344585	360139	344142	331950	317376	311375	322723	312187	329694	335273	320312	354194	807661	759467
Co59	1847.8	1810.0	1973.0	0.1	1.6	0.1	0.1	0.8	2054.9	1959.6	2723.2	2186.3	2082.7	2056.7	2747.0	2234.6
Ni61	378852	380508	400614	11	187	56	24	114	354297	354501	345300	382826	362503	366662	633175	638746
Cu65	3530	1546	1567						80281	4004	169860	14150		57592	53664	76632
Zn67	0.4	0.5		542.1	397.8	429.3	386.3	332.6	0.5		1.0	0.4	0.3			
Ge72	3.4	3.3	3.6	3.8	3.7	3.7	3.7	3.6	4.0	3.6	3.7	3.5	3.2	3.4	10.9	10.0
As75	1306.72	1228.09	1052.00	0.51	1.09	0.37	0.86	0.59	189.58	41.72	489.38	1133.27	1344.62	34.38	27.32	24.66
Se78	416	417	434	207	215	205	156	134	342	326	402	433	417	387	2084	1866
Mo95				0.074			0.122	0.143		0.187			0.095			
Ag107	0.04	0.03	0.11	0.19	0.20	0.10	0.16	0.19	0.55	0.06	0.52	0.32	0.18	0.30	5.07	3.04
Cd111				1.23	0.90	1.09	0.69	0.96					0.14			1.44
Sn120	0.46	0.37	0.65	2.03	2.21	2.13	1.31	1.04	0.13	0.07	0.22	0.37	0.28	0.13	0.47	0.31
Sb121	0.11	0.03	0.04	0.06	0.03	0.02	0.02	0.04	0.03	0.02	0.06		0.02	0.04	0.03	
Te126	218.95	155.70	263.45	0.48	0.28	0.63	0.39	0.20	31.05	7.48	84.34	172.53	195.78	1.57	2.37	2.52
Re185	0.062	0.041	0.047		0.002	0.004			0.019	0.006	0.044	0.043	0.068			0.002
Au197	0.006		0.023	0.010	0.034	0.006	0.001	0.007	0.003	0.009	0.014		0.005	0.015		0.004
Pb208	0.52	0.11	0.17	0.47	0.90	0.38	0.13	0.84	0.31	0.05	2.29	0.03	0.01	1.23	2.50	20.29
Bi209	0.23	0.14	2.50	1.61	1.45	2.00	0.48	0.62	0.79	0.09	5.36	0.36	0.26	2.52	1.28	7.31

Slide	R713-37.3	R713-37.3	R713-37.3	R713-37.3	R713-37.3	R713-37.3	R713-37.3	R713-37.3	R713-37.3	R713-37.3	R713-37.3	R713-37.3	R713-37.3	R713-37.3	R713-37.3	R713-37.3
Ore Type	**Ni-PGE ore**	**Ni-PGE ore**	**Ni-PGE ore**	**Ni-PGE ore**	**Ni-PGE ore**	**Ni-PGE ore**	**Ni-PGE ore**	**Ni-PGE ore**	**Ni-PGE ore**	**Ni-PGE ore**	**Ni-PGE ore**	**Ni-PGE ore**	**Ni-PGE ore**	**Ni-PGE ore**	**Ni-PGE ore**	**Ni-PGE ore**
Spot Name	r713-37 gr2_pt1	r713-37 gr4_pt1	r713-37 gr4_pt2	r713-37 gr5_pt1	r713-37 gr6_pt1	r713-37.3 gr1_pt1	r713-37.3 gr2_pt1	r713-37.3 gr2_pt2	r713-37.3 gr3_pt1	r713-37.3 gr3_pt2	r713-37.3 gr4_pt1	r713-37.3 gr4_pt2	r713-37.3 gr4_pt3	r713-37.3 gr5_pt1	r713-37.3 gr5_pt2	r713-37.3 gr6_pt1
Mineral	**mill**	**mill**	**mill**	**mill**	**mill**	**pn**	**pn**	**pn**	**pn**	**pn**	**pn**	**pn**	**pn**	**pn**	**pn**	**pn**
Ru		0.2	0.225		0.244	6.41					5.95	6.97	0.538			7.71
Rh	1.807		0.025	0.021	0.010	3.330	1.820	1.710		4.540	2.190	3.040	0.138	0.141	0.114	3.470
Pd	15.8	0.97	2.72	2.38	0.88	1.81	10.56	7	29.1	3.68	5.3	6	4.36	51.58	22.79	17.92
Os	3.620	0.017	0.005	0.004	0.010	2.13	1.4	1.43	0.0172	2.84	3.43	4.61	0.006	0.013	0.002	3.92
Ir	1.760	0.048	0.044	0.033	0.115	3.920	1.450	1.590	0.042	4.790	2.520	3.280	0.079	0.243	0.146	4.280
Pt	0.011	0.009		0.017	0.007	0.003	0.015	0.006	0.228		0.003	0.024		0.243	0.494	0.007
S34	1001630	673156	762192	722574	670293	430867	446369	456696	517649	503892	439145	412769	441873	487560	468327	426965
Co59	4818.9	758.3	871.8	2440.3	858.4	2248.8	3636.6	3717.2	5691.0	5237.9	1103.3	1048.9	1148.3	4409.5	6944.5	1358.6
Ni61	641988	631155	677056	636038	620345	508657	504668	521380	642454	563302	498903	487212	540827	559925	527833	480935
Cu65	6268	50454	333693	846625	188357	1514	7446	8036	555581	49173	3007	70848	6161	5395240	3921405	4849
Zn67	1.4					1.2	0.3	20.1	1.7	15.9	0.9	6.9		1.6		
Ge72	13.1	8.9	9.5	9.6	8.7	4.3	4.7	4.4	5.3	5.2	4.2	4.6	4.1	4.9	5.3	4.7
As75	40.03	9.34	10.23	25.98	19.37	14.10	15.11	16.68	19.58	15.33	5.09	5.59	2.84	26.79	31.24	12.37
Se78	2081	1741	1978	1717	1613	699	763	676	789	592	700	797	825	891	970	717
Mo95			0.243		0.068	0.119	0.247		0.286	0.339	0.106		0.104		0.075	
Ag107	0.16	0.03	3.30	2.98	1.22		0.09	0.11	13.82	0.43	0.17	0.11	0.05	9.99	9.55	0.16
Cd111	0.37	0.51		0.14											0.24	
Sn120	0.90	0.08	0.21	0.16	0.08	0.36	0.59	0.38	0.06	0.15	0.26	0.51	0.14	0.15	0.19	0.54
Sb121	0.13	0.06				0.04			0.03	0.05				0.03	0.02	
Te126	219.94	2.86	3.68	2.04	2.72	118.94	264.76	111.99	6.64	57.50	92.91	262.18	3.62	6.10	3.94	253.28
Re185	0.012					0.012	0.010	0.026			0.008	0.008		0.008		0.042
Au197	0.007	0.011	0.021	0.010	0.005	0.008		0.004	0.072	0.003	0.015	0.011		0.217	0.113	0.018
Pb208	0.43	0.39	1.32	4.63	0.02	0.08	0.09	0.23	37.39	0.16	0.66	0.08	2.05	202.28	484.90	0.37
Bi209	1.02	4.93	10.74	8.25	0.85	1.39	0.50	1.37	80.48	0.13	4.58	1.04	1.92	83.80	55.93	1.16

Slide	R713-37.3	R713-37.3
Ore Type	**Ni-PGE ore**	**Ni-PGE ore**
Spot Name	r713-37.3 gr6_pt2	r713-37.3 gr6_pt3
Mineral	**pn**	**pn**
Ru	7.77	8.16
Rh	3.240	3.450
Pd	14.33	14.37
Os	3.05	4.16
Ir	4.070	4.450
Pt		0.007
S34	424950	433355
Co59	1306.2	1443.5
Ni61	501771	506818
Cu65	19277	22575
Zn67	0.6	
Ge72	4.8	5.0
As75	11.99	12.57
Se78	613	721
Mo95	0.179	
Ag107	0.24	0.16
Cd111	0.24	0.10
Sn120	0.37	0.56
Sb121		0.05
Te126	120.75	240.69
Re185	0.025	0.025
Au197	0.003	0.009
Pb208	0.11	2.50
Bi209	0.39	